Technical Report

TR-03-16

Redox zone II

Coupled modeling of groundwater flow, solute transport, chemical reactions and microbial processes in the Äspö island

Javier Samper, Jorge Molinero, Changbing Yang,
Guoxiang Zhang
Universidade Da Coruña

December 2003

Svensk Kärnbränslehantering AB
Swedish Nuclear Fuel
and Waste Management Co
Box 5864
SE-102 40 Stockholm Sweden
Tel 08-459 84 00
+46 8 459 84 00
Fax 08-661 57 19
+46 8 661 57 19

Redox zone II

Coupled modeling of groundwater flow, solute transport, chemical reactions and microbial processes in the Äspö island

Javier Samper, Jorge Molinero, Changbing Yang,
Guoxiang Zhang
Universidade Da Coruña

December 2003

Summary

The Redox Zone Experiment was carried out at the Äspö HRL in order to study the redox behaviour and the hydrochemistry of an isolated vertical fracture zone disturbed by the excavation of an access tunnel. Overall results and interpretation of the Redox Zone Project were reported by /Banwart et al, 1995/. Later, /Banwart et al, 1999/ presented a summary of the hydrochemistry of the Redox Zone Experiment. Coupled groundwater flow and reactive transport models of this experiment were carried out by /Molinero, 2000/ who proposed a revised conceptual model for the hydrogeology of the Redox Zone Experiment which could explain simultaneously measured drawdown and salinity data. The numerical model was found useful to understand the natural system. Several conclusions were drawn about the redox conditions of recharge waters, cation exchange capacity of the fracture zone and the role of mineral phases such as pyrite, calcite, hematite and goethite. This model could reproduce the measured trends of dissolved species, except for bicarbonate and sulphate which are affected by microbially-mediated processes.

In order to explore the role of microbial processes, a coupled numerical model has been constructed which accounts for water flow, reactive transport and microbial processes. The results of this model is presented in this report. This model accounts for groundwater flow and reactive transport in a manner similar to that of /Molinero, 2000/ and extends the preliminary microbial model of /Zhang, 2001/ by accounting for microbially-driven organic matter fermentation and organic matter oxidation. This updated microbial model considers simultaneously the fermentation of particulate organic matter by yeast and the oxidation of dissolved organic matter, a product of fermentation. Dissolved organic matter is produced by yeast and serves also as a substrate for iron-reducing bacteria.

Model results reproduce the observed increase in bicarbonate and sulfaphe concentration, thus adding additional evidence for the possibility of organic matter oxidation as the main source of bicarbonate. Model results indicate that pH and Eh are relatively stable. The dissolution-precipitation trends of hematite, pyrite and calcite also coincide with those indicated by the conceptual model.

A thorough sensitivity analysis has been performed for the most relevant microbial parameters as well as for initial and boundary POC and DOC concentrations. The results of such analysis indicate that computed concentrations of bicarbonate, sulphate and DOC are sensitive to most of the microbial parameters, including specific growth rates, half-saturation constants, proportionality coefficients and yield coefficients. Model results, however, are less sensitive to the yield coefficient of DOC to iron-reducer bacteria. The sensitivity analysis indicates that changes in fermentation microbial parameters affect the growth of the iron-reducer, thus confirming the interconnection of both microbial processes. Computed concentrations of bicarbonate and sulphate are found to be sensitive to changes in the initial concentration of POC and the boundary concentration of DOC, but they lack sensitivity to the initial concentration of DOC and the boundary concentration of POC. The explanation for such result is related to the fact that POC has a low mobility due to its large molecular weight. DOC, however, can migrate downwards.

Although a coupled hydro-bio-geochemical 1-D model can reproduce the observed "unexpected" increase of concentrations of bicarbonate and sulphate at a depth of 70 m, further modelling work is required in order to obtain a similar conclusion under the more realistic two dimensional conditions of the fracture zone.

Contents

1	**Introduction**		**7**
1.1	Background		7
1.2	Objectives		9
1.3	Scope		9
2	**Numerical model of groundwater flow and solute transport**		11
2.1	Introduction		11
2.2	Hydrogeology and hydrochemistry		14
2.3	Hydrogeological conceptual model based on hydrochemical data		16
2.4	Mathematical formulation and first numerical modeling		17
	2.4.1	Mathematical model	17
	2.4.2	Numerical model	18
	2.4.3	Model calibration	20
2.5	Revised hydrogeological conceptual model		21
2.6	Revised numerical model		24
	2.6.1	Model setting	24
	2.6.2	Model calibration and results	29
2.7	Chapter conclusions		34
3	**Numerical model of reactive solute transport**		37
3.1	Hydrochemical and mineralogical background		37
3.2	Hydrochemical modeling of mixing and reactions		41
3.3	Hydrochemical conceptual model		44
3.4	Initial and boundary conditions		47
3.5	Base numerical model		50
3.6	Evaluating the role of the rock landfill		58
3.7	Evaluating the role of seafloor sediments		61
3.8	Chapter conclusions		63
4	**Numerical model of coupled reactive solute transport and microbial processes**		65
4.1	Introduction		65
4.2	Microbes and possible microbial processes at the ÄSPÖ site		65
4.3	Previous microbial model of /Zhang, 2001/		71
4.4	Updated microbial models coupled to hydrogeochemical reactive transport		76
	4.4.1	Updated microbial models	76
	4.4.2	Numerical model set-up	78
	4.4.3	Model calibration	85
	4.4.4	Sensitivity analysis	91
4.5	Chapter conclusions		105

5 Conclusions 107
5.1 Flow and solute transport model 107
5.2 Coupled flow and reactive transport model 107
5.3 Coupled flow, reactive transport and microbial model 108

Acknowledgements 111

References 113

Appendix I Brief description of BIO-CORE 119

1 Introduction

1.1 Background

On March 13th, 1991 the access tunnel of the Äspö HRL intersected a vertical fracture zone at a depth of 70 m below sea level. Prior to tunnel intersection, a borehole was drilled and sampled in order to characterize the undisturbed conditions of groundwater at the tunnel position. These samples provided a reference state against which to compare the evolution of groundwater conditions after tunnel construction. This vertical fracture zone is known within the context of the Äspö HRL as the Redox Zone.

The Redox Zone Experiment carried out at the Äspö HRL provided the opportunity to study the redox behaviour, and the hydrochemistry of an isolated vertical fracture zone disturbed by a tunnel excavation. The Redox Zone Experiment is a long-term in situ experiment with probably one of the largest and most detailed chemical database in the world. The overall results and interpretation of the Redox Zone Project can be found in /Banwart et al, 1995/ who described the methodology and main mineralogical, isotopic, microbiological and hydrochemical studies. Later, /Banwart et al, 1999/ presented a summary of the hydrochemistry of the Redox Zone Experiment.

More recently, /Molinero, 2000/ carried out a numerical model of coupled groundwater flow and reactive solute transport of the Redox Zone Experiment. Inasmuch as the original purpose of the Redox Zone Experiment was mainly the evaluation of redox conditions, more emphasis was given in previous studies to hydrochemical aspects than to hydrodynamic processes. While it was simple to construct a flow numerical model which could reproduce observed drawdowns, the same was not true for a flow and transport numerical model which could explain simultaneously drawdowns and salinities measured at the tunnel and boreholes. /Molinero, 2000/ and /Molinero and Samper, 2004/ proposed a revised conceptual model for the hydrogeology of the Redox Zone Experiment which could explain simultaneously measured drawdown and salinity data. This alternative conceptual model includes the hydrogelogical role of a rock landfill in the west and the Ävrö island in the east. Based on this conceptual model, /Molinero, 2000/ and /Molinero et al, 2000/ performed a fully coupled numerical model of groundwater flow and reactive solute transport. This model accounts for more than 60 homogeneous reactions, including aqueous complexation, acid-base reactions, gas dissolution and redox processes, as well as 5 heterogeneous reactions including mineral dissolution/precipitation and cation exchange. The model was able to reproduce the observed concentrations of most of dissolved species both before and after tunnel construction. The numerical model was found to be useful to understand the natural system. Several conclusions were drawn about the redox conditions of recharge waters, cation exchange capacity of the fracture zone and the role of mineral phases such as pyrite, calcite, hematite and goethite.

However, the behaviour of some relevant chemical species during the experiment still remains unresolved. Even though the numerical model predicts the dissolution of calcite and pyrite, it is unable to reproduce the measured increase of bicarbonate and sulphate in groundwaters. /Molinero, 2000/ used the coupled numerical model to test quantitatively several hydrochemical hypotheses such as alkaline sulphate-rich waters leaching from a rock landfill, and the leaching of seafloor sediment porewaters, among others. After discarding all these hypotheses, it was concluded that microbially-

mediated degradation of organic matter through iron (III) mineral reduction is the most likely chemical process to explain measured bicarbonate behaviour. Then, this increase in bicarbonate concentration could be coupled with adsorption competition processes between bicarbonate and sulphate which could explain the observed behaviour of dissolved sulphate. However, other processes such as methane formation or organic matter fermentation cannot be rejected.

According to /Molinero, 2000/, microbially-mediated processes may affect the hydrochemical conditions at the Äspö site. Incorporating such processes into the current flow and reactive transport numerical models should enable testing the plausibility of these processes by comparing model results to measured data.

Part of the information included in the database such as total and dissolved organic matter were not considered in previous quantitative analyses of the hydrogeological and hydrochemical behaviour of the system. The reason for that is probably the need of sophisticated numerical tools, able to solve simultaneously for groundwater flow, mass transfer, inorganic chemical reactions and microbial processes. Such tools are not commonly available. In fact, even for inorganic reactions, there are just a few codes that are able to solve for fully coupled problems under realistic conditions. The Redox Zone numerical model performed by /Molinero, 2000/ and /Molinero et al, 2000/ constitutes (to our present knowledge) the unique example performed for two dimensional, kilometric-scale, hard rock environment. This numerical model was solved using $CORE^{2D}$ /Samper et al, 2000/, a member of the CORE family of finite element codes developed at the University of A Coruña.

A recent member of the CORE family is BIO-CORE /Zhang and Samper, 2001/ which incorporates the following additional capabilities:

a) A kinetic formulation of mineral dissolution/precipitation, aqueous redox processes and sorption reactions.

b) Biochemical processes. The code includes several conceptual models for microbial processes.

A brief description of the main features of BIO-CORE is included in Appendix I. The availability of this new tool provides the opportunity to improve the numerical model of the Redox Zone Experiment and overcome the difficulties found in the past with some of the most relevant chemical trends measured during the experiment.

Previous works by /Kotelnikova and Pedersen, 1999/ provide much information about microbial population in the granitic groundwater at the Äspö site. They found that total acridine-orange counted $7.3 \times 10^4 - 2.5 \times 10^5$ unattached cells per ml in anaerobic KA2862A groundwater and $2.4 \times 10^5 - 7.7 \times 10^5$ in aerated REX groundwater. In situ microbial population consists of: aerobic heterotrophs (5%), microaerophilic heterotrophs (36%), iron-reducing bacteria (2%), sulphate-reducing bacteria (43%) and methanogenic archaea (7%) /Kotelnikova and Pedersen, 1999/. This means that aerobic, facultative aerobic, anaerobic and obligate anaerobic biodegradations may take place in the system under natural conditions. These processes may play a major role in the geochemical evolution in the Redox Zone. Accounting for these processes should improve our understanding of the geochemical evolution during the experiment.

1.2 Objectives

The main objective of this study is to carry out a coupled numerical model for the hydrogeology and hydrochemistry of the Redox Zone Experiment by accounting for microbially-mediated processes. This model provides a quantitative tool for analyzing and integrating the data collected in this experiment.

The following activities have been carried out in order to achieve this objective:

a) Accounting for microbially-induced processes. Initially it was proposed to investigate the following microbial processes: Organic matter fermentation, microbially-catalyzed iron (III) reduction, and aerobic degradation of dissolved organic matter. Dissolved organic matters are degraded first by using dissolved oxygen as electron acceptor and yield carbon dioxide and bicarbonate. This process requires aerobic conditions and therefore is unlikely to the take place in the Redox fracture zone where redox conditions are reducing for the most part. Organic matter fermentation is the first step of decomposition of organic matters. Fermentation processes destroy insoluble macromolecular organic matters into various soluble organic acids, hydrocarbon chains and cycles which can be further degraded in aerobic, facultative aerobic, anaerobic and fully or obligate anaerobic metabolism. These processes also release nitrogen and sulphur compounds because organic nitrogen and sulphur are common components of proteins and other macromolecular organic matters. Released sulphur compounds are a source of sulphate under aerobic, facultative aerobic and some anaerobic conditions. Microbially-catalyzed iron (III) reduction commonly takes place in the anaerobic parts of the system, and induces an increase in bicarbonate concentration and ferrous mineral precipitation.

b) Performing sensitivity analyses to quantify model uncertainties including: Conceptual model uncertainties (relevance of biochemical processes); and uncertainties in microbial parameters.

c) Deriving conclusions on the role of organic matter and microbial processes in the Redox Zone Experiment.

1.3 Scope

Chapter 2 presents the details of the groundwater flow and conservative solute transport model. Details of the reactive transport model, including the description of the geochemical system is presented in Chapter 3. Chapter 4 provides the details of the coupled water flow, solute transport, chemical reactions and microbial processes. Finally, the main conclusions of this study are presented in Chapter 5.

2 Numerical model of groundwater flow and solute transport

2.1 Introduction

Fractured granites have been selected in several countries as the candidate host rock for building deep geological repositories for high-level radioactive waste disposal. The hosting geological formation of the repository is known as the geological or natural barrier. The reference concept developed by several countries foresees final disposal of waste in metallic containers placed in horizontal or vertical galleries drilled in a granitic formation. Most European countries foresee a bentonite backfill between the canister and the rock (the engineering barrier). In the Swedish reference concept for a radioactive waste repository, spent fuel will be encapsulated in copper canisters which will be deposited in vertical boreholes in horizontal galleries located at 500 m depth in a crystalline rock /SKB, 1995/. Underground facilities will have to be adapted to fracture zones detected during site characterization. Water flow and solute transport through fractured granite is therefore a key factor for the design of a deep geological repository because migration through the hosting granite would be the pathway of radionuclides to the biosphere.

The Äspö Hard Rock Laboratory (Äspö HRL) is a prototype, full-scale underground facility launched and operated by SKB (the Swedish Nuclear Waste Management Company). The Äspö HRL aims at providing a site for research, development and demonstration in a realistic rock environment down to the depth planned for a future deep nuclear waste repository /SKB, 1996/. The Äspö HRL is located in the southeast part of Sweden, 400 km south of Stockholm. The underground facility consists of a 3,600 m long tunnel which starts with an access ramp and runs into two turns down to a depth of 450 m under the Äspö island (Figure 2-1).

On March 13th, 1991, the access tunnel of the Äspö HRL intersected a vertical fracture zone at a depth of 70 m below sea level. Prior to tunnel intersection, a borehole was drilled and sampled in order to characterize the hydrodynamic and hydrochemical conditions of groundwater at the tunnel position. These samples provided a reference state against which to compare the future evolution of groundwater conditions. This vertical fracture zone is known within the context of the Äspö HRL as the Redox Zone because it was used to perform a long-term experiment for evaluating the effects of the construction of the access tunnel on the hydrogeological, hydrochemical and redox conditions prevailing at this fracture zone /Banwart et al, 1994/. A timetable of the main events and experimental activities at the Redox Zone Experiment is presented in Table 2-1.

A detailed geological, mineralogical, hydrodynamic, isotopic, microbiological and hydrochemical characterization was performed both prior and after the tunnel crossed the fracture zone. The fracture zone is approximately vertical and is clearly visible from the access tunnel as a band of water-bearing fractured rock with a thickness of 1 m (Figure 2-2). Figure 2-2 shows a cross-section and a plan view of the fracture zone with the location of the sampling points of the Redox Zone Experiment.

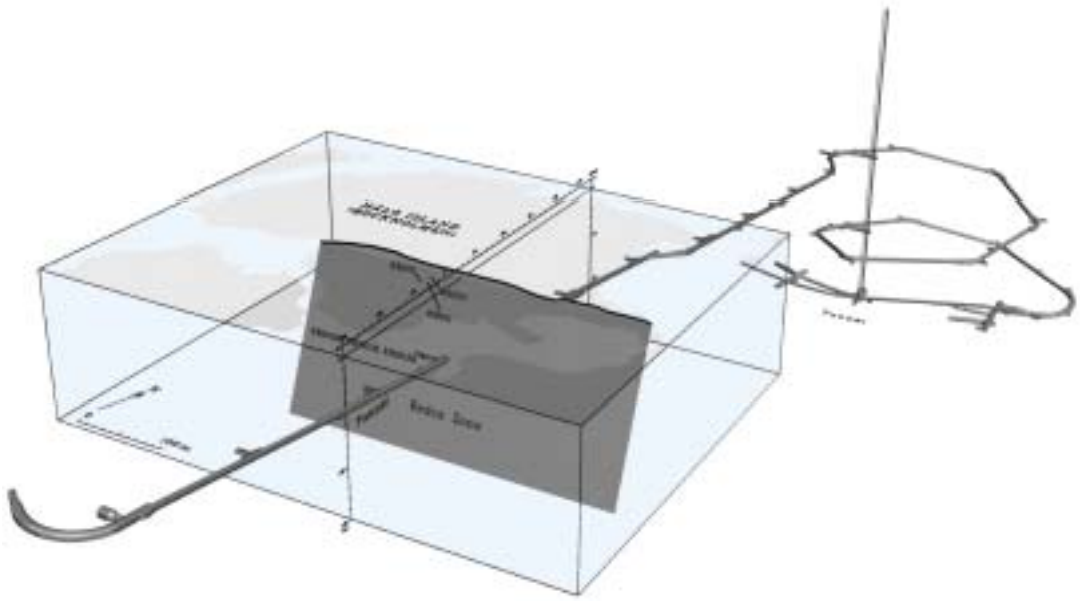

Figure 2-1. *Three-dimensional view of the tunnel and the Redox Fracture Zone. The access ramp to the Äspö Underground Laboratory intersects the fracture zone at a depth of 70 m (figure provided by M. Laaksoharju).*

Table 2-1. Summarized schedule of main events and experimental activities of the Redox Zone Experiment /Banwart et al, 1995/.

Date	Experimental day	Activities
February 20th–21st, 1991	-	Drilling of surface boreholes HBH01 and HBH02
March 9th–10th, 1991	-	Sampling of native groundwater at a depth of 70 m
March 12on–13rd, 1991	0	Tunnel intersects the fracture zone and sampling starts
	47–53	Three boreholes core-drilled into fracture zone from the side of the tunnel (boreholes KR0012B, KR0013B and KR0015B)
	93–114; 149–159	Borehole KR0012B opened with a continuous discharge of 0.3 L/min
	159	Borehole KR0012B closed and borehole KR0013B opened with a discharge of 8–10 L/min
	480	Surface borehole HBH05 percussion-drilled and packed off at 5 m depth
November 11th, 1993	983	End of the experiment

Figure 2-2. *Cross-section and plan view of the Redox Zone Experiment: A) Cross-section view with the location of boreholes drilled from the surface (HBH01, HBH2 and HBH05); and B) Plan view with the location of boreholes drilled from the tunnel at a depth of 70 m (KR0012B, KR0013B and KR0015B).Modified from /Gustafsson et al, 1994/.*

Basic data as well as their interpretation are reported by /Banwart et al, 1995/. Later, /Banwart et al, 1999/ presented a summary of the hydrochemistry of the Redox Zone Experiment. They interpreted hydrochemical and isotopic data using a qualitative description of groundwater flow. Prevailing hydraulic conditions changed drastically first when the access tunnel intersected the fracture zone and later when borehole KR0013B was open to flow. At the vicinity of the tunnel, dilution of the initially saline groundwaters by fresh recharge water is the dominant process controlling the hydrochemistry evolution during the experiment. Most chemical species show dilution trends except for dissolved bicarbonate and sulphate which increase with time due possibly to microbially mediated chemical processes /Zhang, 2001; Samper et al, 2003/.

/Hautojärvi et al, 1994/ performed scoping calculations by means of a flow model of the Redox Zone Experiment in order to support the interpretation of hydrochemical data. A homogeneous domain was assumed in the model due to the lack of data about hydrogeological parameters at that time. The numerical model accounted for variable water density. One of the most remarkable results of the model of /Hautojärvi et al, 1994/ was that the salinity had a minor effect in groundwater flow in this fracture zone. This was expected near the tunnel area where the sink dominates the flow field. In addition, they showed that density variations due to salinity distribution had almost no measurable effects in the computed pressure distribution, even at a distance of 600 m from the tunnel /Hautojärvi et al, 1994/.

Previous interpretations of the experiment are subject to uncertainties mostly related to an oversimplified conceptualization of groundwater flow. In fact, as pointed out by /Banwart et al, 1994, 1999/ the observed water dilution near the tunnel requires a contribution of fresh water greater than the amount of available recharge water on the catchment area.

The main conclusion achieved with the Redox Zone Experiment was that molecular oxygen is apparently removed in the most shallow reaches of the fracture zone /Banwart et al, 1996/. These authors pointed out that anaerobic respiration of the remaining organic carbon explain the input of carbon dioxide and alkalinity to the groundwater. The relevance of this conclusion rests on the fact that any source of organic carbon, such as a soil layer, may provide important protection against penetration of an oxygen front from the surface during construction and operation of an open repository /Banwart et al, 1996/.

Here we present finite element numerical models of groundwater flow and solute transport for the Redox Fracture Zone. A numerical model based on the conceptual model used by /Banwart et al, 1994, 1999/ is presented first. It is shown that this numerical model presents several inconsistencies while is unable to fit simultaneously observed drawdowns and chloride breakthrough curves. Later an alternative flow and transport model is presented which overcomes the limitations of the first model. This revised model is not only consistent with head and concentration data collected prior to tunnel construction, but reproduces simultaneously the observed drawdowns and chloride dilution induced by the construction of the tunnel. Finally we present the main conclusions of this study.

2.2 Hydrogeology and hydrochemistry

Groundwater flow through the Äspö area is controlled mostly by the major tectonic fracture zones and discontinuities /Smellie et al, 1995/. The Redox Fracture Zone is one of such water-conducting zones defined in the hydrogeological conceptual model of the Äspö area /Rhén et al, 1997/. Fracture zones usually have hydraulic conductivities several orders of magnitude larger than the conductivity of adjacent rock domains. /Molinero et al, 2002/ performed a 3-D numerical model of the hydrogeological transient response produced by the construction of the Äspö tunnel and concluded that rock mass domains outside of the fracture zones play no major role on the hydrogeology of the Äspö island.

The Redox Zone outcrops on the small island of Halö which is located between the mainland coastline and the Äspö island (Figure 2-1). The outcrop of the Redox Zone on the Halö island appears as a small topographic depression 10 m wide and 2–3 m deep. At the bottom of this depression, just above the tunnel, there is a layer of soil 0.2 m thick which overlies a zone of reworked sand and gravel extending to a depth of 0.5 m. Below the sand and gravel, a layer of glacial clay extends to a depth of 1 m. Between this glacial clay and the granite bedrock there is a layer of moraine sediments. A percussion borehole drilled from the surface found the rock at a depth of 5 m /Banwart et al, 1995/.

The island of Halö has a slightly undulating topography of well exposed rock, with topographic maxima around 10 m.a.s.l. The geology is characterized by a red to gray porphyritic granite-granodiorite known locally as "Smaland granite" which belongs to the Transcandinavian Granite-Porphyry Belt /Banwart et al, 1999/.

The topography along the fracture zone defines a catchment area on Halö itself of 10,000 m^2. Considering an average rainfall between 500 and 675 mm/year and an average actual evapotranspiration of about 500 mm/year, leaves from 50 to 175 mm/year for runoff and groundwater recharge /Banwart et al, 1995/. Groundwater flow models of the whole Äspö site indicate that groundwater recharge should be from 10% to 20% of the total amount available for runoff and recharge /Banwart et al, 1999/. Therefore, groundwater recharge in fracture zones of the Äspö range from 5 to 35 mm/year.

Available borehole logs indicate that the thickness of the fracture zone decreases with depth from 10 m near the topographic surface to 1 m at a depth of 15 m /Banwart et al, 1999/. /Gustafsson et al, 1994/ performed hydraulic interference tests from which they reported a transmissivity of 4.2×10^{-5} m^2/s at 45 m depth and 1.4×10^{-5} m^2/s at 70 m depth. Estimated values of storativity range from 10^{-5} and 10^{-7} m^{-1}. They also report the results of tracer tests performed in the Redox Zone during the stage in which both borehole KR0013B and the tunnel were discharging. Three conservative tracers were injected in shallow boreholes at 5, 15 and 45 m depth. These tracer tests confirmed the hydraulic connection of injection and discharge points. They reported travel times of 5 days between 45 and 70 m depth, and 30 days between 15 and 70 m depth. From the interpretation of breakthrough curves they obtained a longitudinal dispersivity of 15 to 20 m and a flow porosity from 0.005 to 0.01 for depths ranging from 45 to 70 m.

The water table above the tunnel position was approximately 0.5 m below the surface (i.e. 1.5 m above sea level) before the tunnel intersected the fracture zone. After that, the water table showed a mild decline. According to /Banwart et al, 1994/ the fracture zone can be assumed to be fully saturated during the entire experiment.

Three weeks after the start of the experiment a sharp dilution front arrived to the access tunnel /Banwart et al, 1999/. This appeared as a dramatic decrease in Cl^- and cation concentrations, and an increase in HCO_3^- concentration in the groundwater flowing from the roof of the tunnel. A short time later, dissolved Fe concentrations in the tunnel inflows decreased to near zero for a period of a few weeks. This could be taken as an indication of the arrival of an oxidation front to the tunnel position. In day 159 the discharge borehole was opened for continuous discharge and some time later, another dilution stage, less pronounced than the first one, was observed at some boreholes. Measured Cl^- dilution in borehole KR0015B at a depth of 70 m is shown in Figure 2-3.

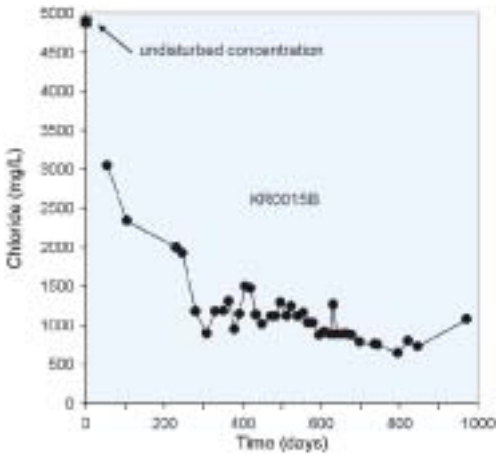

Figure 2-3. *Evolution of measured chloride concentrations at borehole KR0015B showing a strong dilution during the experiment at the tunnel depth (70 m).*

2.3 Hydrogeological conceptual model based on hydrochemical data

Groundwater flow in the Redox Fracture Zone can be assumed to be mainly two-dimensional and contained within the almost vertical plane defined by the fracture zone. According to /Banwart et al, 1995, 1999/ groundwater flows through the fracture zone under natural conditions from the topographically highest points to the discharge areas at the Baltic Sea and some swamp areas.

Systematic sampling of groundwater was done in all the boreholes and tunnel wall during the Redox Zone Experiment. Dilution of the saline native groundwater by fresh recharge water is the dominant process controlling the hydrochemistry evolution during the experiment. /Banwart et al, 1995, 1999/ calculated from chloride data mixing fractions of recharge fresh water and native saline water for samples collected at boreholes located at 70 m depth. These mixing fractions were used to predict ^{18}O values of groundwater samples. In general, a very good agreement was found with measured values. Later, they used their mixing model to predict concentrations of other solutes and assess the role of chemical sink/source terms. Assuming that the chloride content of native saline groundwater remained constant during the experiment, /Banwart et al, 1999/ computed an average dilution of 83% at 70 m depth.

The hydrogeological conceptual model proposed by /Banwart et al, 1999/ for the Redox Zone Experiment can be seen in Figure 2-4. The numerical model of the fracture zone was idealized as 2-D flow in a vertical plane and its domain was extended to the Halö island (Bockholmen). Both the tunnel and the open borehole acted as groundwater sinks, thus creating a convergent flow system /Banwart et al, 1999/. It is assumed that the fracture zone remains saturated during the experiment.

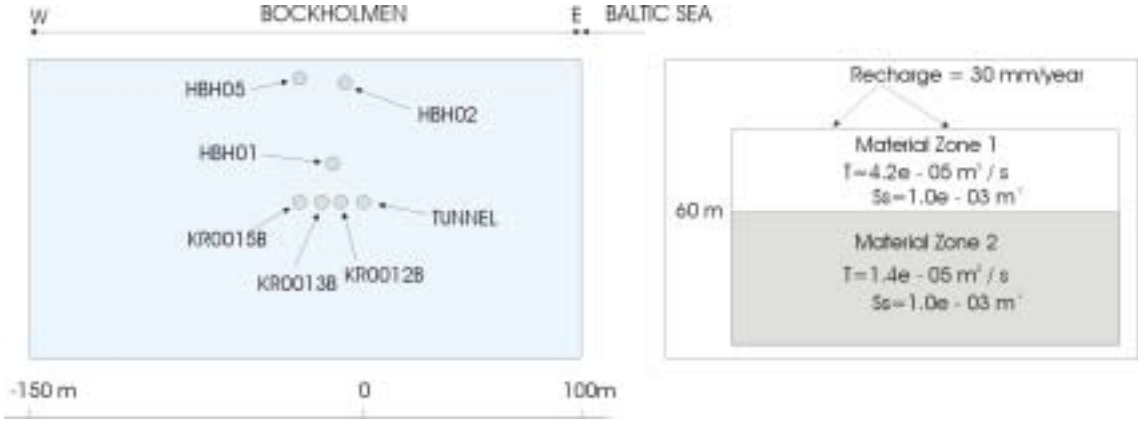

Figure 2-4. *First numerical model of the Redox Zone Experiment: Model domain and location of observation points used for calibration (left); and Material zones and parameters used in the calibration (right).*

2.4 Mathematical formulation and first numerical modeling

2.4.1 Mathematical model

Groundwater flow is governed by the aquifer flow equation:

$$\nabla\cdot\left(\underline{\underline{T}}\nabla h\right)+r=S\frac{\partial h}{\partial t} \qquad (2\text{-}1)$$

where $\underline{\underline{\mathbf{T}}}$ is transmissivity tensor, S is storativity, $\nabla\cdot(\ )$ and $\nabla(\ )$ are the divergence and gradient operators, respectively, r is a sink/source term of water per unit surface, t is time and h is piezometric head.

At the scale of the experiment, changes in water density have a negligible effect on groundwater flow /Hautojärvi et al, 1994/. Therefore, a constant-density groundwater flow model was used.

The model accounts for the following solute transport processes: advection, mechanical dispersion and molecular diffusion. Under these conditions solute transport obeys the well known advection-dispersion equation /Bear, 1972/:

$$\nabla\cdot\left(\phi\underline{\underline{D}}\nabla c\right)-\mathbf{q}\nabla c+r\left(c^{*}-c\right)=\phi\frac{\partial c}{\partial t} \qquad (2\text{-}2)$$

where c is solute concentration, ϕ is porosity, q is specific discharge or Darcy's velocity given by $\mathbf{q}=-\underline{\underline{K}}\nabla h$, c^{*} is the concentration of sink/source water and $\underline{\underline{\mathbf{D}}}$ is the dispersion tensor which includes both mechanical dispersion and molecular diffusion.

Flow and solute transport simulations were carried out with CORE$^{2D©}$ /Samper et al, 2000/, a finite element code for solving groundwater flow, heat transfer and multicomponent reactive solute transport in partially or fully saturated media. CORE$^{2D©}$ can handle heterogeneous and anisotropic media. Both steady-state and transient flow regimes can be simulated. Groundwater flow boundary conditions include prescribed head (Dirichlet), water flux (Neumann) and mixed (Cauchy). Solute transport boundary conditions include: (1) prescribed solute flux, (2) prescribed concentrations, and (3) solute sources associated to fluid sources.

2.4.2 Numerical model

The model domain covers 250 m in length and 140 m in depth (Figure 2-4) and starts (t=0) on March 13th, 1991, when the access tunnel intersected the fracture zone. The fracture plane is assumed to be heterogeneous. Two zones with different hydrodynamic parameters were considered (Figure 2-4). The shallow zone has a transmissivity greater than that of the deep zone. Selected flow parameters were derived from /Gustafsson et al, 1994/ and are shown in Figure 2-4. Dispersivities and porosity were derived from tracer tests performed by /Gustafsson et al, 1994/. A porosity of 0.01, a longitudinal dispersivity of 25 m, and a transverse dispersivity of 5 m were used for both layers. Figure 2-4 shows the location of observation points used for comparing computed values to measured data.

The numerical grid for spatial discretization contains 1,154 nodes and 2,228 triangular finite elements. The mesh was progressively refined near the open borehole (KR0013B) and near the Baltic estuary where the largest gradients of hydraulic heads and solute concentrations are expected to take place. The modeling time horizon was discretized into 900 time steps having durations ranging from 0.4 (at the beginning of the experiment) to 2.7 days (at the final stages of the experiment).

Groundwater flow boundary conditions are shown in Figure 2-5. A constant recharge of 30 mm/year was prescribed along the upper boundary. At both sides and at the bottom of the model domain a Cauchy boundary condition was specified according to which water flux is equal to a leakage coefficient times the difference between an external head and the head on the boundary. Large leakage coefficients were used initially (on the order of 1,000 d^{-1}). The external head was assumed to be equal to 5 m. The tunnel and the open borehole (KR0013B) were considered to be internal boundaries with prescribed flow rates of 0.9 L/min and 7.6 L/min, respectively. A time function was used to simulate the opening of the borehole on day 159 (Figure 2-5). Initial heads were computed from the solution of a steady state problem corresponding to undisturbed conditions without tunnel and open boreholes.

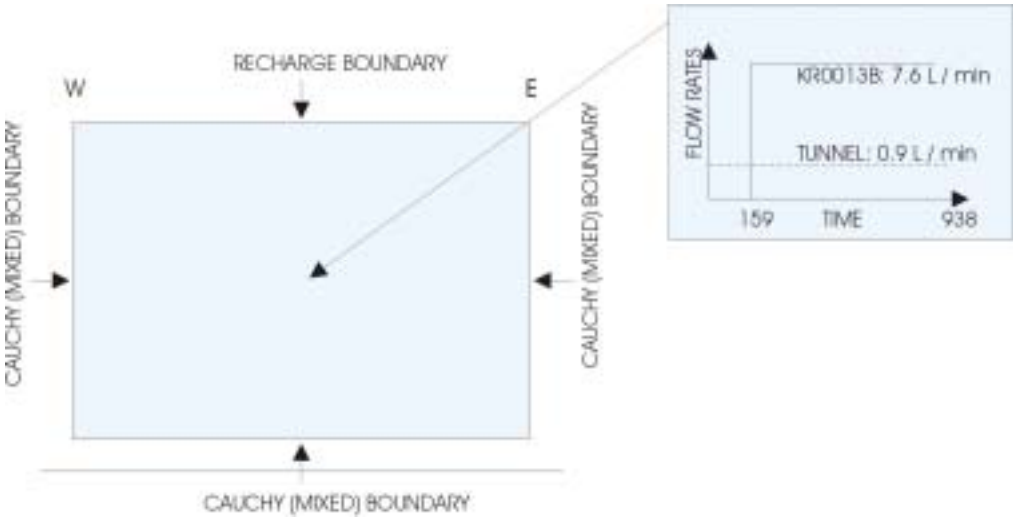

Figure 2-5. *Boundary conditions for groundwater flow (left) and flow rate time functions used in the first numerical model.*

Boundary conditions for solute transport include: prescribed concentration of fresh water recharge along the upper boundary and saline native groundwater concentration on the bottom boundary. Measured Baltic estuary concentration was prescribed at the upper-east corner of the domain. Concentrations at nodes lying along the sides of the domain were assumed constant in time and equal to their initial values. There are few available data for defining these initial concentrations. Available information for the conditions prior to the starting of the experiment include measured values for the Baltic estuary water, samples of very shallow fresh water and a sample of native saline groundwater at a depth of 70 m. It is well known that island aquifers have a fresh groundwater lens with a maximum thickness under recharge zones (usually the highest topographic points). The transition between fresh and saline water in coastal aquifers under natural conditions is generally thin and usually idealized as a sharp interface /Custodio, 1983/. The interface has a nearly parabolic shape, with the thickness of the fresh water lens approaching zero near the coastline. Based on the Dupuit-Forcheimer assumption of horizontal groundwater flow and assuming a sharp interface between fresh and saline water, the depth to the interface in a water table aquifer can be obtained from /Custodio, 1983/:

$$Z^2 = \frac{2q_o x - Wx^2}{K\beta(1+\beta)} \qquad (2\text{-}3)$$

where:

$$\beta = \frac{\gamma_s - \gamma_f}{\gamma_f}$$

Z = depth to the interface

q_o = Darcy velocity of the fresh water in the aquifer

x = distance from the coastline

W = aquifer recharge

K = hydraulic conductivity

γ_s = specific weight of saline water

γ_f = specific weight of fresh water

Based on kriging interpolation of field measurements, /Laaksoharju et al, 1995/ estimated that under natural conditions the interface between fresh and saline water is at a depth between 45 and 70 m at the tunnel vertical, which is consistent with a fresh-saline water interface computed with Equation 2-3 and a recharge value of 120 mm/year. It should be noticed that a recharge value of 120 mm/year along the fracture zone amounts to a recharge of 15 mm/year infiltrated on the catchment associated to the fracture zone depression.

2.4.3 Model calibration

Calibration of the numerical model of the Redox Zone Experiment was performed by comparing numerical results with measured hydraulic heads at borehole HBH01 (see Figures 2-2 and 2-4) and chloride concentrations at boreholes HBH01, HBH02, KR0012B and KR0015B (also shown in Figures 2-2 and 2-4). While it was straightforward to calibrate a groundwater flow model by fitting observed drawdowns at borehole HBH01, the same was not true for a simultaneous calibration of flow and solute transport fitting measured drawdowns and salinities at all available observation points. Calibration of flow parameters allowed fitting measured heads at borehole HBH01, but computed Cl^- concentrations were much greater than measured values at all boreholes. On the other hand, it was possible to reproduce measured concentrations by adjusting the leakage coefficients of the bottom boundary, which control the flux of saline water coming from the bottom boundary. The model fits observed chloride data when these leakage coefficients are decreased significantly, but computes drawdowns at borehole HBH01 which are much greater than measured values /Molinero, 2000/.

According to /Banwart et al, 1995, 1999/, the maximum recharge of fresh water at Halö island into the experiment area ranges from 1.0 to 3.3 L/min. However, the observed dilution at the tunnel and boreholes requires much more fresh water than that amount. /Banwart et al, 1995, 1999/ concluded that there should be another source of fresh water in addition to the recharge over Halö island. They proposed the possibility of "lateral flows" induced by tunnel construction. The results of our first numerical model are consistent with the statements of /Banwart et al, 1995, 1999/ because an additional source of fresh water is required in order to fit simultaneously measured drawdowns and chloride data.

The best fit to measured head data and observed chloride concentrations evolution at KR0012B and KR0015B boreholes is obtained with a Dirichlet condition at the shallow parts of the east and west boundaries associated with fresh water inflow (Figure 2-6). This modification of the boundary conditions allows for more fresh water reaching the tunnel "laterally". Then, the numerical model shows a good agreement with measured hydraulic heads and an acceptable fit to measured chloride concentrations (Figure 2-6). This numerical model, however, lacks soundness because it assumes the occurrence of fresh water just beneath the Baltic sea. This assumption is undoubtly unrealistic and should be revised.

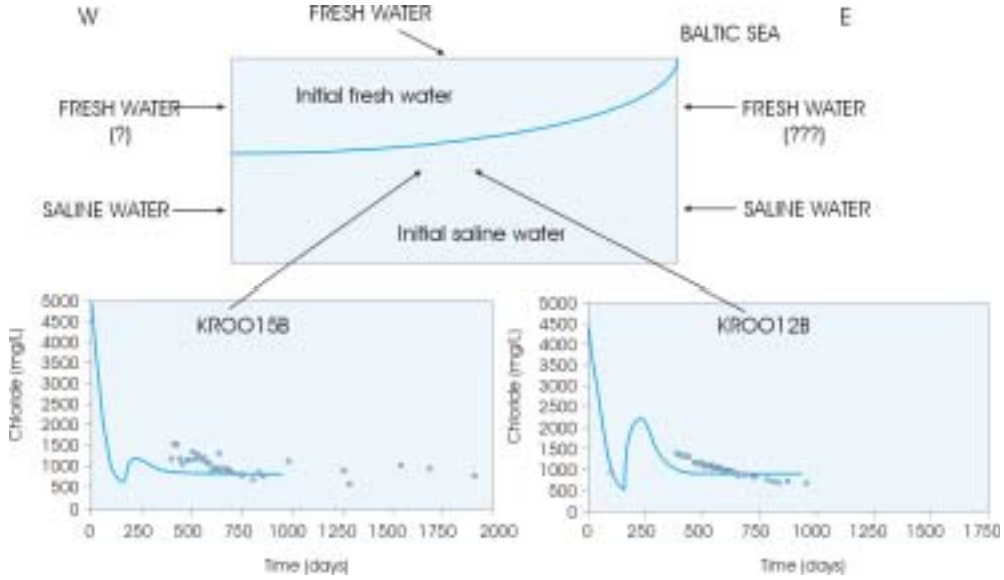

Figure 2-6. *Computed and measured chloride concentrations at a depth of 70 m. This run provides the best results achieved with the first numerical model.*

2.5 Revised hydrogeological conceptual model

In order to overcome the drawbacks of the previous numerical model, the conceptual flow and transport model was fully revised. Contrary to the previous conceptual model which was derived mostly from hydrochemical data, the revised conceptual model was constructed using simultaneously all available hydrodynamic and hydrochemical data. In addition, special care was taken in setting appropriate boundary conditions and locations. As a first step, the topography and geometry of the study area was revised.

Figure 2-7a shows an old map of the Äspö area where Bockholmen appears as a small island not connected to Halö. Recent reports show that Bockholmen and Halö are connected. In fact, the system Halö-Bockholmen forms a peninsula connected to the mainland at Simpevarp. Figure 2-7b shows an aerial picture of the Redox Zone area, and a mapping of the fracture zone outcrop. It can be noticed that Bockholmen island is actually connected with Halö. This connection is made by means of a landfill built during the construction of the Oskarshamn Nuclear Power Plant which is located in the vicinity of the study area. The landfill has two parts, an ancient part covered by grass and little trees, and a new landfill zone (Figure 2-7b). The new landfill is mainly made of blocks of granite and concrete although sand, clay and cement are also present. The landfill is directly in contact with the Redox Zone. In fact, the fracture zone outcrop is covered by the landfill (Figure 2-7b). The fracture zone is not in contact with the Baltic Sea on the west boundary, but under a blocky rock landfill which constitutes the highest topographic point on the west area. The east boundary of Bockholmen is in contact with a narrow and shallow estuary (50–100 m wide and some few m deep). Beyond the estuary there is a big island (Ävrö island).

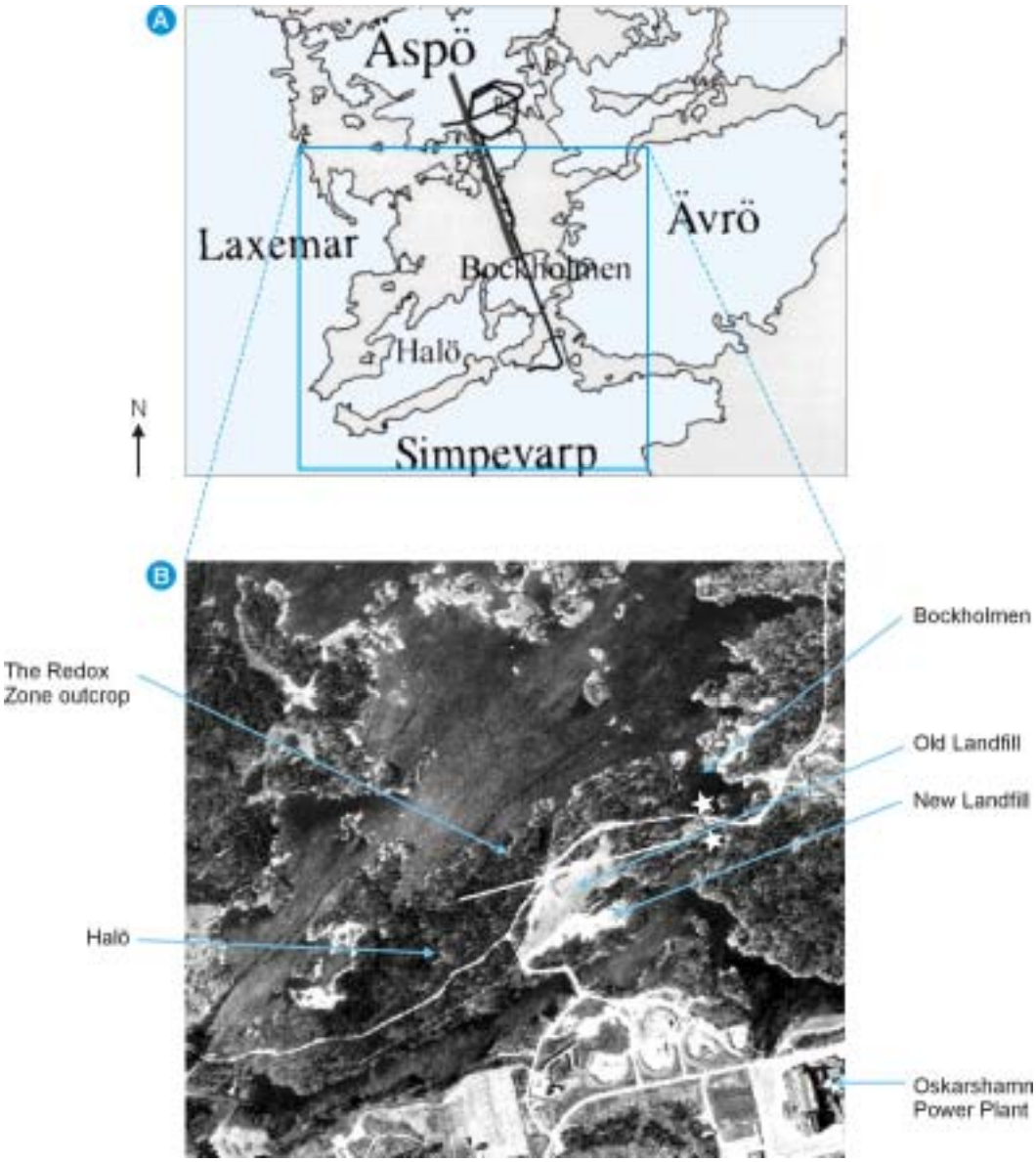

Figure 2-7. *A) Map of the Äspö area showing the location of Äspö, Ävrö and Bockholmen islands. Halö is a peninsula connected to the mainland at Simpevarp. B) Aerial view of the Redox Zone site showing the trace of the fracture zone outcrop. The Oskarsham Power Plant is located at Simpevarp. In front of the Power Plant, Bockholmen appears connected with Halö by means of a big rock landfill. The fracture zone goes under the landfill and it is in contact with the Baltic estuary, which separates Bockholmen and Ävrö island. Star symbols represent the location of water samples used to characterize the chemical composition of the estuary. (Aerial picture with the authorisation from Swedish Lanfméteaverket 1999. From GSD-Ekonomic map 507-99-236).*

Figure 2-8 shows a scheme of the revised conceptual model for the hydrogeology of the Redox Zone for natural conditions. The model domain is extended in order to reach natural groundwater boundaries which in this case coincide with groundwater divides. To the west, the central point of the landfill constitutes the highest topographic point. To the east, beyond the Baltic estuary, the model was extended to the groundwater divide of the Ävrö island. This conceptual model envisages two shallow fresh water lenses, one under Bockholmen and another beneath the Ävrö island. Under natural conditions both shallow hydrogeological systems are independent. Shallow groundwater flows from recharge zones to the Baltic estuary. Saline-fresh water interfaces reach their maximum depths under the recharge zones and tend to zero at the Baltic estuary. Figure 2-9 shows a sketch of the hydrogeological conceptual model when the tunnel intersected the fracture and at the end of the experiment. During the first 148 days the tunnel is the only groundwater sink at 70 m depth, with an average discharge of 0.9 L/min. Some of the flow lines going naturally from Bockholmen to the Baltic estuary are intercepted by the tunnel (Figure 2-9a). Borehole KR0013B was opened after 149 days with a constant discharge of 7.6 L/min. Some time later, the hydraulic disturbance reaches the Baltic area, allowing the bypass of the fresh water from Ävrö towards the tunnel (Figure 2-9b). The propagation of drawdowns towards the east caused the flushing of the saline groundwater wedge located under the Baltic estuary towards the tunnel. Once the saline wedge was flushed, fresh water coming from both sides (Bockholmen and Ävrö) caused the observed dilution at all boreholes. It should be noticed that this revised conceptual model is consistent with having a flux of fresh water beneath the Baltic estuary.

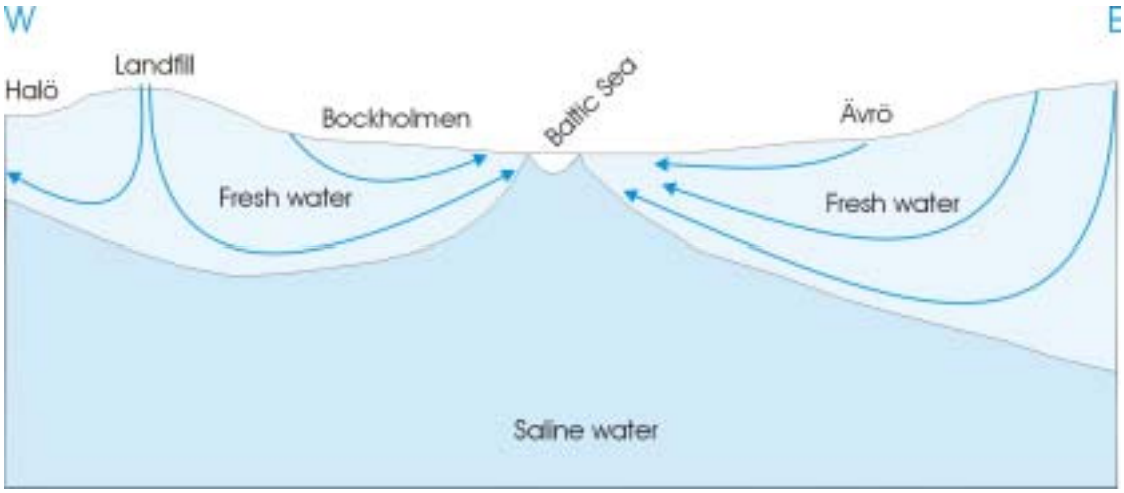

Figure 2-8. *Alternative hydrogeological conceptual model of the Redox Zone under undisturbed natural conditions.*

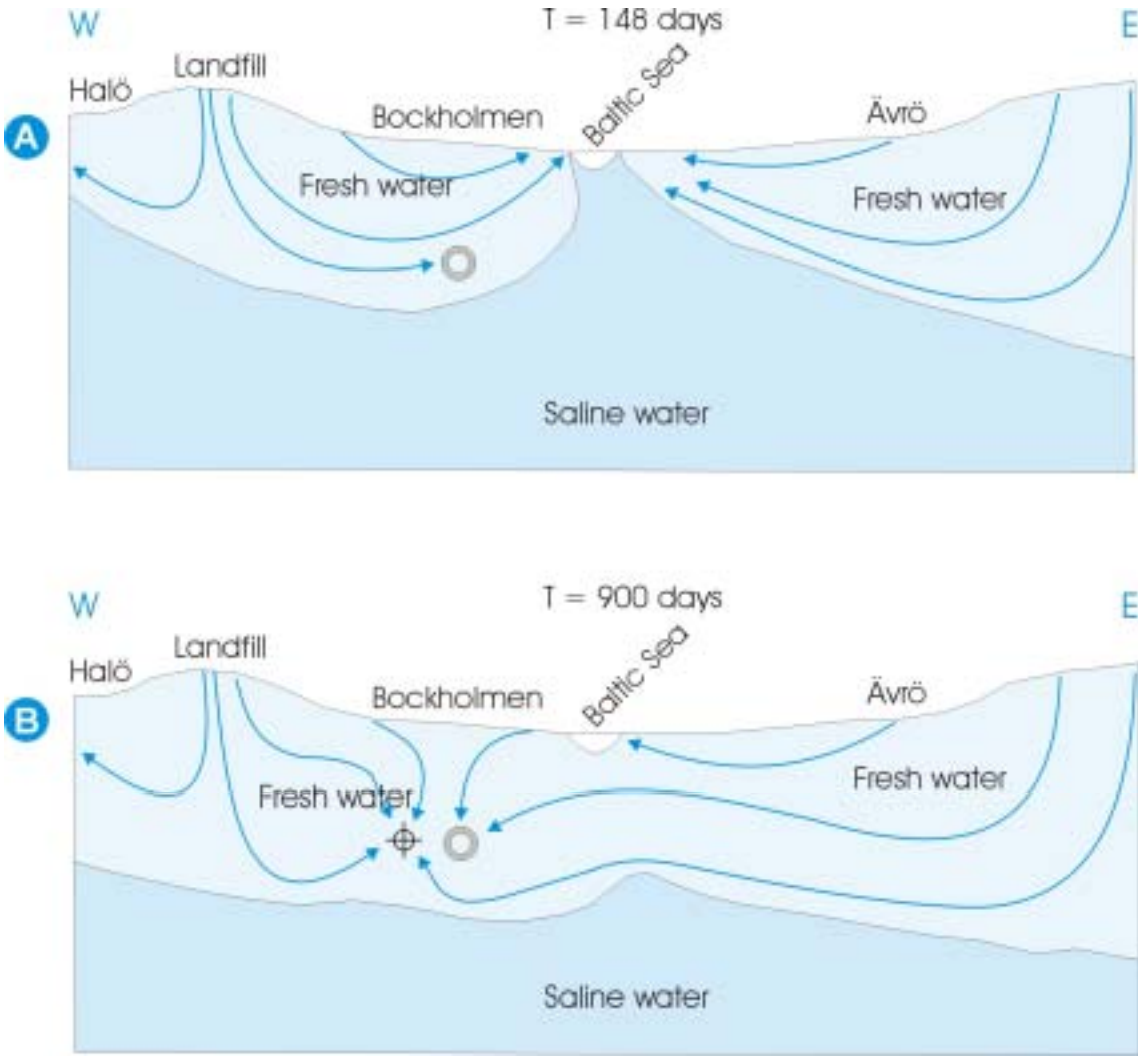

Figure 2-9. *Alternative hydrogeological conceptual model of the Redox Zone under disturbed conditions: A) Just prior to the opening borehole KR0013B; and B) At the end of the experiment.*

2.6 Revised numerical model

2.6.1 Model setting

A second numerical model of the Redox Zone was performed based on the revised conceptual model of Figures 2-8 and 2-9. The domain of this numerical model is extended laterally in order to reach natural groundwater boundaries, thus overcoming unnecessary and unrealistic assumptions about "lateral flows". The model domain was also extended in depth to minimize uncertainties about the bottom boundary.

The trace of the model is shown in the three-dimensional topographic view of the Äspö site (Figure 2-10). It is nearly 1 km long and extends from Ävrö in the east to Bockholmen in the west. The Baltic Estuary lies between Ävrö and Bockholmen (Figure 2-10). Lateral boundaries coincide with groundwater divides.

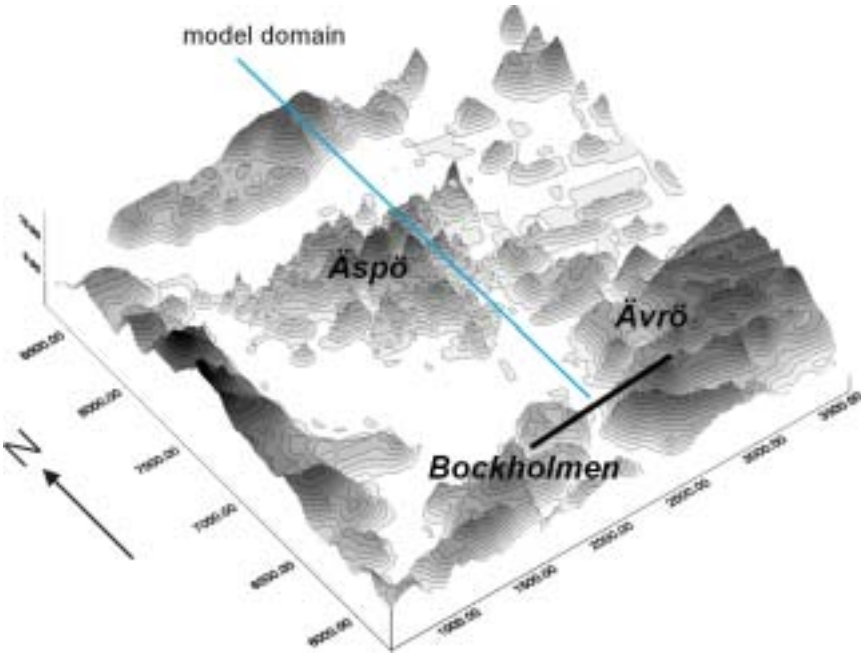

Figure 2-10. *Three-dimensional topographic surface of the Äspö site showing the trace of the extended model domain.*

A revised finite element mesh was needed to cope with the extended model domain. It contains 1,049 nodes and 1,985 triangular elements (Figure 2-11). The mesh was refined near the tunnel and boreholes, as well as in the surroundings of the Baltic Estuary where large head and concentration gradients are expected. The size of the elements increases gradually towards the east and bottom boundaries where less accuracy is required.

A zonation scheme was used in order to account for the vertical heterogeneity of the Redox Zone (Figure 2-11). The model domain is divided into several material zones each of them containing a set of elements which share the same hydrodynamic and transport parameters. Material zones include: zone #1 which extends from the surface to a depth of 50 m, zone #2 which covers from 50 to 150 m depth and, the lowermost zone #3 which extends from 150 m to the bottom of the flow domain (Figure 2-11). Zones #4 and #5 correspond to seafloor Baltic sediments and the landfill, respectively (Figure 2-11).

Left and right boundaries coincide with groundwater divides and are assumed impermeable. A recharge of 30 mm/year is prescribed on the upper boundary, except along the Baltic Sea area where hydraulic head is prescribed to a value of 0 m. Head at the bottom boundary was prescribed to a value large enough to prevent fresh water from reaching the bottom boundary, i.e. no flow path originating at the water table reaches the bottom boundary at a depth of 300 m. This is consistent with chemical data collected at the Äspö site prior to tunnel construction which indicate a Cl^- content of 8,000 mg/L at a depth of 300 m /Laaksoharju and Wallin, 1997/. Similar to the preliminary numerical model, flow rates at the tunnel and borehole KR0013B were prescribed to their measured values.

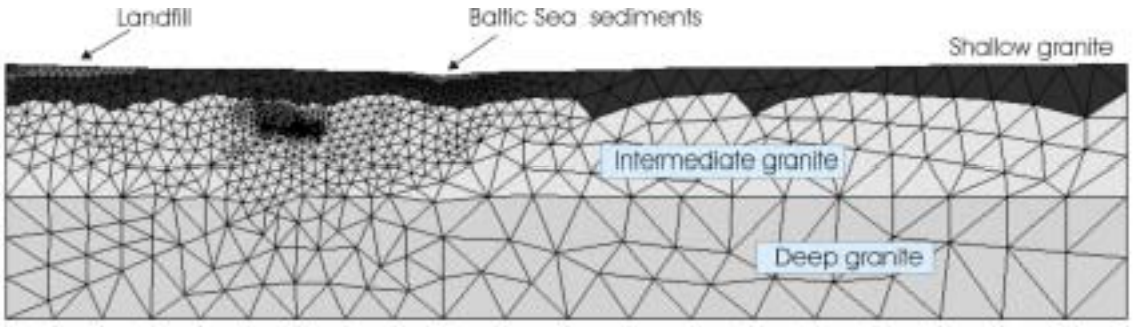

Figure 2-11. *Finite element mesh used for the revised numerical model of the Redox Zone. The mesh is refined near the tunnel, boreholes and Baltic estuary. Zonation accou5nts for spatial heterogeneity. 5 material zones are considered, three for the granite, one for the rock landfill and one other for Baltic seafloor sediments.*

Boundary conditions for solute transport include saline native groundwater concentrations at the bottom boundary and fresh recharge groundwater concentrations at the upper boundary, except on the sea, where the Baltic water composition is prescribed. The largest uncertainty for solute transport boundary conditions occurs at the bottom boundary. Although chemical data under natural conditions were available only at a depth of 70 m, there were chemical data available from other fracture zones intersected by the Äspö tunnel at deeper locations. Concentrations of most chemical species decrease with depth except for Mg^{2+} and SiO_2 /Molinero, 2000/. These data were used to estimate the chemical composition of groundwater at a depth of 300 m /Molinero, 2000/. Chemical data of saline, recharge and Baltic waters used in the numerical model are listed in Table 2-2.

Table 2-2. Chemical composition of boundary waters used in the revised numerical model of the Redox Zone Experiment.

Chemical component	Recharge fresh water (mol/L)	Baltic estuary water (mol/L)	Bottom saline water (mol/L)
Cl^-	1.69×10^{-4}	1.00×10^{-1}	2.25×10^{-1}
Ca^{2+}	9.58×10^{-4}	2.43×10^{-3}	4.96×10^{-2}
Mg^{2+}	1.64×10^{-4}	5.43×10^{-3}	8.10×10^{-3}
Na^+	6.69×10^{-4}	8.52×10^{-2}	1.09×10^{-1}
Sr^{2+}	2.51×10^{-6}	2.45×10^{-4}	2.45×10^{-4}
Li^+	1.44×10^{-6}	4.61×10^{-5}	8.00×10^{-5}
Fe^{2+}	1.00×10^{-5}	1.13×10^{-5}	1.13×10^{-5}
K^+	6.65×10^{-5}	2.33×10^{-4}	4.50×10^{-4}
SiO_2	9.98×10^{-5}	9.32×10^{-5}	9.32×10^{-5}
HCO_3^-	2.24×10^{-3}	1.47×10^{-3}	1.05×10^{-3}
SO_4^{2-}	2.50×10^{-4}	3.38×10^{-3}	4.95×10^{-3}

Under natural conditions hydraulic heads are assumed at steady state and were obtained from the solution of the steady-state flow equation (Figure 2-12a). It can be noticed that there is no flow of fresh water crossing the bottom boundary. The contour plot of hydraulic heads indicates that there are flow lines initiating at the bottom boundary which discharge at the Baltic Sea. These flow lines are consistent with the occurrence of regional flows from Laxemar and Ävrö, as described by the regional Äspö flow model of /Svensson, 1997/. The computed water table is everywhere below the ground surface. At the tunnel vertical, the computed elevation of the water table is 1.05 m which is consistent with the values reported by /Banwart et al, 1999/.

The uncertainty of initial conditions for groundwater chemistry is greater than that of initial heads. Available information prior to the construction of the tunnel indicates the occurrence of a fresh-saline water interface at a depth between 45 and 70 m. The salinity distribution under natural conditions should be consistent with the steady state flow regime prevailing during the last thousands of years. According to /Laaksoharju and Wallin, 1997/, the geographical distribution of the Äspö area has been stable for the last 2,000 years. Prior to that time, the Äspö area was covered by the Litorina Sea (an ancient stage of the actual Baltic Sea) during a period of around 6,000 years during which saline water infiltrated through fracture zones. Therefore, the present time salinity distribution at emerged islands should be the result of a continuous flushing and replacement of saline water by shallow fresh groundwater flowing from the recharge zones to the Baltic Sea during the last 2,000 years. Long-term runs of the flow and transport numerical model were performed under natural conditions in order to check the consistency of this hypothesis. In these runs, it was assumed that the whole domain contained initially saline groundwater. The numerical model was run until steady-state concentrations were attained. This happened after 4,000 days. Figure 2-12b shows a contour plot of computed steady-state chloride concentrations which agrees qualitatively with the expected distribution based on the revised conceptual model of Figure 2-9. The revised numerical model covers a time horizon of 4983 days. The first 4,000 days are used to reach steady-state natural conditions and the rest corresponds to the transient stage of the Redox Zone Experiment itself. In this manner, initial conditions of the Redox Zone Experiment are self-generated by the numerical model in each run.

Initial estimates of flow and transport model parameters were derived from /Gustafsson et al, 1994/ and are listed in Table 2-3.

The transport model was solved for the following chemical species: Cl^-, Ca^{2+}, Mg^{2+}, Na^+, Sr^{2+}, Li^+, Fe^{2+}, SiO_2, K^+, HCO_3^- and SO_4^{2-}. In this stage, all of them were assumed to be conservative, i.e. no chemical interactions were considered. As pointed out by /Molinero, 2000/ and /Molinero et al, 2003/ some of them are subject to chemical reactions such as cation exchange and mineral dissolution-precipitation. Multi-component reactive transport models of the Redox Zone Experiment are presented by /Molinero, 2000/ and /Molinero et al, 2003/.

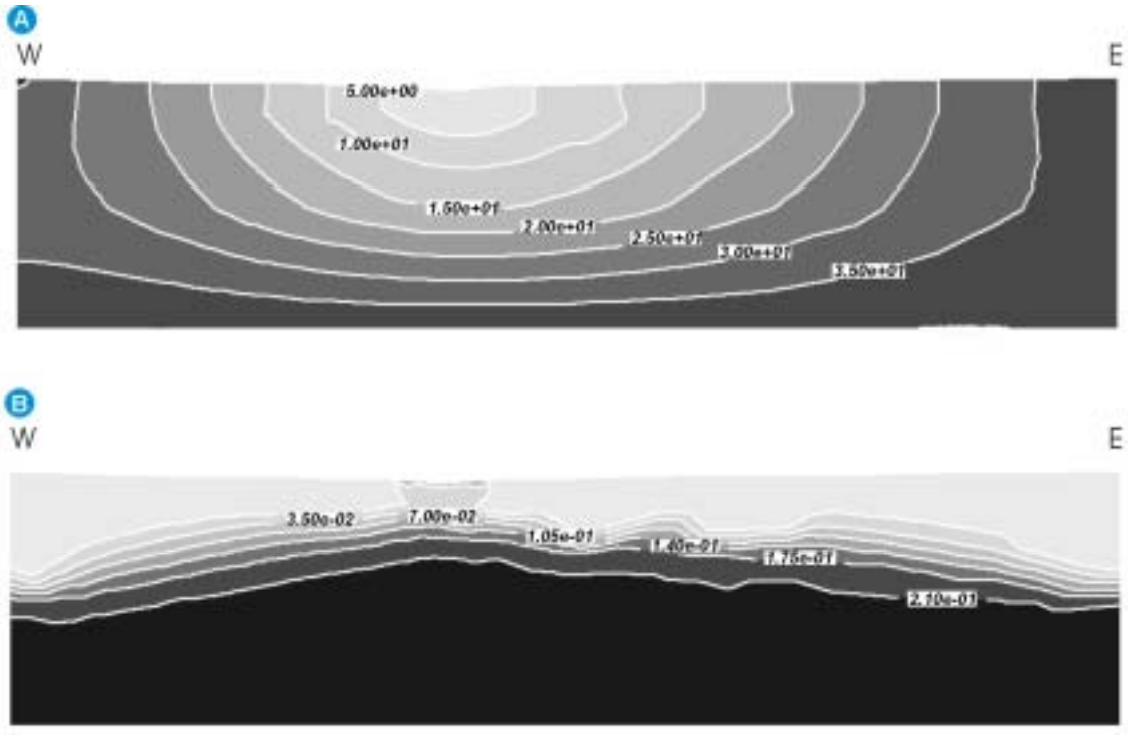

Figure 2-12. *Computed steady-state natural conditions of A) hydraulic heads (results are in dm) and B) chloride concentrations (mol/L).*

Table 2-3. Flow and solute transport parameters of the revised numerical model. Only transmissivities were calibrated. Other parameters remained unchanged during calibration.

Material Zone	Transmissivities (m^2/day)		Storativities	Porosity	Longi-tudinal dispers-ivity (m)	Trans-verse dispers-ivities (m)
	Calibrated		Not calibrated			
	Initial guess	Final	Initial guess	Initial guess	Initial guess	Initial guess
Shallow granite (depth: 0–40 m)	15	100	4×10^{-3}	0.01	30	15
Intermediate granite (depth: 40–80 m)	0.24	0.1	4×10^{-3}	0.01	30	15
Deep granite (depth: 80–300 m)	0.024	0.05	4×10^{-3}	0.01	30	15
Baltic seafloor sediments	10^{-4}	10^{-4}	4×10^{-3}	0.1	30	15
Rock landfill	2	100	4×10^{-3}	0.01	30	15

2.6.2 Model calibration and results

Parameters and boundary conditions for the revised numerical model were assigned by using available prior information as discussed above. For some parameters this information is limited and therefore uncertain. To overcome the uncertainties of prior information, the values of some parameters and boundary conditions were adjusted during model calibration. Transmissivities of the three granite layers and solute concentrations at the bottom boundary were calibrated by a trial-and-error procedure. Optimum values were derived by fitting computed heads and concentrations to measured values of: 1) solute concentrations under natural conditions at the tunnel location, 2) transient drawdowns at borehole HBH01, 3) breakthrough curves of Br^{-}, Mg^{2+}, Cl^{-}, Li^{+} and Sr^{2+} at boreholes KR0015B and KR0012B, and 4) chloride breakthrough curves at shallower depths (boreholes HBH01 and HBH02). Initial and calibrated parameter values are listed in Table 2-3. Figure 2-13 shows a comparison of measured and computed concentrations for undisturbed conditions at the tunnel location. This figure includes the most relevant chemical species considered in the numerical model. In general, model performance is adequate for all chemical species except for sulphate, bicarbonate and iron which, as pointed out by others /Banwart, 1997, 1999; Molinero, 2000/, are strongly affected by chemical and microbial processes.

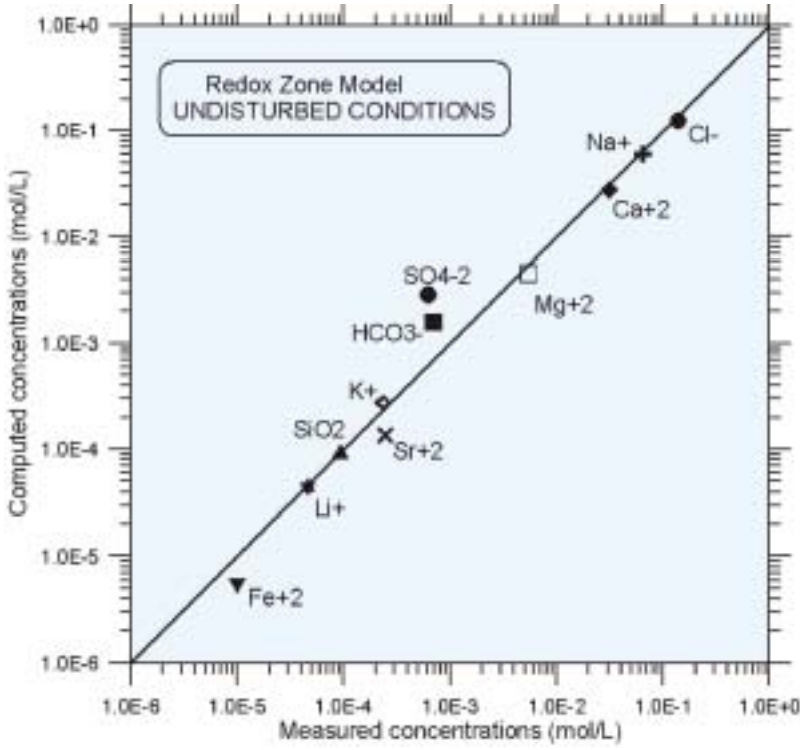

Figure 2-13. *Computed versus measured concentrations at the tunnel for natural conditions.*

Computed heads and concentrations for undisturbed conditions (Figure 2-12) were used as initial conditions for the transient-state numerical model of the Redox Zone Experiment.

Model calibration required increasing the transmissivity of the upper and bottommost layers, while that of the intermediate layer was reduced from 0.24 to 0.1 m^2/d. Calibrated transmissivities decrease with depth. This is consistent with the decrease of the fracture zone thickness with depth and with the general trend observed in the Äspö area of decreasing permeabilities with depth.

Figure 2-14 shows contour plots of hydraulic heads at : a) t = 145 days, when only the tunnel is discharging groundwater, b) t = 163 days, when borehole KR0013B is open and c) t = 906 days, at the end of the experiment. These plots clearly illustrate the propagation of the hydraulic perturbation induced by the tunnel and open borehole. Such perturbation extends beyond the Baltic Estuary. Computed hydraulic heads match the measured heads at borehole HBH01 located at a depth of 45 m (Figure 2-15). This borehole is the only available observation point with recorded groundwater heads evolution during the Redox Zone Experiment.

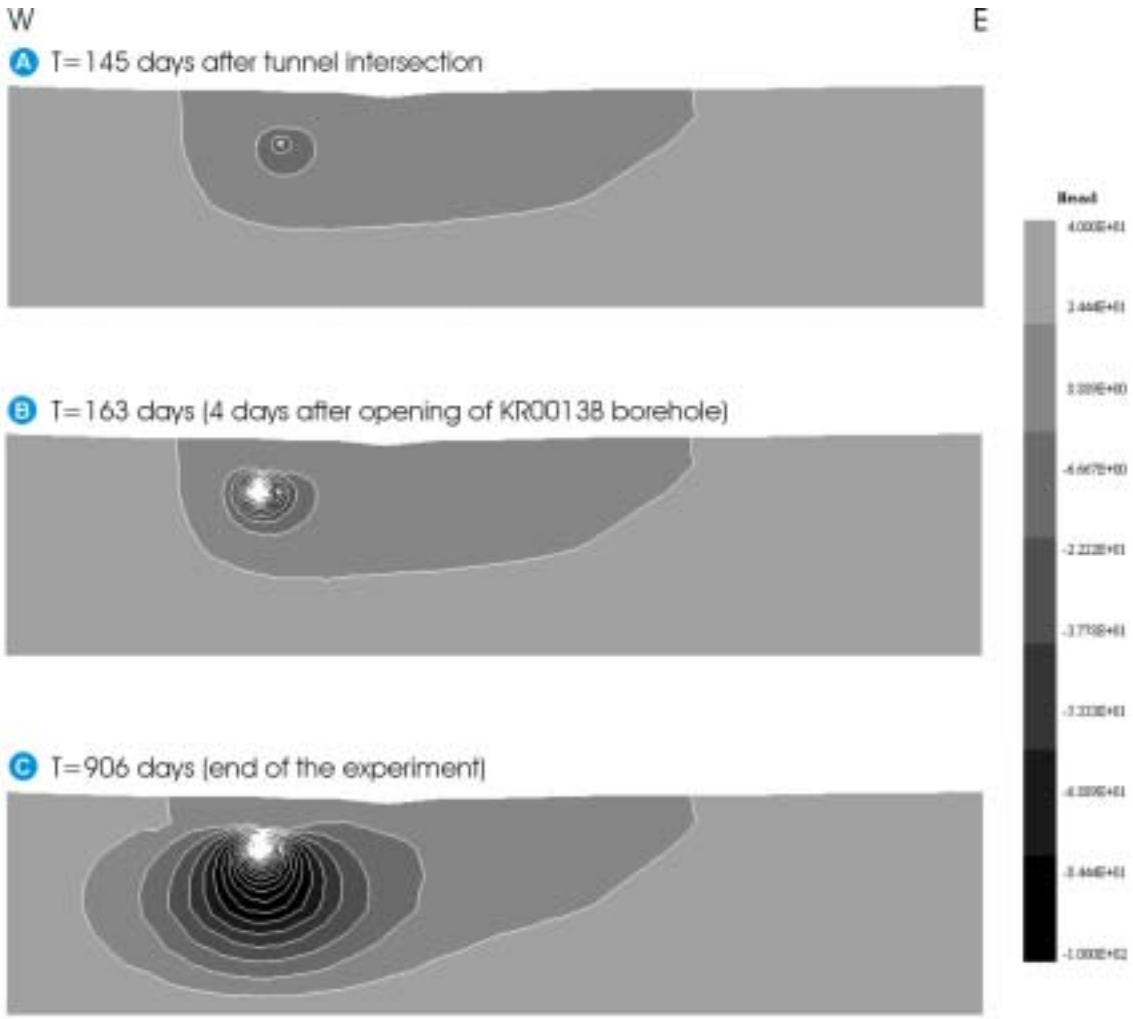

Figure 2-14. *Contour plots of computed hydraulic heads (dm) at: A)145 days after tunnel intersection; B) 163 days (just after opening of borehole KR0013B); and C) 906 days (at the end of the experiment).*

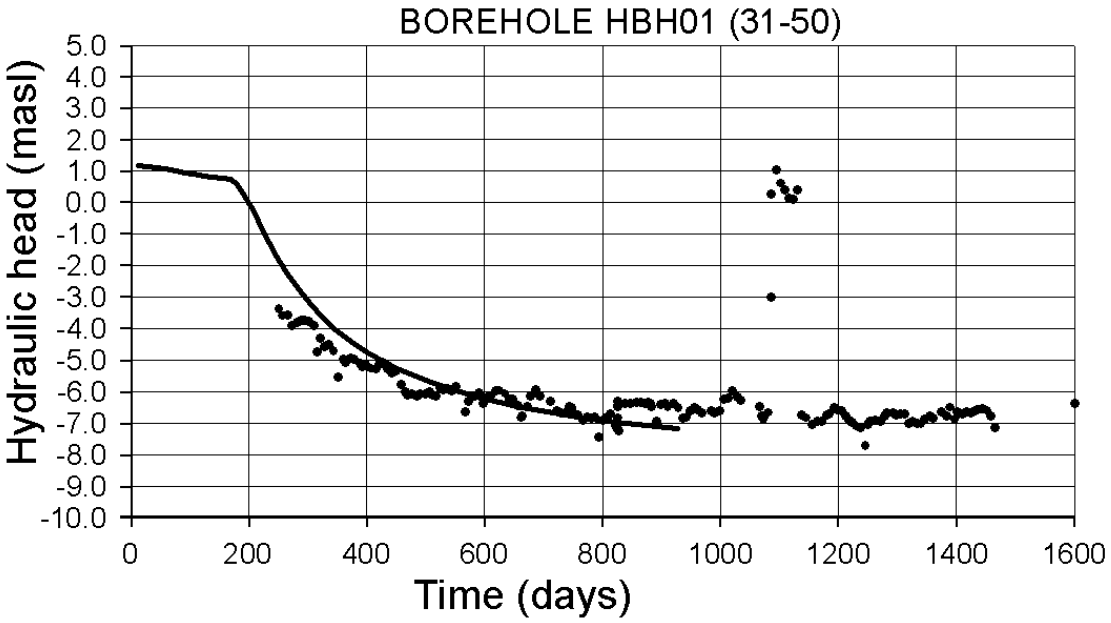

Figure 2-15. *Computed (line) and measured (symbols) hydraulic heads (m) at borehole HBH01 (45 m depth).*

Contour plots of computed chloride concentrations at t=0, 254 and 906 days are shown in Figure 2-16. It can be seen that the main effect of tunnel construction and borehole opening is an important increase in the flux of shallow fresh water coming from both Laxemar (west) and Ävrö (east). Such flux causes a noticeable dilution and a decrease of chloride concentrations in the vicinity of the tunnel.

Figure 2-17 shows a comparison of measured and computed chloride concentrations at several depths. At a depth of 15 m (borehole HBH02, Figure 2-17a) no change in chloride concentrations were detected during the experiment. Fresh recharge groundwater dominates at this location during al the experiment. At a depth of 45 m (borehole HBH01), on the contrary, a relevant increase of chloride concentrations is computed after 250 days (Figure 2-17b). Data were not available at borehole HBH01 under natural conditions. Still, computed concentrations match the measurements after 400 days. The computed increase in chloride concentration at borehole HBH01 is due to the arrival of saline water coming from the saline wedge under the Baltic estuary which is flushed by fresh water coming from Ävrö. Figures 2-17c and 2-17d show measured and computed values of chloride concentrations at a depth of 70 m (near the tunnel). It can be seen that the model matches the measured concentrations under undisturbed conditions. It also reproduces the dilution curves measured at both boreholes. Model results match perfectly the dilution curve of borehole KR0015B (Figure 2-17d). However, some discrepancies are detected for the first 300 days at borehole KR0012B (Figure 2-17c). Boreholes KR0015B and KR0012B are located 10 m apart from the open borehole (KR0013B), so there is a distance of 20 m between both observation points (see Figures 2-2 and 2-4).

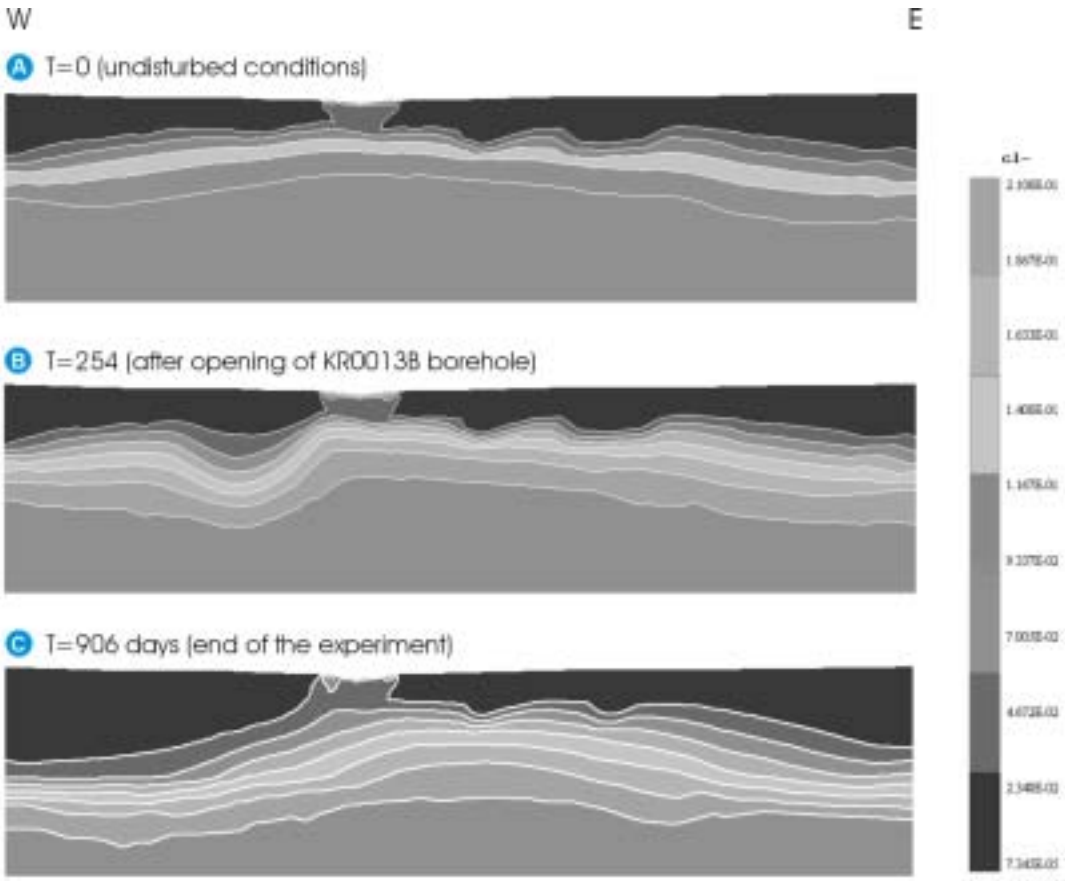

Figure 2-16. *Contour plots of computed chloride concentrations (mol/L) at: A) undisturbed conditions; B) 254 days after tunnel intersection; and C) 906 days (at the end of the experiment).*

Measured data show a higher initial dilution at borehole KR0012B than at KR0015B, while the numerical model provides almost the same results at both boreholes. It should be noticed that a dispersivity of 30 m was adopted, based on field tracer tests. This dispersivity is larger than the separation between the boreholes. Therefore, a large mixing is expected which is confirmed by the fact that concentrations at both boreholes become similar after 300 days. The large initial dilution recorded at borehole KR0012B but not at borehole KR0015B could be caused by local heterogeneities which are not considered in the numerical model. In addition to changes in fracture zone thickness, reported transmissivities at the Äspö site show variations up to 2 orders of magnitude in a single fracture zone /Rhén et al, 1997/. This local heterogeneity is present in the Redox fracture Zone and is consistent with the differences in flow rates measured at the tunnel (0.9 L/min) and the open borehole KR0013B (7.6 L/min) which are only 20 m apart from each other. The numerical model covers a kilometric domain and accounts for large-scale heterogeneities associated to changes in thickness. However, it does not account for small-scale heterogeneities. A proper characterization of the latter would have required additional permeability data which in this case were not available. Therefore, our numerical model is expected to capture long-term trends taking place at a large scale while its ability to reproduce small-scale and short-term fluctuations is limited.

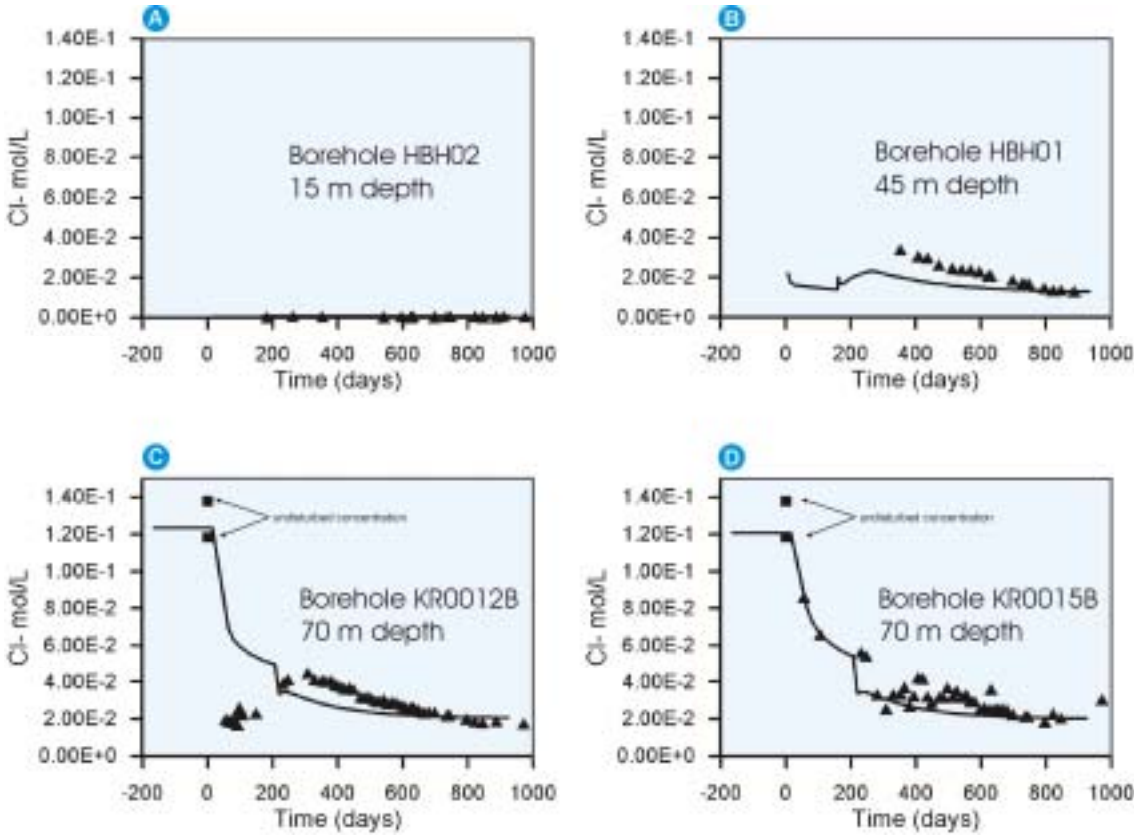

Figure 2-17. *Measured (symbols) and computed (lines) chloride concentrations at control points: A) HBH02 (15 m depth); B) HBH01 (45 m depth); C) KR0012B (70 m depth); and D) KR0015B (70 m depth). T=0 when tunnel intersected the fracture zone.*

A comprehensive sensitivity analysis was performed. No other possible combinations of parameters were found that could produce the same initial chloride concentrations at the tunnel depth (Figure 2-13), the evolution of measured groundwater heads (Figure 2-15), and the evolution of chloride concentrations at control points (Figure 2-17).

The numerical model reproduces also the measured evolution of the concentration of other quasi-conservative species (Figure 2-18a, b and c). This figure shows also the concentrations measured at undisturbed conditions. It can be seen the consistency between field measurements and computed initial conditions for the Redox Zone Experiment.

Similar to what was observed for undisturbed conditions (Figure 2-13), the largest discrepancies between computed and measured concentrations occur for dissolved sulphate, bicarbonate, iron and sodium (Figure 2-18d). Modeling the evolution of these reactive species requires accounting for the chemical processes affecting them which are not considered in the present model. Several hypotheses have been proposed to explain hydrochemical facies and processes occurring at the Äspö site /Banwart et al, 1995, 1996, 1999; Laaksoharju et al, 1999; Banwart, 1999/. These hypotheses have been tested quantitatively by means of coupled groundwater flow and reactive transport models /Molinero, 2000; Molinero et al, 2000; Molinero et al, 2003/. It should be mentioned that these reactive transport models are based on the numerical models of flow and solute transport presented in this paper.

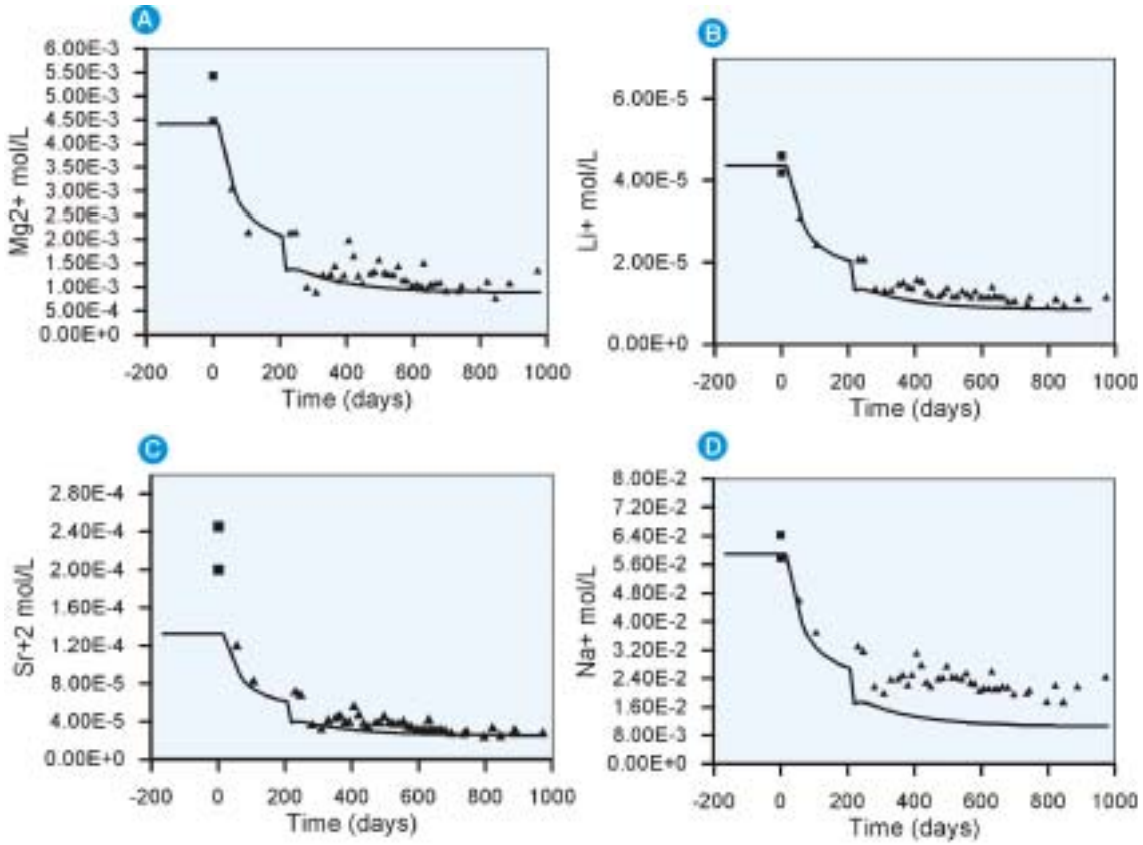

Figure 2-18. *Measured (symbols) and computed (lines) concentrations of: A) Magnesium; B) Lithium; C) Strontium; and D) Sodium at borehole KR0015B (70 m depth).*

2.7 Chapter conclusions

Finite element numerical models of groundwater flow and solute transport of the Redox Zone Experiment have been presented which have proved to be useful for evaluating the effects of the construction of the access tunnel on the hydrogeological and hydrochemical conditions of this fracture zone. The first model was constructed on the basis of the conceptual model used by /Banwart et al, 1994, 1999/ to interpret hydrochemical data. This numerical model exhibits clear inconsistencies and fails to reproduce simultaneously the observed drawdowns and the decrease in salinity at the tunnel location. The limitations of this model are overcome by revising Banwart's hydrogeological conceptual model. An improved conceptual and numerical flow and transport model has been presented which relies directly on available hydrogeological and transport parameters, is based on the identification of appropriate flow and transport boundary conditions and uses, when needed, solute data extrapolated from nearby fracture zones. This revised model is consistent with head and concentration data collected prior to tunnel construction and its results match both observed drawdowns and the chemical dilution induced by the construction of the tunnel.

A major outcome of this study is that quantitative analyses of hydrochemical data should rely on sound conceptual flow and transport models in order to ensure consistency of hydrochemical and hydrogeological data /NEA, 1999/. Numerical modeling of water flow and solute transport provides an appropriate framework for

checking the consistency of hydrodynamic and hydrochemical data. This framework can be subsequently used for quantitative analyses of complex chemically-reactive species by means of reactive transport models /Molinero, 2000; Molinero et al, 2003/ which may even incorporate the role of biological processes /Zhang 2001; Samper et al, 2003/.

As a broader conclusion regarding mixing freshwater induced by the tunnel construction, our results confirm that this is a relevant process for a potential repository at least for the conditions prevailing in the Scandinavian region. Chemical data from deeper portions of Äspö tunnel indicate that freshwater mixing takes place whenever the tunnel intersects a major fracture zone /Molinero, 2000/. Most of the measured inflows to the tunnel take place along fracture zones. This is also confirmed by numerical models /Molinero et al, 2002/. Therefore, the relevance of fresh water mixing at a potential repository will be determined by the intersection of the repository with one of such fracture zones.

3 Numerical model of reactive solute transport

3.1 Hydrochemical and mineralogical background

In order to study the hydrochemical evolution of the groundwater system, systematic sampling of water was done at the boreholes and tunnel wall during the Redox Zone Experiment. The main results of the Redox Zone Experiment are reported in /Banwart et al, 1995/ and an excellent summary of the experiment can be found in /Banwart et al, 1999/.

Three weeks after the start of the experiment a sharp dilution front arrived to the access tunnel. This appeared as a dramatic decrease in Cl^- and cation concentrations, and an increase in HCO_3^- concentration in the groundwater flowing from the roof of the tunnel. A short time later, dissolved Fe concentrations in the tunnel inflows decreased to near zero for a period of a few weeks. This could be taken as an indication of the arrival of an oxidation front to the tunnel position /Banwart et al, 1999/.

Figure 3-1 shows the time evolution of dissolved Cl^- and Fe(tot) concentrations measured in the tunnel. After the initial dilution, the fracture zone at 70 m depth became increasingly saline. In day 159 the discharge borehole was opened for continuous discharge. Some time later, another dilution stage, less pronounced than the first one, is observed at some boreholes (very clearly at KR0013B and KR0012B). Figure 3-2 shows the Cl^- concentrations measured at boreholes KR0012B and KR0015B. One can see in this figure the measured dilution at a depth of 70 m. According to /Banwart et al, 1999/, after 50 days both the significant dissolved Fe concentrations at all sample locations and the stable and continuously measured redox potentials (within the range $-150 < Eh < -100$) indicate that anoxic conditions prevail in the fracture zone. pH remained constant near a value of 8 through out the experiment /Banwart et al, 1999/.

HCO_3^- and SO_4^{2-} concentrations increase significantly during the experiment at the sampling points located at 70 m depth (Figure 3-3). During the last part of the experiment the concentration of most solutes remains relatively constant (Figures 3-2 and 3-3). /Banwart et al, 1999/ understand the stabilization of concentrations as an indication of steady conditions for transport and chemical processes in the area of the experiment.

The overall results and interpretation of the Redox Zone Project were reported by /Banwart et al, 1995/. This report includes the methodology and the results of the mineralogical, isotopic, microbiological and hydrochemical studies.

Dilution of the saline native groundwater by fresh recharge water is the dominant process controlling the hydrochemistry evolution during the experiment /Banwart et al, 1995/. From chloride data, /Banwart et al, 1995, 1999/ calculated mixing fractions of recharge fresh water and native saline water for water samples collected at the three boreholes located at 70 m depth. These mixing factors were used to predict ^{18}O values of groundwater samples. In general, a very good agreement was found with measured values. Later, they used the mixing model to predict the concentration of other solutes, in order to assess the role of chemical reactions.

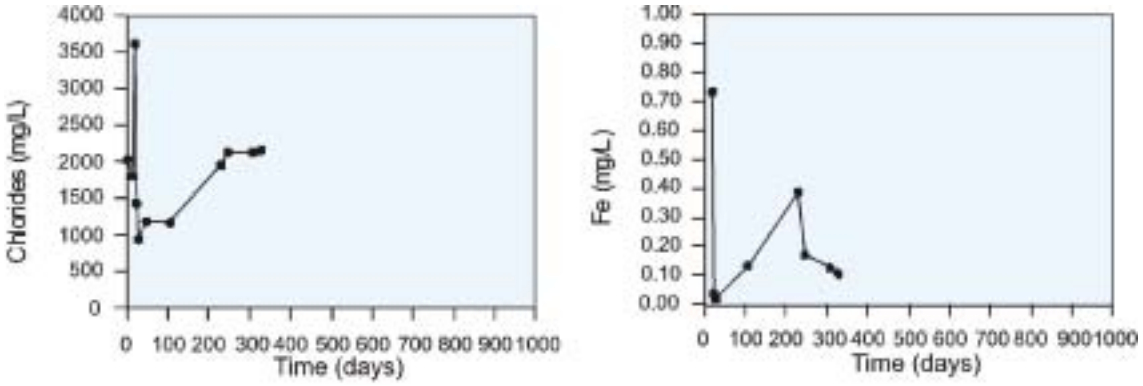

Figure 3-1. *Chloride and dissolved Fe concentration evolution measured at the tunnel wall. There are not available chemical data for the tunnel after 400 days.*

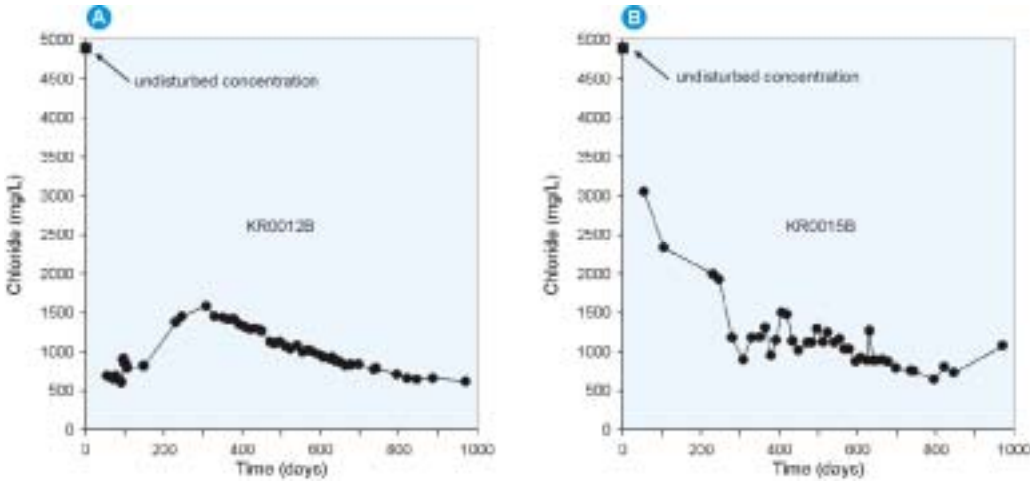

Figure 3-2. *Chloride concentration evolution measured at A) KR0012B borehole and, B) KR0015B borehole. A strong dilution is recorded during the experiment at tunnel depth (70 m).*

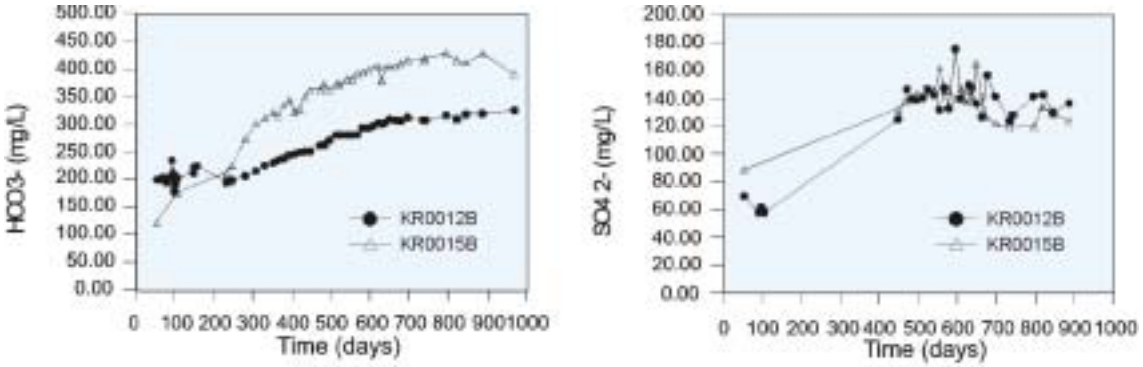

Figure 3-3. *Bicarbonate and sulphate concentration evolution measured at KR0012B and KR0015B boreholes. These boreholes are located at both sides of the open borehole KR0013B.*

Chloride dilution was greater in boreholes KR0012B and KR0015B, located 10 m on each side of the discharge borehole (KR0013B). Assuming constant chlorinity for the native saline groundwater during the experiment, /Banwart et al, 1999/ computed an average dilution on each borehole of 83%.

When the mixing modeling was extended to the rest of solutes, significant sources for HCO_3^-, SO_4^{2-} and Na^+ were found. On the other hand, a less relevant sink for Ca^{2+} was identified.

/Viani and Bruton, 1997/ demonstrate that the behaviour of Na^+ and Ca^{2+} is consistent with cation exchange, with preferential exchange of dissolved Ca^{2+} and displacement of exchanged Na^+ during the dilution of saline groundwater.

Isotopic /Banwart et al, 1995, 1996/ and microbiological /Pedersen et al, 1995/ studies conclusively ruled out SO_4^{2-} reduction during the experiment, and provide significant evidence supporting Fe(III) reduction as respiration pathway for oxidation of organic C in the fracture zone. Results reported by /Tullborg and Gustaffson, 1999/ illustrate the large increase in ^{14}C activity measured in both dissolved organic and inorganic C during the experiment, providing evidence for a source of young organic C oxidizing into the groundwater. Significant amounts of dissolved CH_4 were also found in the fracture zone /Banwart et al, 1996/.

/Bruton and Viani, 1997/ propose that anion exchange due to adsorption competition between HCO_3^- and SO_4^{2-} may occur, with HCO_3^- dominating the surfaces almost completely at the near neutral pH. However, they also conclude that the total adsorption capacity expected for the fracture zone, is likely to be too small for anion exchange to have a significant impact on dissolved SO_4^{2-}. /Banwart, 1997/ carried out calculations of the adsorption equilibrium and concluded that if anion exchange occurs, the adsorption capacity would have to be on the order of 0.2 mol/L to explain the increase of SO_4^{2-} concentrations observed during the experiment.

There is no conclusive explanation for the increase in dissolved SO_4^{2-} /Banwart et al, 1999/. Sulphur isotope data /Wallin, 1995/ show that SO_4^{2-} originating from either sea water, deeper groundwater or atmospheric deposition would not be consistent with the isotopic signature of dissolved SO_4^{2-} at sampled boreholes. /Banwart et al, 1999/ state that the hypothesis of anion exchange is an attractive explanation, mainly because any change in the isotopic composition would be reflected identically for ions in solution or those adsorbed.

/Pitkänen et al, 1999/ suggest that an unknown source of groundwater with high SO_4^{2-} concentration is entering the fracture zone during the experiment, which may explain the observed increase in SO_4^{2-} concentration. On the other hand, /Banwart et al, 1999/ argue that this groundwater source would then have $[Mg^{2+}]/[Cl^-]$ and $[K^+]/[Cl^-]$ ratios that must be the same as the native saline groundwater, in order to be consistent with the behaviour of these ions during the experiment.

In spite of the fact that isotopic studies ruled out the dissolution of calcite as being the main process responsible for the increase in HCO_3^- concentrations /Wallin et al, 1995/, thermodynamic calculations show that shallow groundwater (0–15 m) is unsaturated with respect to calcite /Banwart et al, 1999/. Then, dissolution of this mineral could be expected to take place during the experiment. Figure 3-4 shows the scheme of the hydrochemical conceptual model for the Redox Zone Experiment as proposed by /Banwart et al, 1999/.

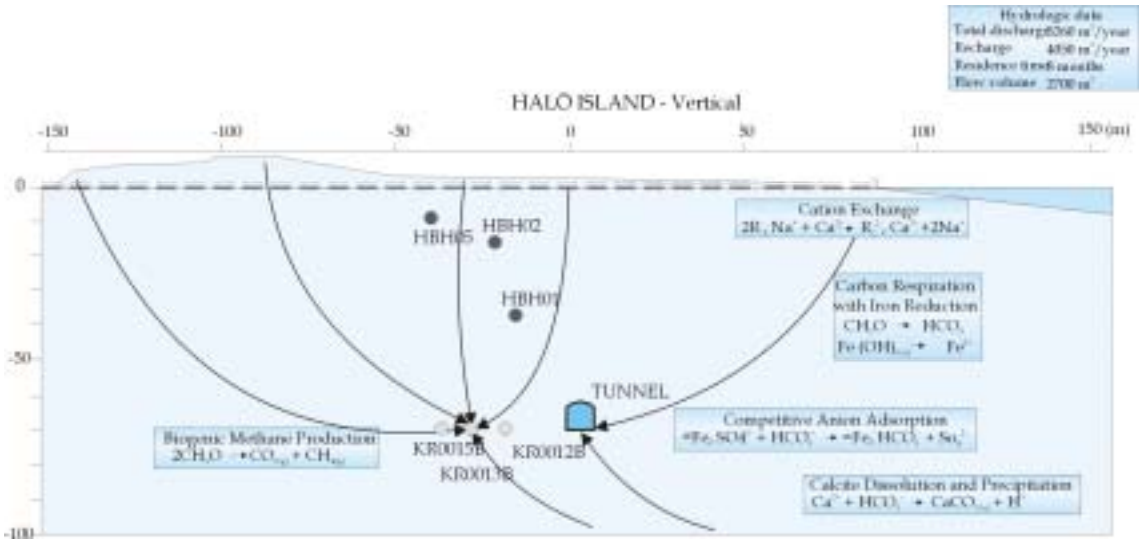

Figure 3-4. *Conceptual model of hydrogeochemistry for the Redox Zone under disturbed conditions. (Modified from /Banwart et al, 1999/).*

/Tullborg, 1995/ reports the main results of the mineralogical and geochemical studies of the Redox Zone Experiment. Figure 3-5 shows a summary of the fracture zone mineralogy and the Fe(II) content of host rock and fracture minerals, based on characterization of drill cores coming from the three boreholes in the side tunnel.

Between the fresh rock granite and the fracture zone there is an altered transition zone. This altered band shows obvious signs of oxidation and weathering, and the most remarkable facts are /Tullborg, 1995/:

1) Biotite is completely altered and replaced mainly by chlorite.

2) Plagioclase grains are altered to albite+sericite+epidote.

3) Quartz is intensely recrystallized.

4) Micro-grains of pyrite are more frequent than in the fresh granite.

In the fracture zone, dominating minerals are chlorite, calcite, epidote, clay minerals, hematite/FeOOH, and less frequently also fluorite and pyrite. The results reported by /Tullborg, 1995/ show a strong evidence about the occurrence of different generations of calcite. Two different types of clay minerals were also identified; illite and swelling clay minerals (smectite or mixed layer clay minerals).

/Tullborg, 1995/ found strong correlation between the grain size of the fracture fillings and mineralogy. This author reported that generally, the larger pieces (> 1 mm) consist of red stained hydrothermally altered granite, whereas the smaller grains (< 0.5 mm) usually are mono-mineralic. K-feldspars, quartz, chlorite and altered plagioclase (clay minerals) are the dominating minerals at that fraction, but also calcite, epidote, FeOOH, laumonite and prehnite occur. In the < 2 mm fraction, mixed layer clay minerals dominate, but significant portions of chlorite and illite are also present.

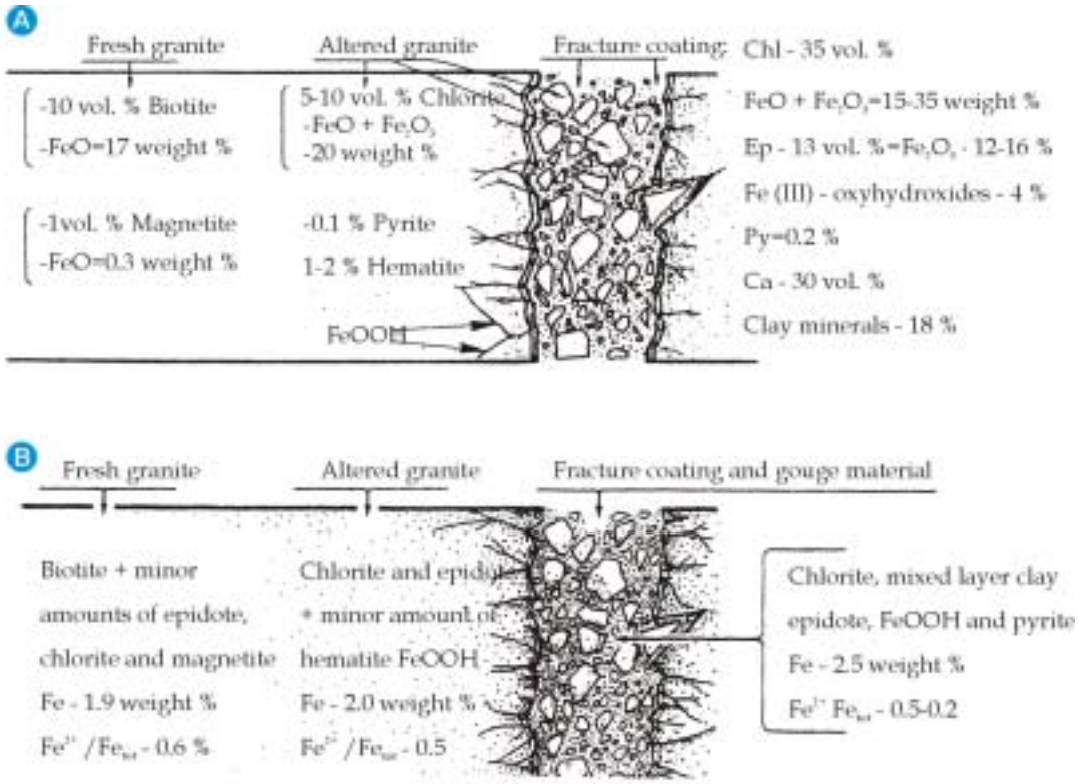

Figure 3-5. *Mineralogy (A) and iron availability (B) in a profile from thr fresh granite to the fracture zone (Modified from /Tullborg, 1995/).*

3.2 Hydrochemical modeling of mixing and reactions

Prior to reactive transport modeling, a number of static hydrochemical calculations were performed. The numerical convergence of the iterative procedure for reactive transport calculations is highly dependent on the initial guess of primary dissolved species. It is known that in order to obtain adequate initial values of concentrations it is useful to use standard hydrochemical speciation codes /Samper et al, 1998/. In addition, hydrochemical speciation is useful to identify the most relevant dissolved species.

It was already pointed that dilution of the saline native groundwater by fresh recharge water is the dominant process controlling the hydrochemical evolution during the Redox Zone Experiment /Banwart et al, 1995/. This was the reason why, in addition to pure speciation of fresh and saline groundwaters (end-members), hydrochemical speciation of binary mixtures between both end-members was also carried out. The scope of binary mixing calculations was to obtain information about the hydrochemical behaviour of the system, prior to proceed with coupled flow and reactive transport modeling.

Binary mixtures were computed with EQ3/6 /Wolery, 1979/. Selected end-members for binary mixtures were the saline native water sampled prior to tunnel intersection (undisturbed sample) and a fresh water sample collected at a depth of 5 m. Table 3-1 shows the main chemical characteristics of both end-members. The methodology consisted on mixing saline native groundwater with fresh recharge water in the following relations saline/fresh water: 100/0, 90/10, 80/20, 70/30, 60/40, 50/50, 40/60, 30/70, 20/80 and 10/90. Speciation calculations were performed for each mixing step and computed results were used as the initial conditions for the next one.

Table 3-1 Chemical composition of native and shallow groundwaters. Concentrations are in mg/L.

Characteristics	Saline Water (KA0483A)	Fresh water (HBH05)
Depth (m)	70	5
T (ºC)	9	8
pH	7.5	7.5
Na^{+}	1480	15.4
Ca^{2+}	1250	38.4
Mg^{2+}	132	4
K^{+}	9.1	2.6
Fe^{2+}	0.54	0.822
Mn^{2+}	0.94	0.36
Li^{+}	0.32	0.01
Sr^{2+}	21.5	0.22
Cl^{-}	4890	11.2
HCO_3^{-}	42	137
SO_4^{2-}	60	23
Br^{-}	30.2	–
$SiO_{2(aq)}$	5.6	6

Thermodynamic calculations were made accounting also for mineral dissolution/precipitation reactions including goethite, pyrite, calcite and quartz, according to:

$$FeOOH(s) + 2H^{+} = 1.5H_2O + Fe^{+2} + 0.25O_2(aq)$$

$$SiO_2(s) = SiO_2(aq)$$

$$FeS_2(s) + H_2O + 3.5O_2(aq) = 2H^{+} + 2SO_4^{-2} + Fe^{+2}$$

$$CaCO_3(s) + H^{+} = Ca^{+2} + HCO_3^{-}$$

These mineral phases were selected based on mineralogical characterization results /Tullborg, 1995/.

There are not available data for measured redox potentials. Therefore, it was needed to assume some values. It is known that redox potentials at a depth of 70 m were in the range of –150 and –100 mV during the experiment /Banwart et al, 1996/. Figure 3-6 shows a phase diagram with the solubility limits of goethite as a function of Eh. A value of –145 mV is obtained when undisturbed measured Fe^{+2} concentration is in equilibrium with goethite (Figure 3-6). Then a Eh value of –145 mV was assumed for native saline water. A greater uncertainty exists for the redox conditions of fresh recharge water. This was the reason why 3 different possibilities were considered (Figure 3-7): 1) Fresh recharge water is in equilibrium with atmospheric oxygen (oxidizing water), 2) fresh recharge water has a Eh value equals to –150 mV and, 3) fresh recharge water has a Eh value equals to –250 mV (highly reducing water).

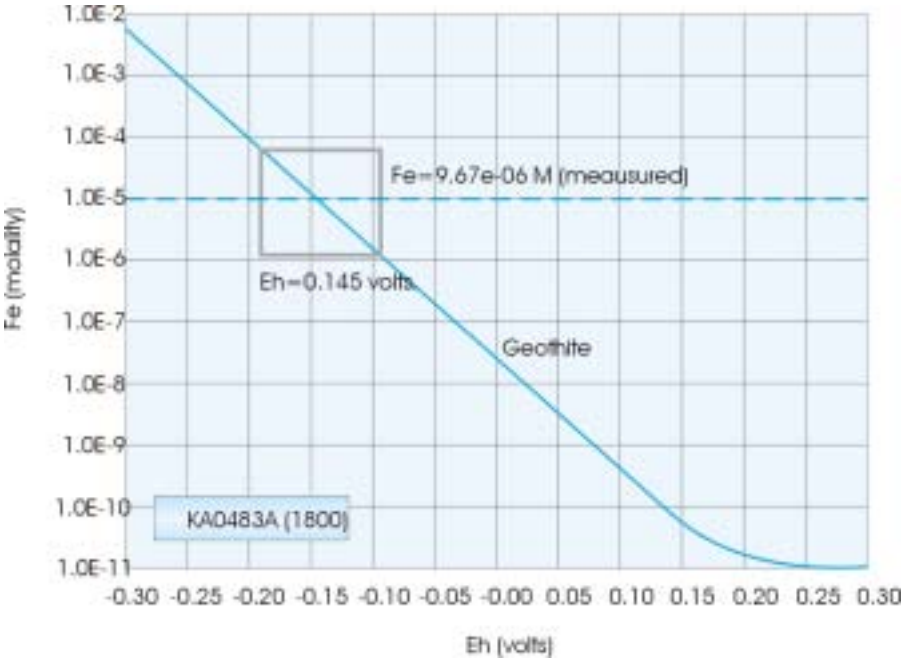

Figure 3-6. *Phase diagram showing the solubility limits of goethite as a function of Eh. Measured dissolved iron in equilibrium with goethite gives a Eh value equals to –0.145 V.*

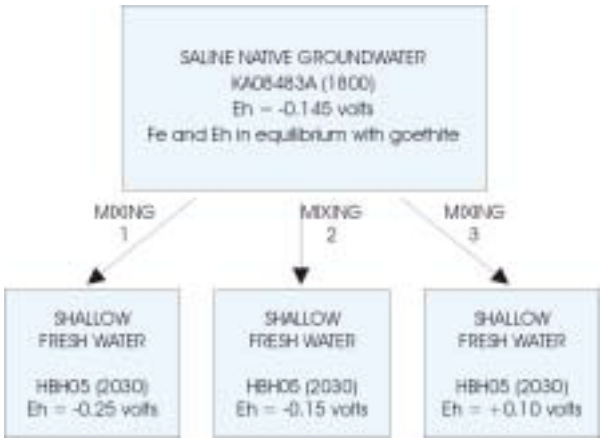

Figure 3-7. *Scheme of the three different possibilities considered for binary mixtures.*

Figure 3-8 shows computed results for binary mixtures. Mineral dissolution (negative values) and precipitation (positive values) is shown as a function of the saline native groundwater proportion (Figure 3-8). It can be noticed that pyrite, calcite and quartz precipitate (positive values) while goethite dissolves (negative values) when saline native groundwater is diluted with fresh recharge water. Quantitatively, dissolution-precipitation processes are more important when fresh recharge water is highly reducing. However, for Eh values above –150 mV mineral behaviour is not sensitive to the redox conditions of the fresh recharge water.

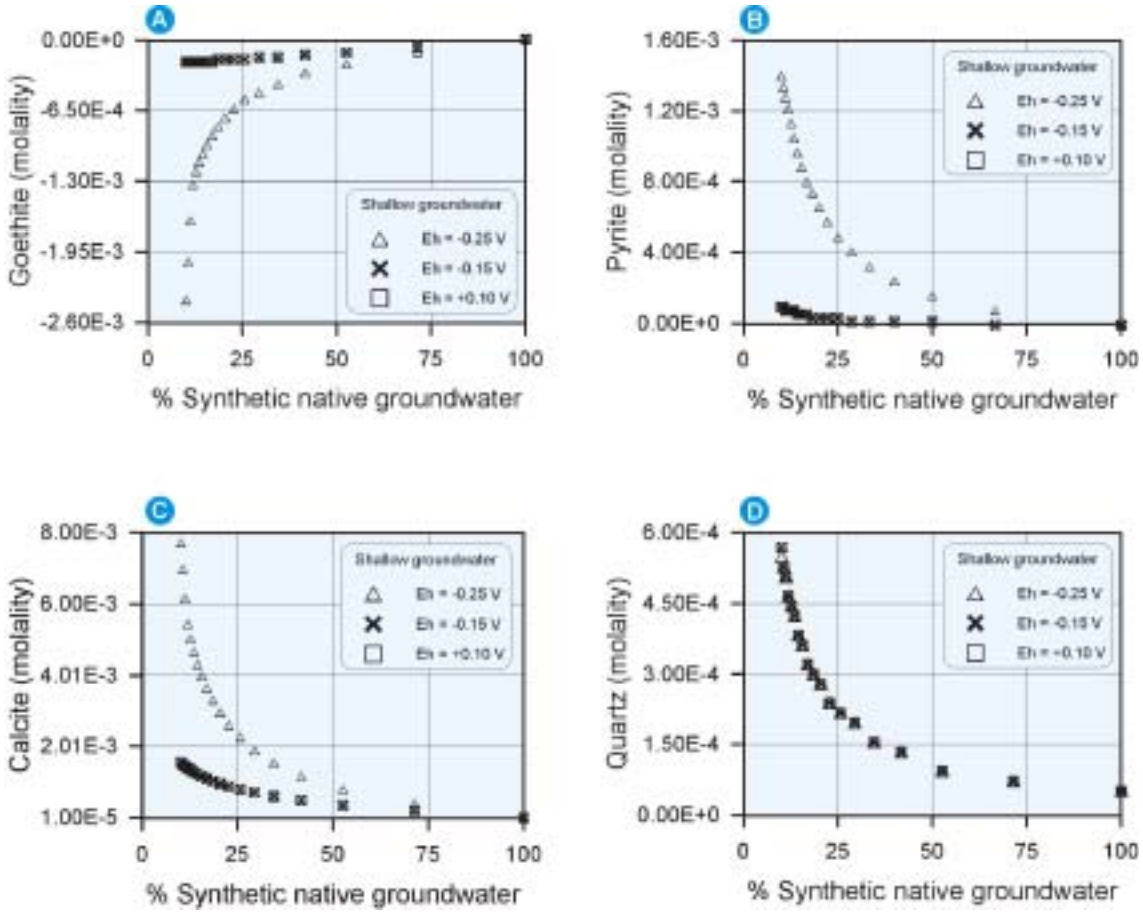

Figure 3-8. *Computed mineral behaviour in binary mixture calculations. A) Goethite evolution. B) Pyrite evolution. C) Calcite evolution. D) Quartz evolution. Positive numbers indicate precipitation and vice versa.*

3.3 Hydrochemical conceptual model

After hydrochemical speciation using EQ3/6 program /Wolery, 1979/, the most relevant aqueous species were selected to be included into the reactive transport model. Finally, 68 homogeneous reactions including aqueous complexation, acid-base and redox processes were considered. Chemical reaction stoichiometry and detailed thermodynamic database can be found in /Molinero, 2000/.

Following reported results about mineralogical studies of the Redox Zone /Tullborg, 1995/, 4 mineral phases were included in the reactive transport model. These minerals are calcite, quartz, goethite and pyrite, as in the hydrochemical modeling of mixing and reactions. Mineral dissolution-precipitation was modeled assuming local equilibrium. Thermodynamic parameters (equilibrium constants) are also listed in /Molinero, 2000/.

/Tullborg, 1995/ reports the occurrence of both ferric oxides and oxihydroxides mineral phases. However, by assuming the local equilibrium approach it is not possible to include both minerals together in the same model. Figure 3-9 shows a phase diagram with the solubility limits of iron minerals as a function of Eh. It can be noticed in Figure 3-9 that hematite and goethite show parallel solubility limits, so there are not common equilibrium points for both minerals. In addition to that, both ferric minerals

have independent equilibrium points with pyrite (see the square in Figure 3-9). Both equilibrium points seem more or less consistent with undisturbed conditions of the Redox Zone (Eh and dissolved Fe concentration measured at the undisturbed native water sample at a depth of 70 m).

From a thermodynamic point of view, hematite formation is more stable than goethite when they are in equilibrium with aqueous solutions. Figure 3-10 shows a Pourbaix diagram for iron mineral phases. Pourbaix diagrams /Pourbaix, 1945; Pourbaix and Zubov, 1963; Garrels and Christ, 1965; Beverskog and Puigdomenech, 1996/, also called potential pH diagrams, are thermodynamic maps. The Pourbaix diagram can be seen as a map in the chemical space, summarizing thermodynamic information in a compact and useful manner /Beverskog and Puigdomenech, 1996/. Pourbaix diagram shown in Figure 3-10 was computed for total iron and sulphate concentrations equal to the measured values of undisturbed native water of the Redox Zone. Thermodynamic calculations and graphical display of the Pourbaix diagram was performed with the code MEDUSA /Puigdomenech, 1999/. Figure 3-10 shows that, considering the Redox Zone measured concentrations and chemical conditions ($7 < pH < 8$; $-0.2V < Eh < -0.1V$), data are located in the equilibrium boundary between pyrite and hematite.

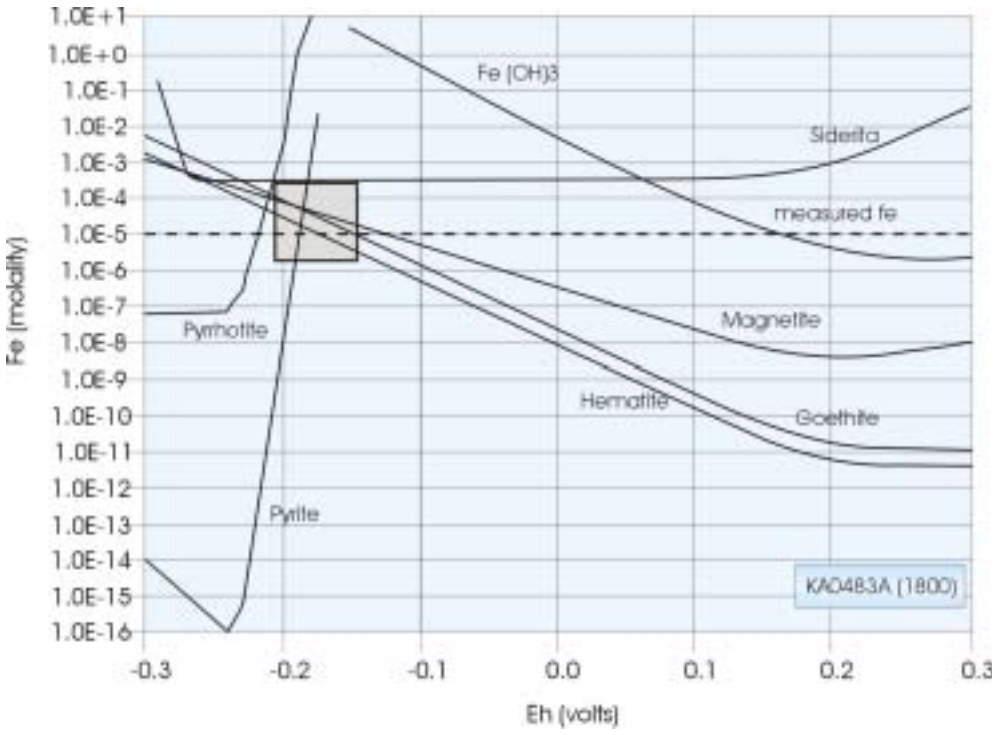

Figure 3-9. *Phase diagram showing the solubility limits of iron minerals as a function of Eh.*

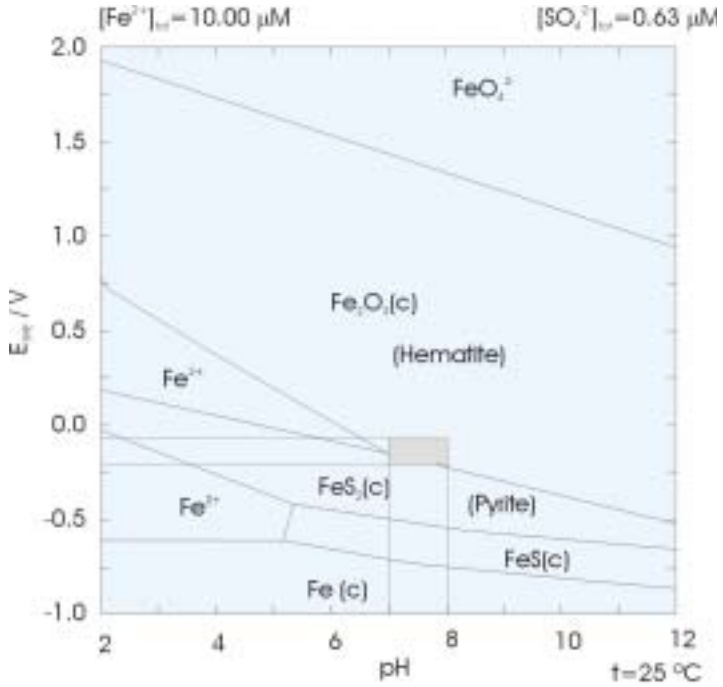

Figure 3-10. *Pourbaix diagram for measured dissolved iron and sulphate of the undisturbed native groundwater of the Redox Zone. Grey square illustrates the thermodynamic field for measured chemical conditions of the Redox Zone.*

However, reported experimental existence of both hematite and goethite mineral phases in many natural systems indicates that goethite formation is perhaps favoured on kinetic grounds /Beverskog and Puigdomenech, 1996/. This is the case of the Redox Zone where the occurrence of goethite together with hematite was clearly recognized in the fracture zone /Tullborg, 1995/. From a practical point of view, /Beverskog and Puigdomenech, 1996/ propose that the choice of oxide or oxihydroxide of Fe(III) to be considered in a given system can also be based on non-thermodynamic arguments. Of course, if hematite is not considered in the system then goethite can also reach equilibrium with pyrite (see Figure 3-9). Finally, in spite of hematite being thermodynamically more favourable, goethite was selected as the ferric mineral phase to be included in the numerical model in order to be consistent with field observations. However, the uncertainty about the most appropriate ferric mineral phase is analyzed in following sections.

Another heterogeneous chemical process included in the conceptual model of the Redox Zone Experiment is cation exchange /Molinero, 2000/. /Viani and Bruton, 1997/ estimated the exchange capacity of the Redox Zone to be on the range between 0.06 and 0.2 equivalents of exchanger per liter of groundwater, based on matching hydrochemical model results to observed Na^+ and Ca^{2+} groundwater concentrations. On the other hand, /Banwart et al, 1995/ present two estimates:

1) 0.083 eq/L based on fitting mass balance and cation exchange mass action equations to observed concentration of Na^+ in Äspö groundwaters.

2) 0.004–0.03 eq/L based on the observed fracture mineralogy, fracture fill porosity and CEC values for various clay minerals.

Then a great uncertainty exists for the cation exchange capacity of the Redox Zone. This uncertainty constitutes an interesting point to be explored with the coupled flow and reactive transport model.

3.4 Initial and boundary conditions

Hydrochemical concentrations used for either Baltic sea, fresh recharge water and 300 m deep bottom groundwater were introduced in Chapter 2 to set up the conservative transport numerical model (see /Molinero, 2000/ for details). As was shown in the hydrochemical modeling of binary mixtures, a main uncertainty was detected concerning the redox potential of fresh recharge waters infiltrating on the top of the fracture zone. Two extreme conjectures can be considered to cope with this uncertainty:

1) Recharge fresh water is oxidizing, with an oxygen fugacity in equilibrium with atmospheric oxygen partial pressure.

2) Recharge fresh water is reducing once it reaches the water table. Dissolved oxygen of surface water infiltrating through a soil could be depleted by interaction with organic matter and/or minerals.

As mentioned before, there are not Eh field measurements for shallow groundwater of the Redox Zone. Both extreme possibilities were numerically tested with the reactive transport model. Long term runs of the coupled flow and reactive transport numerical model were performed to simulate the undisturbed conditions in order to check the hydrochemical behaviour of the system under different assumptions.

The firstly tested scenario consisted on considering oxidizing fresh water on the upper boundary. Dissolved oxygen of the upper boundary water was constrained to a fugacity in equilibrium with atmospheric oxygen partial pressure. The numerical model was run for simulating 6,000 days. Figure 3-11 shows computed results of pyrite concentrations at 1,000 days and 6,000 days. Computed results show an important dissolution of pyrite at the shallow fresh water system. Figure 3-11 illustrates the advance in time of the pyrite dissolution front.

/Tullborg, 1995/ reports values of pyrite around 0.1% in volume at a depth of 70 m. If this is the natural amount of pyrite in the fracture zone, and considering that the present day hydrological conditions can be supposed as being constant at least for the last 2,000 years, then pyrite depletion at the shallowest part of the Redox Zone can be expected if we consider oxidizing infiltration water. Should this be true, two different mineral zones should be expected into the fracture zone under natural conditions (prior to tunnel construction). The two mineral zones would coincide with the water distribution at natural conditions: a fresh water zone in which pyrite would be probably dissolved during the last 2,000 years, and a deeper saline water zone with about a 0.1% in volume of pyrite. A new run of the numerical model was performed accounting for this distribution of mineral zones. Figure 3-12 shows computed values of Eh for this scenario. One can see in this figure that the new mineral distribution produces a clear, sharp redox interface between oxidizing fresh waters and reducing deeper saline waters.

Figure 3-11. *Computed results of pyrite concentrations for the first considered conjecture: upper boundary water is oxidizing. A) Computed results al 1,000 days. B) Computed results at 6,000 days. Comparison of both figures illustrates the advance of the pyrite dissolution front within the shallow fresh water system.*

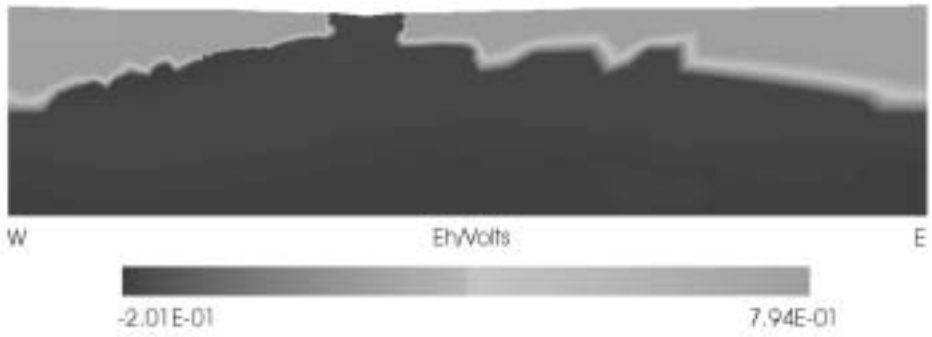

Figure 3-12. *Computed steady-state of Eh values for natural conditions when depletion of pyrite is considered in the shallow fresh water systems. A clear sharp redox interface is computed for this scenario.*

Finally, the second proposed conjecture was tested. Reducing fresh water was assumed on the upper boundary, with an Eh value constrained to be in equilibrium with existing minerals. In this case, the domain was supposed mineralogically homogeneous, what is to say, only one mineral zone containing calcite, goethite, pyrite and quartz was assumed for the whole domain. Figure 3-13 shows computed values of Eh for this second hypothesis. As expected, a totally different Eh distribution is obtained. Computed Eh values for this scenario are reducing everywhere, showing maximum values of about –177 mV at the fresh-saline water interface (Figure 3-13).

Even though there is no available information about the redox conditions for the shallow groundwater of the fracture zone, there are a number of chemical analyses of shallow groundwaters collected in borehole HBH05 during the Redox Zone Experiment. HBH05 borehole samples were collected at a depth of 5 m after tunnel intersection, so it can be assumed that these samples are representative of fresh recharge water on the top of the fracture zone. Measured dissolved iron within these shallow fresh water samples ranges between 10^{-4} and 10^{-6} mol/L (Figure 3-14a).

Computed numerical results of dissolved iron at a depth of 5 m (obtained with both conjectures about the redox state of recharge water) are compared at Figure 3-14b. It can be noticed that considering reducing water on the upper boundary leads to a much better agreement with measured data than in the case of surface oxidizing waters. Then, from Figure 3-14b it can be concluded that reducing fresh water is the most likely hypothesis for the hydrochemical boundary condition on the top of the fracture zone.

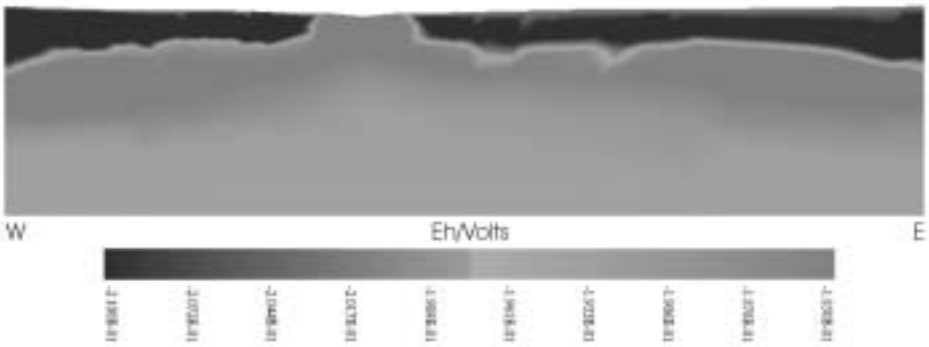

Figure 3-13. *Computed steady-state of Eh values for natural conditions when a reducing water top boundary condition is prescribed. In this case the maximum values of Eh are computed at the saline-fresh water interface.*

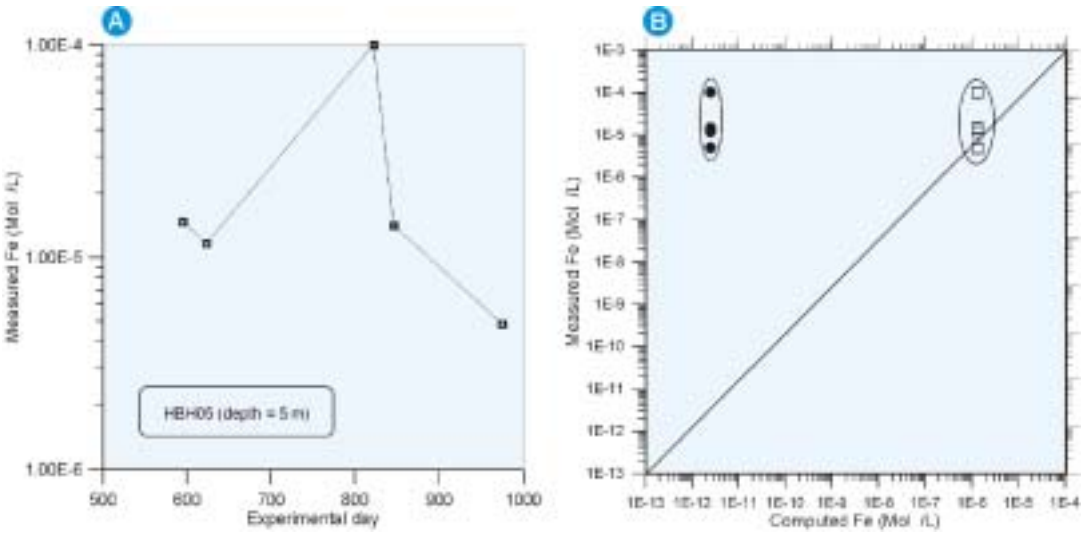

Figure 3-14. *A) Measured dissolved iron at borehole HBH05 (5 m deep).*
B) Comparison between measured and computed dissolved iron at a depth of 5 m for both considered hypotheses about the redox conditions of shallow fresh water. Considering reducing waters on the upper boundary leads to a much better agreement with measured values.

3.5 Base numerical model

Figures 3-15 through 3-18 show computed mineral concentrations on day 983 (at the end of the experiment). In this figures positive values indicate mineral precipitation and vice versa. It is worth noting that behaviour of goethite, pyrite and calcite is controlled by the fresh-saline water interface (Figures 3-15 through 3-17). The position of this interface is modified by the hydrologic disturbance produced by tunnel construction and opening of the KR0013B borehole, as was shown in previous sections. The tunnel and the open borehole produce a net dilution within the tunnel surroundings (at a depth of 70 m), as a result of the important increase of shallow fresh water coming from the fresh-water lenses located at both sides of the Baltic Sea. The tunnel and the open borehole constitute water sinks towards which groundwater flows radially. The mixing of different kinds of water in the tunnel vicinity produces changes on water compositions, which at the same time influence mineral saturation indexes. This is the reason why the most relevant changes in mineral behaviour are computed within the tunnel surroundings (Figures 3-15 through 3-17). The Baltic coast is also another location where relevant mineral changes are computed, because different waters are also put in contact there (Baltic estuary water and shallow fresh water). Figure 3-18 illustrates that, in the case of quartz, noticeable precipitation is computed in the Baltic Coast while no relevant mineral changes are computed in the tunnel surroundings.

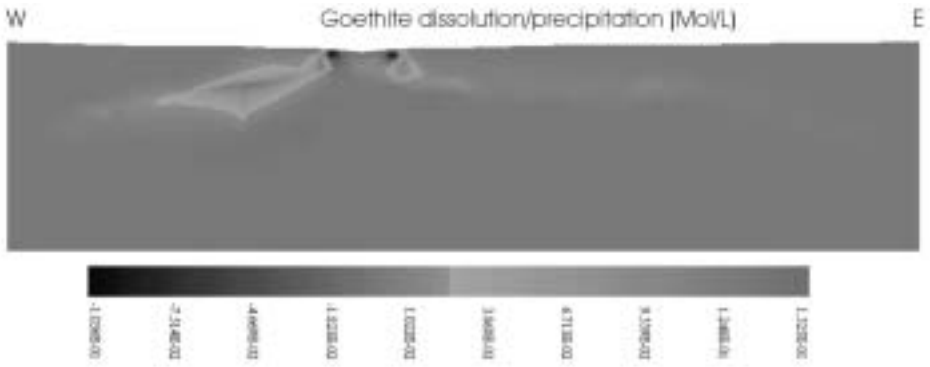

Figure 3-15. *Computed dissolution/precipitation of goethite on day 908. Positive numbers indicate precipitation and vice versa.*

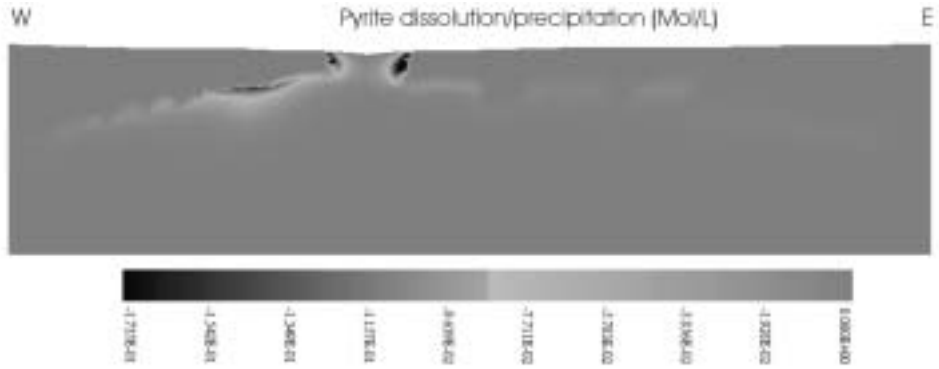

Figure 3-16. *Computed dissolution/precipitation of pyrite on day 908. Positive numbers indicate precipitation and vice versa.*

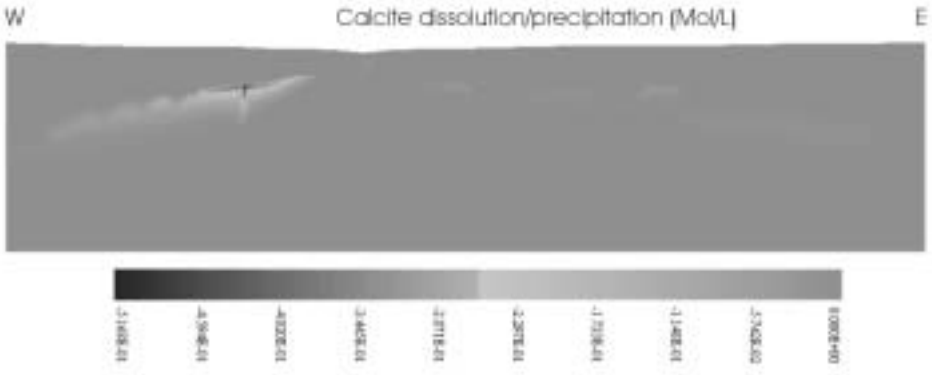

Figure 3-17. *Computed dissolution/precipitation of calcite on day 908. Positive numbers indicate precipitation and vice versa.*

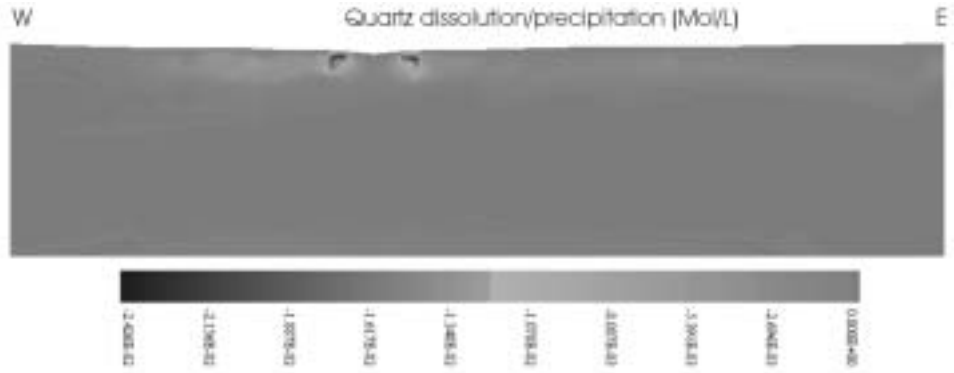

Figure 3-18. *Computed dissolution/precipitation of quartz on day 908. Positive numbers indicate precipitation and vice versa.*

Looking at the tunnel surroundings in Figures 3-15 through 3-17 one can see that the numerical model computes dissolution of calcite and pyrite and precipitation of goethite. This finding was unexpected at the beginning because it is exactly the opposite behaviour predicted by mixing and reaction modeling shown in the previous section.

Figure 3-19 shows computed mineral distribution versus time at the tunnel position. It is possible to notice that the qualitative behaviour of all minerals is opposite to that computed by using the binary mixtures and reactions model (see Section 3.2). One can see in Figure 3-19 that the larger the dilution the greater the numerically computed dissolution of pyrite, calcite and quartz, and the higher the precipitation of goethite.

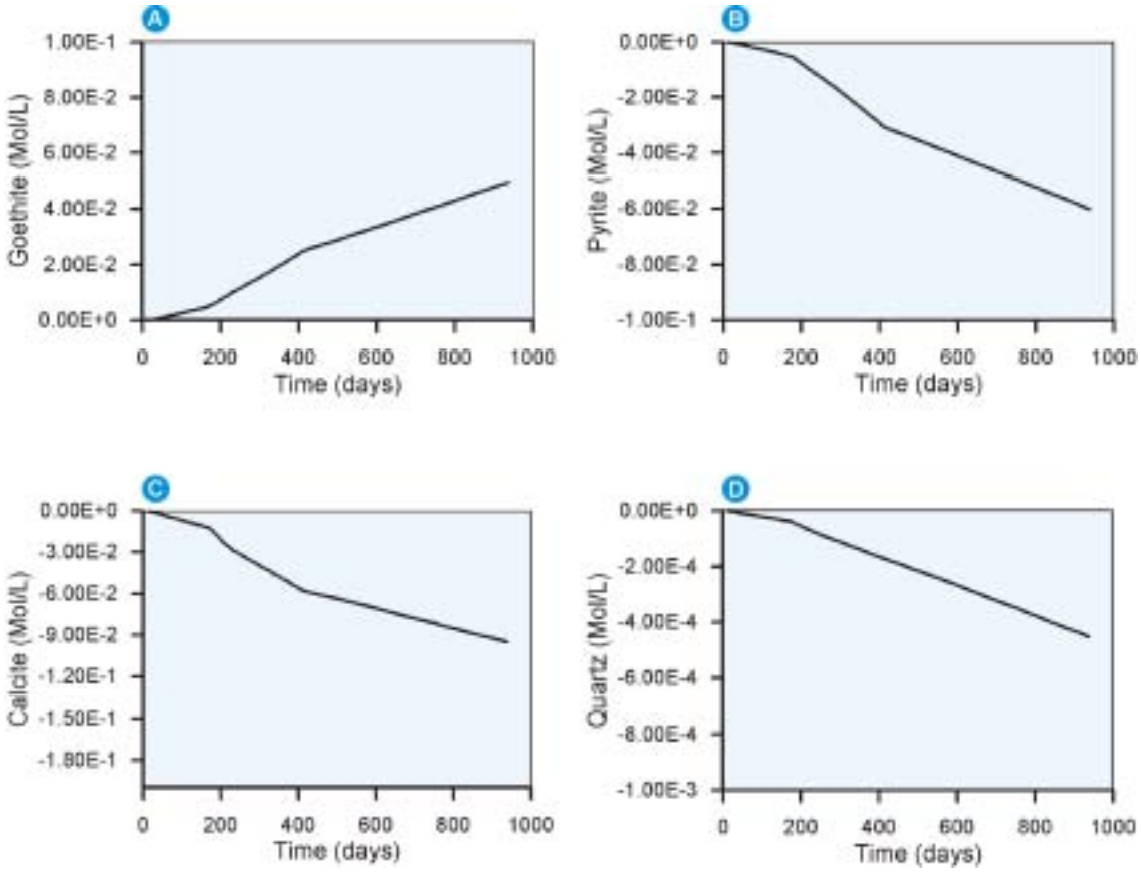

Figure 3-19. *Computed mineral behaviour at the tunnel location: A) Goethite, B) Pyrite, C) Calcite and D) Quartz. By comparison with Figure 3-8 it can be noticed that the reactive solute transport numerical model predicts qualitative opposite patterns than mixing and reactions hydrochemical model.*

The explanation for this apparent lack of coherence is that for binary mixing calculations the selected end-member for fresh water was a water sample collected at a depth of 5 m (at borehole HBH05). This water sample is chemically the same as that prescribed on the upper boundary of the coupled flow and reactive solute transport numerical model. However, the mixing of waters actually takes place at a depth of 70 m, which means that boundary fresh waters must travel from the surface to the tunnel. Binary mixing and reaction model presented in Section 3.2 does not account for the chemical interaction between the fresh water and the solid phases within the first 70 m of aquifer. Finally, fresh waters reaching tunnel location are actually different than those very shallow waters, and then mixing and reaction models based on end-members are unable to represent the real system. On the contrary, the coupled flow and reactive solute transport numerical model accounts for water-solid interactions in the whole model domain, so it is able to give a better representation of the actual mixing happening within the tunnel surroundings.

Looking at the computed values of dissolved species a major change with respect to conservative numerical model results was observed for iron concentrations. Figure 3-20 shows a comparison between computed dissolved iron with both, conservative and reactive solute transport numerical model. It must be reminded that the numerical model under-predicted measured iron concentrations when chemical equations were not considered (see Chapter 2). However, coupled flow and reactive solute transport numerical model computes iron concentrations noticeably larger than those measured concentrations (Figure 3-20).

Computed dissolved iron concentrations are mainly controlled by heterogeneous reactions involving pyrite and goethite. As was discussed in Section 3.1, mineralogical studies report the simultaneous occurrence of both ferric oxides and oxihydroxides (hematite and goethite) within the Redox Zone. However, both mineral could not be considered together in the model, because there is not a common equilibrium point for these ferric minerals together with pyrite. In spite of hematite is thermodynamically more stable (see Section 3.3), goethite was finally included within the numerical model as the ferric mineral phase due to field evidences, and also because it is known that in many natural systems goethite formation is favoured for kinetic reasons /Beverskog and Puigdomenech, 1996/.

A new run of the groundwater flow and reactive solute transport numerical model was performed considering hematite as the ferric mineral phase instead of goethite. Figure 3-21 shows a comparison between computed dissolved iron concentrations at borehole KR0015B (depth of 70 m). One can see in Figure 3-21 that a much better agreement is obtained when goethite is replaced by hematite. Hematite seems the most appropriate ferric mineral phase for simulating the Redox Zone Experiment assuming the Local Equilibrium Approach (Figure 3-21).

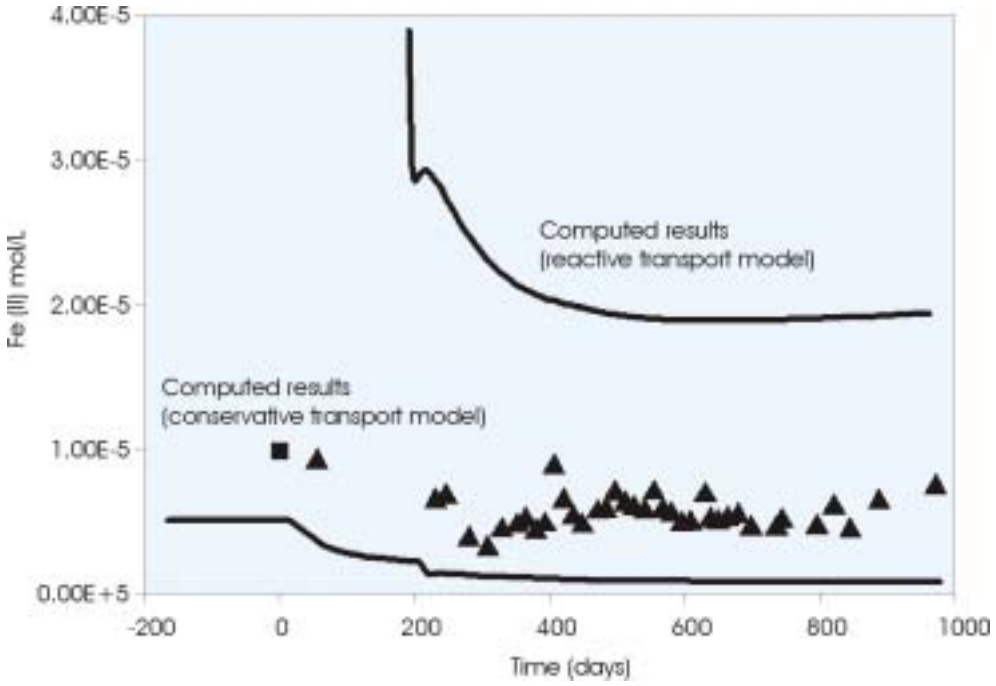

Figure 3-20. *Comparison between computed results of dissolved iron concentrations obtained with the conservative solute transport model and the reactive transport model. Measured values (symbols) lie in the middle of both computed results.*

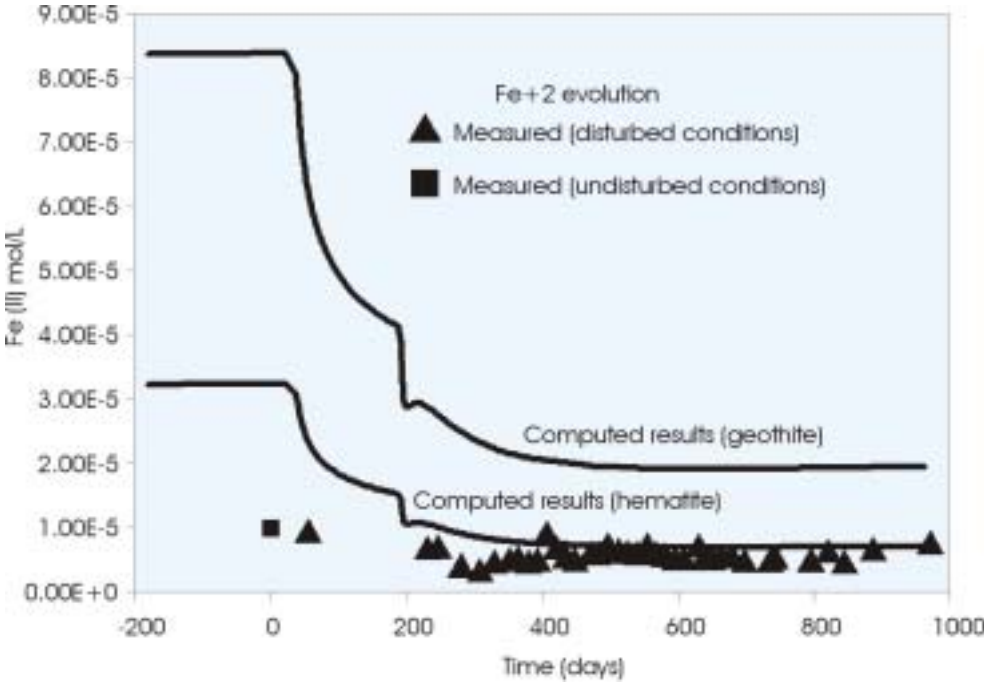

Figure 3-21. *Comparison between computed dissolved iron concentrations considering goethite and hematite as the ferric mineral phase in the reactive transport model. Considering hematite in the numerical model leads to much better agreements with measured values (symbols).*

The coupled groundwater flow and reactive solute transport numerical model was also used to study the role of cation exchange processes during the Redox Zone Experiment. As was commented previously an important uncertainty was detected about the Cation Exchange Capacity (CEC) of the Redox Zone. Mineralogical studies /Tullborg, 1995/ estimate the clay content of the fracture zone as being 0.5% in weight. However, fracture zones gouge materials are often lost during mineral sampling. Usually the smaller the mineral size the higher the lost fraction during sampling. /Banwart et al, 1995/ estimate the cation exchange capacity of the Redox Zone as 0.03 equiv./L based on fracture zone mineralogy, clay abundance (they assume 0.5%) and standard values of CEC of clay minerals. On the other hand, /Viani and Bruton, 1997/ estimated the exchange capacity of Äspö fracture zones to be up to 0.2 equiv./L, based on matching static hydrochemical model results to observed Na^+ and Ca^{2+} groundwater concentrations. Then, estimating CEC values by hydrochemical modeling leads to much higher values than estimations based on observed clay content.

Figure 3-22 shows a comparison between measured Na^+ concentrations and numerically computed values. Computed results with 2 model runs are shown in Figure 3-22. One of the model runs adopted a total CEC value of 0.06 Mol/L, while the second run was performed with a CEC value which was one order of magnitude higher. Computed results using a CEC of 0.6 Mol/L leads to a much better agreement with respect to measured Na^+ concentrations (Figure 3-22).

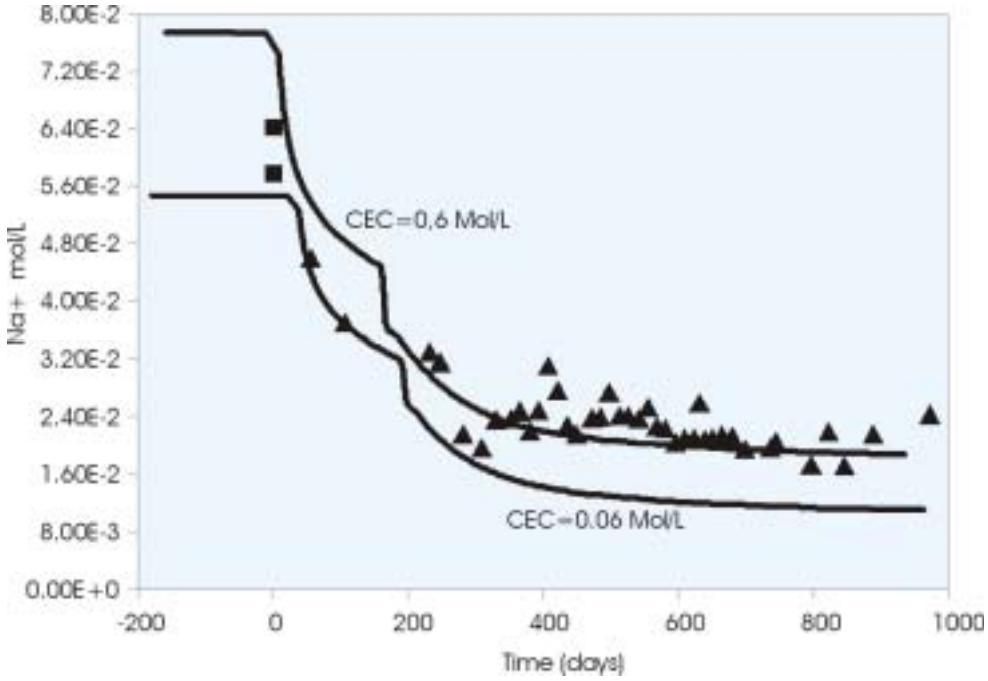

Figure 3-22. *Comparison between measured sodium concentrations and numerically computed concentrations using a total CEC value of 0.06 Mol/L and 0.6 Mol/L.*

/Banwart et al, 1995/ reported standard values of CEC for pure mixed-layer clay minerals in a range between 0.4 and 1.4 Mol/Kg. Assuming a CEC value of 1 Mol per Kg of clay, a clay porosity of 30% and a clay mineral density of 2.6 Kg/L, leads to an exchange capacity for pure mixed-layer clay minerals of 6 Mol/L. Then, numerically derived CEC value for the fracture zone (0.6 Mol/L; see Figure 3-22) indicates that the clay content should be around 10% in the Redox Zone. This estimation of CEC for clay minerals is based on simple considerations and standard values, and must be taken as a first guess estimation. Looking at coupled flow and reactive transport model it is thought that actual clay content within the Redox Zone should be closer to 5 % better than to 0.5 % (proposed by mineralogical characterization).

It has been shown that the groundwater flow and reactive solute transport model is able to improve computed results for dissolved iron and sodium, compared to conservative transport model results shown in Chapter 2. In addition to these species, relevant deviations from the conservative behaviour were also detected for bicarbonates and sulphates. Figure 3-23 shows computed and measured concentrations of bicarbonates and sulphates. It can be noticed that the reactive solute transport numerical model is not able to reproduce measured values.

Both, measured bicarbonates and sulphates show a drastic concentration increase during the Redox Zone Experiment. As was commented previously (Section 3.1), carbon isotopes studies point clearly towards microbially mediated organic matter degradation as being the most probable source for bicarbonates. Organic matter degradation frequently occurs in groundwaters, but it can be catalyzed by many kinds of bacteria. /Banwart et al, 1995, 1999/ and /Banwart, 1999/ propose microbially mediated iron reduction as the responsible process to explain the recorded behaviour of bicarbonates. This chemical process can be summarized as:

$$4\ Fe(OH)_{3(s)} + CH_2O + 7\ H^+ \rightarrow 4Fe^{2+} + HCO_3^- + 10\ H_2O$$

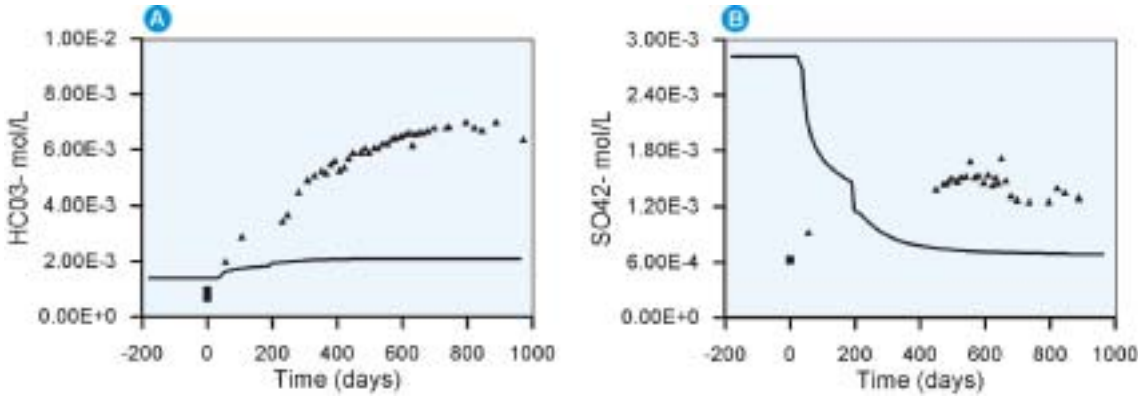

Figure 3-23. *Comparison between measured (symbols) and computed (lines) concentrations of A) bicarbonates and B) sulphates, at borehole KR0015B (depth of 70 m).*

However, there are also other possibilities such as /Wikberg et al, 1997/:

Fermentation: $CH_2O \rightarrow 1/3\ CO_2 + 1/3\ C_2H_6O$

Sulphate reduction: $CH_2O + ½\ SO_4^{2-} + ½\ H^+ \rightarrow CO_2 + 1/2\ HS^- + H_2O$

Methane formation: $CH_2O + ½\ CO_2 \rightarrow CO_2 + 1/2\ CH_4$

Sulphate reduction does not seem to be responsible for bicarbonate increase because isotopic studies rule out this possibility during the Redox Zone Experiment /Wallin, 1995/. In fact, the most probable process is that proposed by /Banwart, 1999/ because microbiological studies performed in the Redox Zone /Pedersen et al, 1995/ found relevant populations of iron reducing bacteria.

On the other hand, there is not a conclusive explanation for the sulphate behaviour. Looking at Figure 3-23b it is possible to appreciate that numerically computed sulphate concentrations are much higher than measured values at the initial time (undisturbed conditions; before time = 0). In fact, it seems really to be a problem related with assumed sulphate boundary conditions. Prescribed sulphate concentration on the bottom boundary was derived (as for the rest of dissolved species) by analyzing available samples collected prior to the tunnel construction at the Äspö site. This analysis indicates a sulphate concentration of about 400 mg/L at a depth of 300 m. Sulphate concentration (under undisturbed conditions) at a depth of 70 m was 60 mg/L. /Pedersen et al, 1995/ reports that no presence of sulphate reducing bacteria was found within the Redox Zone during the experiment, which is consistent with isotopic results reported by /Wallin, 1995/. However, /Pedersen et al, 1995/ states that sulphate reducing bacteria are definitely not absent in the Äspö area, because they appeared in other parts of the tunnel, mainly in those zones of the tunnel going under the bottom of the Baltic Sea. /Lovley, 1991/ argued that the iron reducing bacteria can out-compete the sulphate reducing bacteria by keeping the concentration of electron donors too low for sulphate reducers. There were not any microbiological investigation undertaken at the Redox Zone prior to the start of the experiment. Therefore, the undisturbed microbiological situation is unknown. /Pedersen et al, 1995/ states that it is not impossible that sulphate reducers were present before the experiment and then, they could have been out-competed by the iron reducers once the flow system was modified by the tunnel construction. In fact, we know that fresh groundwater flowing towards the

tunnel actually increases the input of suitable electron donors (organic matter) in the tunnel surroundings. The increase of organic matter could have enhanced the activity of iron reducing bacteria, which at the same time could inhibit (out-competition) the growth of sulphate reducer microorganisms.

Figure 3-24 shows computed sulphate concentrations evolution when sulphate concentrations at the bottom boundary (at a depth of 300 m) was prescribed equals to the measured value of the Redox Zone undisturbed sample (at a depth of 70 m). It can be appreciated that the computed results are much more consistent for the beginning of the experiment (time = 0) than using the previous boundary condition (Figure 3-23b). This analysis supports the hypothesis of that sulphate reducing bacteria could be present in the fracture zone, prior to tunnel intersection, keeping sulphate concentrations at 300 m depth at a similar value to that measured at a depth of 70 m.

However, the recorded increase of sulphate concentrations during the Redox Zone Experiment (before time = 0) still remains unresolved (Figure 3-24). As was pointed in Section 3.1 /Banwart et al, 1999/ propose anion exchange due to adsorption competition between bicarbonates and sulphates as an explanation to measured sulphate behaviour. However, this hypothesis is questioned by /Bruton and Viani, 1997/ because the expected anion adsorption capacity for the Redox Zone is estimated to be too low at the geochemical conditions prevailing within the fracture zone. Coupled groundwater flow and reactive solute transport numerical model has been used for testing different hypotheses concerning sulphate behaviour.

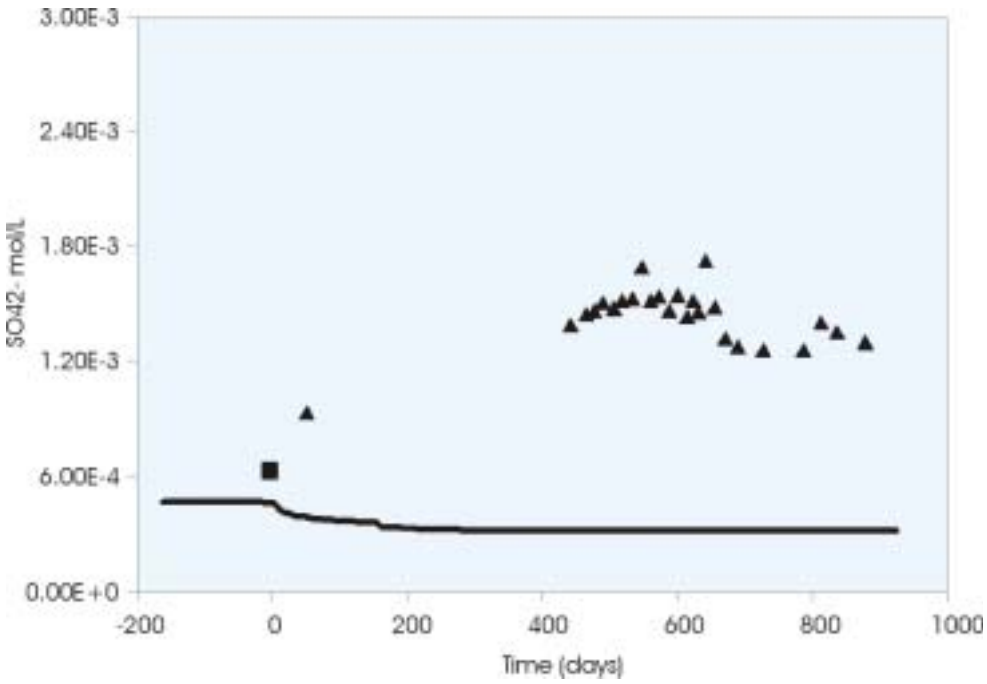

Figure 3-24. *Measured (symbols) and computed (line) sulphate concentrations. In this run, the bottom boundary condition for sulphate was assumed equal to that measured at a depth of 70 m.*

3.6 Evaluating the role of the rock landfill

As was commented in Chapter 2 the occurrence of the rock landfill on Halö (Figure 3-7) provides a logical explanation for the additional source of fresh water required in order to reach measured dilution at 70 m deep boreholes (see the conceptual model; Figures 2-8 and 2-9). In addition, it was found that the rock landfill contains a large amount of concrete and cement.

The chemistry of cement is complicated and much work remains to be done even to establish the thermodynamic properties of its components /Steefel and Lichtner, 1994/. The two most important phases in the hydration of a calcium-rich cement are portlandite ($Ca(OH)_2$) and various calcium silicate hydrates. The presence of these two phases leads to pore water compositions with high OH^- and low silica activities /Atkins and Glasser, 1992; Berner, 1992; Reardon, 1992; Steefel and Lichtner, 1994/. The alkalies are present in cement in the form of solid solutions with readily-soluble sulphates /Steefel and Lichtner, 1994/. One of the most typical sulphate minerals in cements is the ettringite (a highly soluble calcium and aluminium sulphate). Then, the rock landfill of Halö could constitute a potential source for sulphate, which could be responsible of the relevant increase on sulphate concentrations recorded during the Redox Zone Experiment (see Figures 3-23 and 3-24).

A new run of the flow and reactive solute transport numerical model was performed in order to evaluate quantitatively this hypothesis. The new run accounts for a different initial water zone on the landfill area (Figure 3-25). There is not available information about pore waters of the landfill area, so it was needed to adopt some assumptions. /Steefel and Lichtner, 1994/ performed a study about water-rock interaction adjacent to cement-bearing nuclear waste repositories. These authors proposed a synthetic-standard chemical composition for cement pore waters based on hydrochemical modeling. Table 3-2 shows the chemical characteristics of this cement pore-water as proposed by /Steefel and Lichtner, 1994/. In this table are included the main assumptions (constrains) used by these authors to derive the synthetic water composition. Additional details (such as thermodynamic parameters) can be consulted in /Molinero, 2000/.

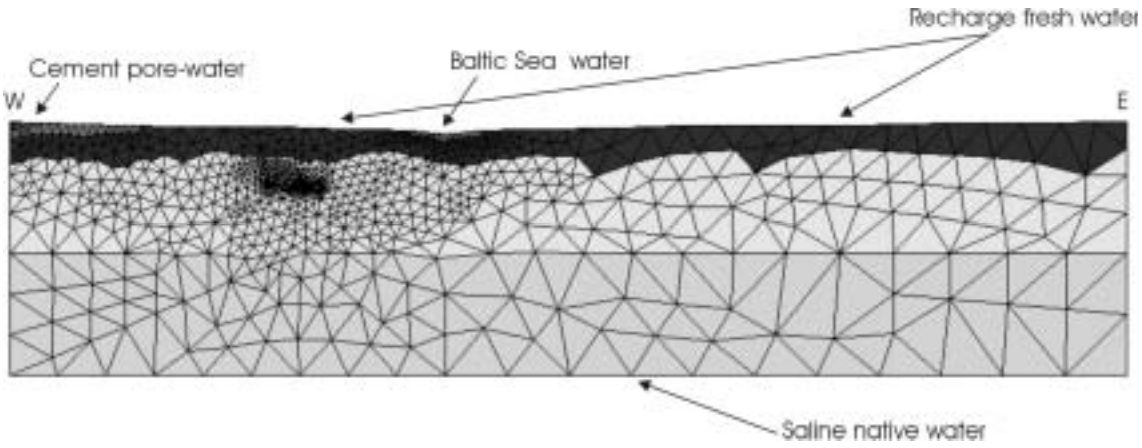

Figure 3-25. *Hydrochemical boundary conditions of the numerical model for evaluating the role of the rock landfill.*

Table 3-2. Solute concentrations (Mol/L) and constrains used for the landfill pore water.

Chemical	Concentration	Constrain
OH^-	3.49×10^{-2}	Charge balance
$Al(OH)_4^-$	1.48×10^{-5}	Katoite
K^+	6.65×10^{-5}	Recharge water
Na^+	6.69×10^{-4}	Recharge water
Ca^{2+}	9.51×10^{-3}	Portlandite
Mg^{2+}	4.92×10^{-9}	Brucite
SiO_2	9.04×10^{-6}	Foshagite
HCO_3^-	1.59×10^{-6}	Calcite
SO_4^{2-}	2.16×10^{-3}	Ettringite
Cl^-	1.69×10^{-4}	Recharge water
T (ºC)	25	
pH	12.45	

As in all previously performed runs of the reactive transport numerical model, this new run accounting for the rock landfill pore waters covers a time horizon of 5,000 days in order to reach consistent initial conditions for any change done in the numerical model. In this manner, the initial 4,000 days of the numerical model are used to simulate natural undisturbed conditions, prior to the hydraulic disturbance produced by the presence of the tunnel.

Figure 3-26 shows computed results of sulphate concentrations distribution for both, undisturbed conditions and the final time of the Redox Zone Experiment. It can be seen in Figure 3-26a that considering the potential influence of the landfill, a typical plume of landfill-leachate (as proposed by /Freeze and Cherry, 1979/) is numerically computed for the undisturbed conditions of the Redox Zone Experiment. The influence of the rock landfill (in terms of sulphate concentrations) reaches the future tunnel location. However, flow and reactive transport numerical modeling predicts an attenuation of the landfill-leachate plume at the end of the experiment (Figure 3-26b). It can be noticed in Figure 3-26 that after reaching new steady-state concentrations for disturbed conditions, the landfill-leachate plume becomes shorter (Figure 3-26b).

Figure 3-27 shows computed sulphate concentrations behaviour within the tunnel surroundings (borehole KR0015B). Numerically computed results show a better agreement with measured undisturbed concentrations (time = 0) if the rock landfill is considered (it can be checked by comparing Figures 3-24 and 3-27). However, the presence of the rock landfill is not a plausible explanation for the important sulphate increase measured near the tunnel during the Redox Zone Experiment. The occurrence of the rock landfill produces a slight increase in sulphate concentrations for undisturbed conditions but, a sulphate dilution is computed during the experiment around the tunnel (Figure 3-27). This computed sulphate dilution is due to the arrival of both, deep and shallow groundwaters, which have lower values of dissolved sulphate than the landfill-leachate water.

Figure 3-26. *Numerically computed sulphate concentrations distribution (Mol/L). A) Undisturbed conditions, prior to tunnel intersection. B) End of the experiment (983 days after tunnel intersection).*

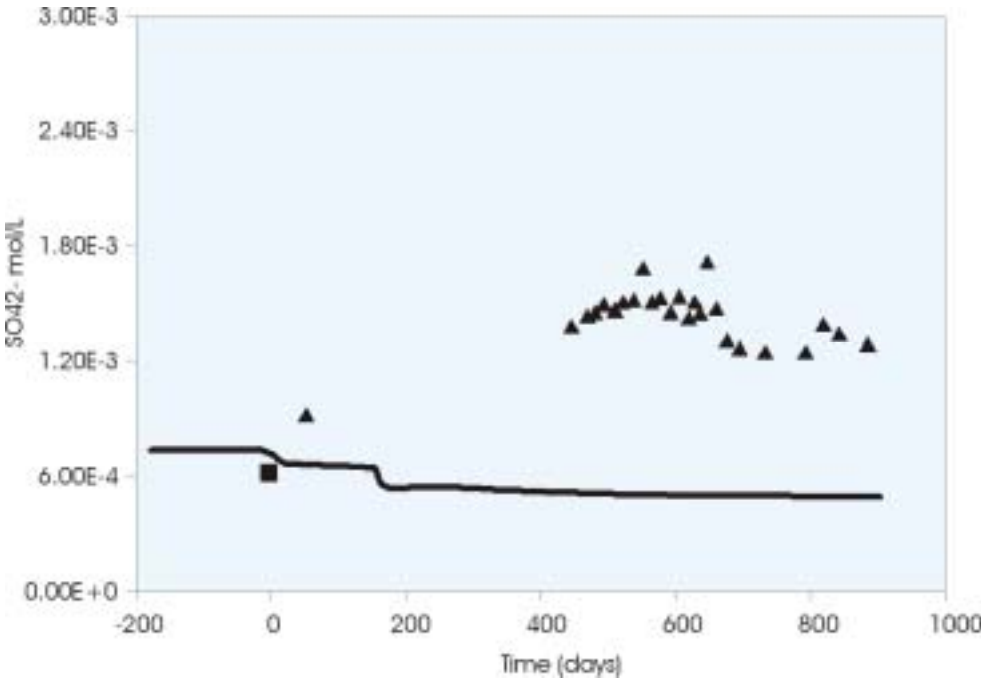

Figure 3-27. *Measured (symbols) and computed (lines) sulphate concentrations during the Redox Zone Experiment, at borehole KR0015B. Numerical results rule out the possibility of the rock landfill being responsible for measured sulphate behaviour.*

3.7 Evaluating the role of seafloor sediments

Different types of sediments exist on the shallowest part of the Äspö area, as a result of the paleogeographical evolution of the Baltic Shield during the Quaternary Period. Sediments of the archipelago surrounding the island of Äspö have been extensively studied by /Sundblad et al, 1991/, /Landström et al, 1994/ and /Sundblad and Mathiasson, 1994/. The general stratigraphy of the clay sediments in the Baltic seafloor is composed by three main units:

Glacial clay and silt (usually varved due to an annually rythm in the sedimentation)

Transition clay

Postglacial mud /Sunblad et al, 1991/.

These seafloor sediments are loaded with monosulphides, dominated by iron sulphides, with a typical smell of H_2S /Wallin, 1995/. Pore water analyses in the deeper silty layers of the sediments show extremely high concentrations in sulphate, indicating that an extensive oxidation of monosulphates is going on /Wallin, 1995/. Obviously, monosulphides produced during bacterial sulphate reduction in the past are now being oxidized causing high sulphate concentrations in that part of the sedimentary column. Probably, fresh water discharge from the shallow groundwater systems to the Baltic estuaries is preferentially concentrated in these silty (even sandy) layers which should have higher hydraulic conductivity than clay and mud layers. /Sundblad et al, 1991/ report sulphate concentrations within Baltic sediment pore waters up to 2,350 mg/L.

The hydraulic disturbance produced by tunnel and borehole reaches the Baltic estuary location (see Figure 3-14), and groundwater flows from this position to the tunnel surroundings during the Redox Zone Experiment. Then, seafloor sediments could also constitute a sulphate source in the Redox Zone Experiment. To evaluate this conjecture, a new run of the flow and solute transport numerical model was performed. The only difference of this new run (with respect to the base run) was a change in the Baltic water composition (by sediment pore water composition). Measured pore water in the sediment core SAS-21 /Sunblad et al, 1991/ was selected because the highest sulphate concentration (2,350 mg/L) was measured within this core. Then, the most favourable scenario is selected for testing this hypothesis. Chemical composition of the seafloor sediments pore water used in the numerical model can be consulted in /Molinero, 2000/.

Figure 3-28 shows sulphate concentration distribution computed numerically. It can be seen that, as expected, a sulphate-rich plume is developed from the Baltic estuary to the tunnel surroundings. A comparison between measured and numerically computed sulphate concentrations (versus time) within the tunnel surroundings is shown in Figure 3-29. A slight increase in sulphate concentrations is computed around the tunnel due to the arrival of Baltic influence (Figure 3-29; after 200 days). However, measured sulphate shows a more drastic increase than computed values (Figure 3-29).

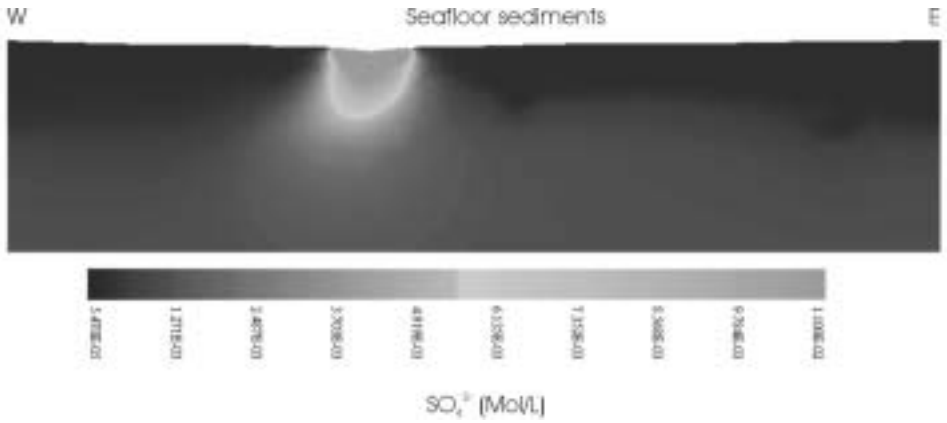

Figure 3-28. *Numerically computed sulphate concentrations distribution (Mol/L) at the end of the experiment.*

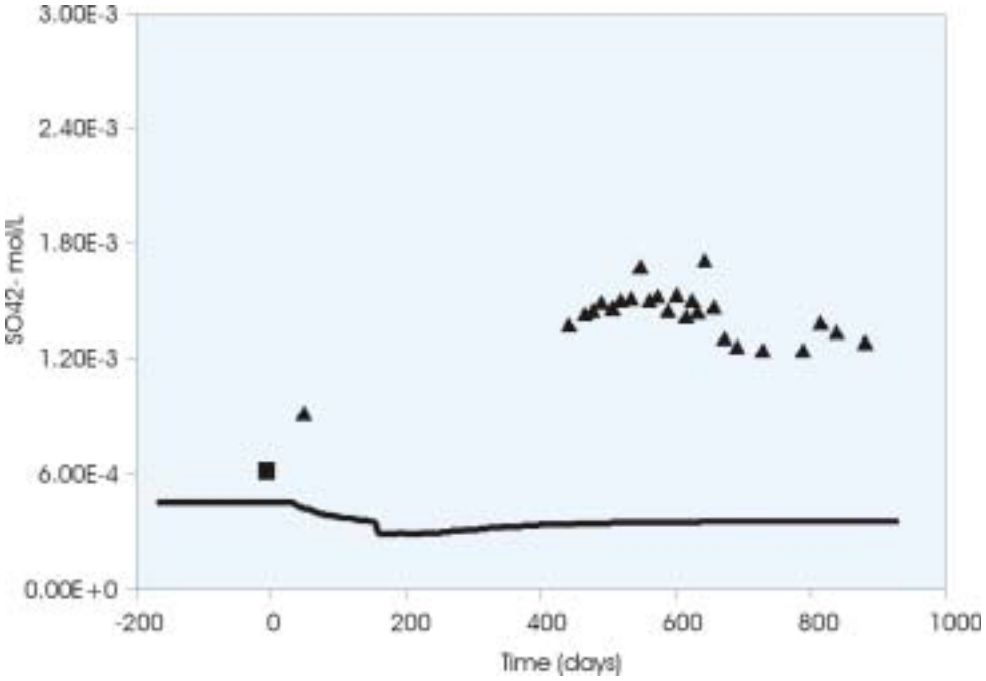

Figure 3- 29. *Measured (symbols) and computed (lines) sulphate concentrations during the Redox Zone Experiment, at borehole KR0015B. Numerical results indicate that seafloor sediments cannot be the only source of sulphate during the Redox Zone Experiment.*

The $\delta^{34}S$ isotope signatures of the dissolved sulphate suggest a multiple source of sulphur /Wallin, 1995/. The early readings of the dissolved sulphate are all significantly higher than at the end of the experiment and the mean values were around + 19 per mil, strongly indicating a marine signature as one possible sulphur source /Wallin, 1995/. /Wallin, 1995/ states that the significant lowering of the $\delta^{34}S$ recorded along the experiment suggests that the sulphur contribution could be mainly oxidation of late precipitates of monosulphides in a previously semi-open bacterial sulphate reducing environment. This kind of environment is similar to that described for the seafloor sediments. However, it has been shown that this hypothesis is unable to explain quantitatively the measured sulphate increase in the Redox Zone Experiment.

Numerical results indicate that seafloor sediments constitute a source of sulphate (which in addition is consistent with isotopic studies) which, however, cannot explain measured concentrations. Additional sources of sulphate must exist in order to explain field measurements.

3.8 Chapter conclusions

The flow and transport model shown in Chapter 2 was used to perform coupled groundwater flow and reactive solute transport simulations of the Redox Zone Experiment. The reactive transport numerical model accounts for more than 60 homogeneous reactions, including aqueous complexation, acid-base, gas dissolution and redox processes, as well as 5 heterogeneous reactions including mineral dissolution/precipitation and cation exchange. The model reproduces the observed concentrations of most dissolved species both before and after tunnel construction.

Numerical analyses indicate that fresh recharge waters have reducing conditions which are consistent with measured values of dissolved iron at a depth of 5 m. In addition, it was found that hematite is the iron mineral phase controlling dissolved iron in groundwaters.

Numerical calibration of the cation exchange capacity leads to a value higher than that evaluated on the basis of reported clay contents. Numerical results are consistent with an average clay content on the order of 5%.

Although calcite dissolution takes place in the surroundings of the tunnel, this process is not able to explain the increase of bicarbonate concentrations measured near the tunnel. Microbially-mediated degradation of organic matter through iron (III) mineral reduction is the most likely chemical process to explain such observations. A performed analysis of measured data of bicarbonate, iron, ^{13}C and ^{14}C in water samples collected at different boreholes allows one to suppose that the rock landfill could be a "hot spot" for organic matter degradation.

The model predicts also the dissolution of pyrite around the tunnel but this process cannot explain the measured sulphate evolution. Numerical results support the hypothesis of that sulphate reducing bacteria could be present in the fracture zone prior to tunnel intersection. After the start of the experiment, fresh groundwater flowing towards the tunnel increases the input of suitable electron donors (organic matter) in the tunnel surroundings. This could have enhanced the activity of iron reducing bacteria, which at the same time could inhibit the growth of sulphate reducer microorganisms by out-competition.

The coupled groundwater flow and reactive solute transport numerical model was used to test additional hydrochemical hypotheses. Numerical results rule out the possibility of a source of sulphate coming from alkaline sulphate-rich waters leaching from a nearby rock landfill. They also rule out the hypothesis of dissolution of iron monosulphides within Baltic seafloor sediments as being responsible for the evolution of sulphate. By discarding these hypotheses one may conclude that competitive anion adsorption is the most likely geochemical process influencing sulphate behaviour during the Redox Zone Experiment.

Coupled flow and reactive transport numerical model results are markedly different than those computed with a model of pure mixing and chemical reactions. Computed results not only are different but they show opposite trends in mineral behaviour. It can be concluded that end-members mixing and reaction models are inappropriate for modeling hydrodynamic systems.

4 Numerical model of coupled reactive solute transport and microbial processes

4.1 Introduction

This chapter deals with coupling microbial processes and the inorganic reactive transport model presented in the previous chapter.

As pointed out in Chapter 3, the groundwater flow and reactive transport model was able to reproduce measured behaviour of groundwater heads and the evolution of most dissolved species. However, it was not possible to represent properly measured evolution of dissolved bicarbonates and sulphates during the Redox Zone Experiment, probably because these species are affected by microbially-driven reactions.

Different models have been developed in order to account for microbial processes. First of all, a two dimensional model was attempted, including a simplified conceptual model for microbial reactions. However, the large CPU time required to solve such a model together with the poor convergence behaviour led us to consider a simpler 1D reactive transport model. Based on the 1D model, microbial parameters were calibrated easier. Then, a thorough sensitivity analysis was performed for most of the microbial parameters.

Microbially-driven organic matter fermentation and oxidation by iron-reducer are considered as the dominant microbial processes controlling the redox status and the concentration evolution of bicarbonate and sulphate.

4.2 Microbes and possible microbial processes at the ÄSPÖ site

The REX Project of Äspö was launched to study O_2 depletion processes by creating a controlled oxidizing perturbation in a deep rock environment at the Äspö HRL. Oxygen was injected into a fracture zone and water samples were collected which were used for microbiological research. /Kotelnikova and Pedersen, 1999/ report that:

(1) Groundwater in fracture zone and the surface of the granite contain abundant and diverse microbial populations. The populations include not only anaerobic microorganisms as could be expected in the reduced environment, but also facultative aerobic and microaerophilic organisms (see Table.4.1).

(2) Several microbially-catalyzed reactions may theoretically contribute to biomass production in accordance to available nutrients for biomass production.

(3) Both attached and dissolved microorganisms could be responsible for the oxygen depletion observed under in situ conditions.

Table 4-1. Microbial population in the groundwater of KA2862A (section 7.4–16 m), sampled during the REX experiment directly from the borehole /Kotelnikova and Pedersen, 1999/.

Date	07/07/98	28/01/99	12/03/99
Time after oxygen injection (day)	28	14	12
Total microbial counts (AODC), (cells/L)	2.02×10^5	1.12×10^5	7.31×10^4
Aerobic heterotrophic microorganisms (cells/ml)	2.40×10^4	5.18×10^3	0
Microaerophilic heterotrophic microorganisms (cells/ml)	2.90×10^3	4.08×10^4	555
Microaerophilic methane-oxidizing bacteria group I (cells/ml)	1.49×10^4	31	21
Aerobic hydrogen-oxidizing bacteria (cells/ml)	4600	50	0
Anaerobic sulphate-reducing bacteria (cells/ml)	1800	2.50×10^4	2.95×10^4
Anaerobic iron-reducing bacteria (cells/ml)	1335	1010	1010
Anaerobic methane-producing archea (cells/ml)	46	4080	0

Table 4-1 lists the microbial populations detected in the groundwater in borehole KA2862A (2862 m from the entrance of the tunnel) which demonstrates a very diverse microbial flora. Data in Table 4-1 indicate that, in the section of 7.4–16.0 m, after oxygen injection (which can be an inhibition to the iron- and sulphate-reducing bacteria), iron- and sulphate-reducing bacteria still appear with pronounced numbers. The number of iron-reducing organisms increases from 1.2–2.3% in borehole KA2862A to 0.2–55% in the REX chamber after a low oxygen pulse. The viable counts of sulphate- and iron-reducing bacteria are negatively correlated with increasing redox potential.

A wide variety of microorganisms, including fungi, facultatively anaerobic bacteria, and strict anaerobes are capable of reducing iron. Some of these organisms are capable of oxidizing completely organic compounds to CO_2, while others are incomplete oxidizers. Iron-reducing bacteria are known to catalyze the oxidation of aromatic compounds, including important intermediates of anaerobic decay. Some iron-reducers are capable of using a variety of electron acceptors, including Mn(IV), U(VI), NO_3^-, NO_2^-, SO_4^- and even oxygen.

/Kotelnikova and Pedersen, 1999/ detailed a microbial speciation in the groundwater of the fracture zone and the relevant metabolisms including the required organic matter and electron acceptors for each microbe.

Water samples for microbial investigation of the REX experiment were collected from section 7.4–16 m. Microbial population in the deeper groundwater of the fracture zone should show some differences due to the fact that the redox potential at depth is more reducing. Samples were usually collected after an oxygen injection which inhibits anaerobic organisms such as iron reducer and sulphate reducer. However, samples from shallow groundwater have shown a large content of iron-reducers. In favourable conditions (enough carbon source and ferric minerals) the bacteria can be further activated.

An increase in HCO_3^- and SO_4^{2-} concentrations in the groundwater leaking from the roof of the tunnel and boreholes KR0012B, KR0013B and KR0015B was observed (see Chapter 3 and Figure 4-1). /Banwart et al, 1999/ and /Banwart, 1999/ suggested that the source of HCO_3^- was the degradation of organic matter coming from the shallow fresh water. Microbiological investigations demonstrate a high diverse microbial activity that supports this hypothesis. /Kotelnikova and Pedersen, 1998/ detailed a microbial speciation and the relevant metabolisms including the required organic matter and electron acceptors for each microbe. The final product of organic matter in biodegradation processes is HCO_3^- or CO_2, although many intermediate products may also appear. Except for anion exchange, this is the unique possible source of HCO_3^- because the prevailing quasi saturation and/or oversaturation with respect to calcite precludes calcite dissolution.

As shown in Figure 4-1, the evolution of dissolved sulphate is similar to that of bicarbonate. In addition, bicarbonate concentrations at KR0012B and KR0015B show a positive correlation to the concentration of dissolved organic matter (DOC), although available DOC data show a wide scatter (Figure 4-2). This observation provides additional evidence for the source of bicarbonate being biodegradation of DOC.

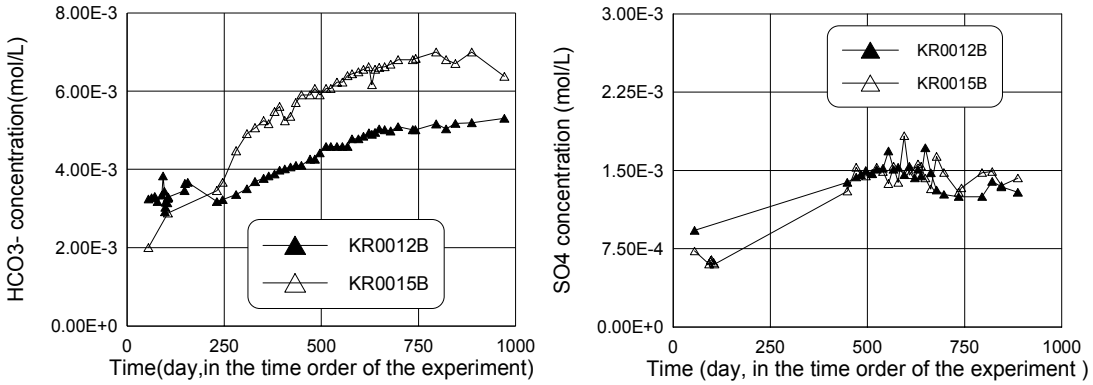

Figure 4-1. *Bicarbonate and sulphate concentrations measured at KR0012B and KR0015B boreholes. These boreholes are located at both sides of the open borehole KR0013B.*

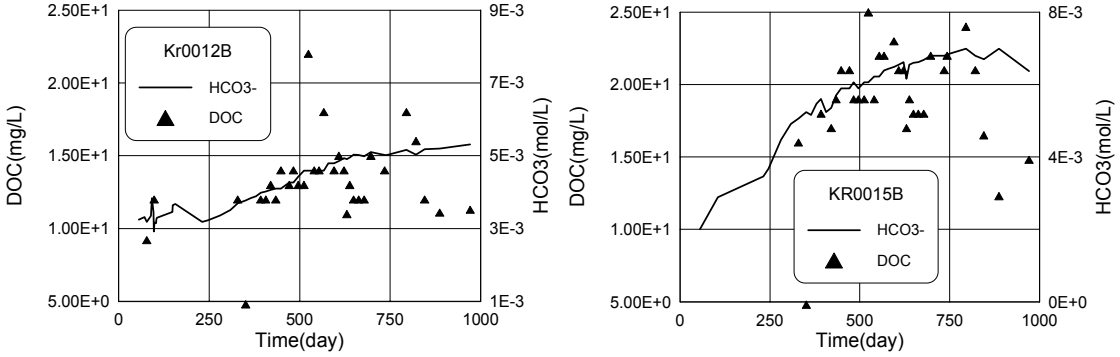

Figure 4-2. *Concentration time evolution of bicarbonate at KR0012B and KR0015B are correlated with concentration of DOC.*

Possible sources of sulphate include: (1) dissolution of minerals such as pyrite and gypsum; (2) recharge water containing high concentration of sulphate /Pitkänen et al, 1999/ and (3) anionic exchange between bicarbonate and sulphate /Bruton and Viani, 1997/.

At first, mineralogical investigation concluded that there is not enough amount of gypsum to be dissolved. The solubility of both gypsum and pyrite in the geochemical conditions of the fracture zone rules out the possibility of a sulphate source coming from the dissolution of these minerals.

The hypothesis of a source of water containing high sulphate concentration is not consistent with available data. If there were a high sulphate containing recharge water, data from boreholes HBH02B and HBH05B at 15 m and 10 m depth, respectively should show it first. In fact, sulphate concentrations at HBH02 and HBH05B are low and stable. In addition, sulphate concentrations at HBH01B (35 m deep) show the same behaviour to that of KR0012B and KR0015B (Figures 4-1 and 4-3). Borehole HBH01B is almost vertically below HBH02B and is at downstream of both HBH02B and HBH05B. How can it be that sulphate is high downstream and low upstream?. /Molinero, 2000/ tested the hypothesis of a sulphate-rich source of water leaching from a nearby rock landfill. Model results clearly discard this hypothesis.

The key for anionic exchange is that sufficient exchange capacity is required. /Banwart, 1997/ carried out calculations of the adsorption equilibrium and concluded that if anion exchange occurs, the adsorption capacity should be on the order of 0.2 mol/L in order to explain the increase of SO_4^{2-} concentrations observed during the experiment. It is worth to point out that /Bruton and Viani, 1997/ proposed that anion exchange may occur. However, based on the laboratory batch experiments, these authors also concluded that the total adsorption capacity in the fracture zone is too small to occur a significant anion exchange which could induce a pronounced increase in sulphate concentration.

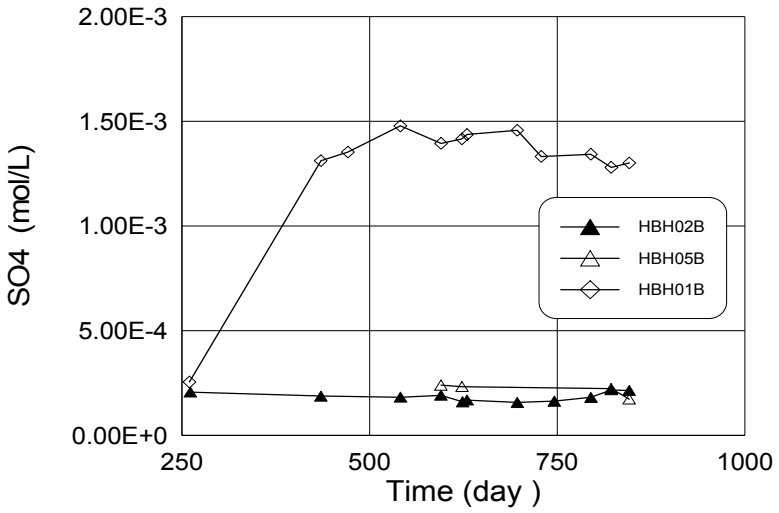

Figure 4-3. *Sulphate concentrations measured at boreholes HBH02B and HBH05B which are low and very stable compared to those at HBH01B and KR0012B and KR0015B.*

One has to look for another sulphate source in order to explain the observed sulphate concentration evolution. There is an organic-rich sediment layer with a thickness of 0.2 m composed of deposition of organic litter from the pine canopy which overlies a zone of reworked sand and gravel. Organic litters from pine canopy contain resin. A typical component of resin is organic sulphur. In addition, as the fossilized resin, amber is also a sulphur-containing 'mineral'. The famous Baltic amber contains up to 0.46% sulphur which is inherited from resin*. So, organic sulphur (sulphur containing organic matter) is a possible source of sulphate. Otherwise, Baltic sea sediments also contains abundant organic sulphur.

Organic sulphur is firstly fermented in the shallow anaerobic zone (the possible depth is 10–20 m) releasing intermediate dissolved organic matter, such as fatty acids and aromatic compounds, sulphur compound (sulphate or hydrogen sulphate) and possibly ammonium:

$$\text{Org.S} + H_2O \rightarrow \text{Fatty acids} + \text{aromatic compounds} + \text{sulphur compound} \quad (4\text{-}1)$$

Microbiological investigations /Kotelnikova and Pedersen, 1999/ in the REX experiment indicate that fermentation is a common microbial process taking place in the fracture zone which is carried out by anaerobic *rods* and *cocci*.

In the redox condition of deeper fracture zones HS^- is unstable and is oxidized by Fe(III) or Mn(IV) according to:

$$HS^- + Fe^{3+}_{(\text{mineral source})} + 4H_2O = SO_4^{2-} + Fe^{2+} + 9H^+ \quad (4\text{-}2)$$

This is the overall reaction which may take place with several intermediate steps. However, the redox potential of the equilibrium pair $HS^- \Leftrightarrow SO_4^{2-}$ is much lower than that of $Fe^{3+} \Leftrightarrow Fe^{2+}$. This means that in an environment containing sufficient Fe(III) minerals HS^- should be eventually oxidized into SO_4^{2-}. This can be a significant source of sulphate.

In addition, as a product of fermentation, dissolved organic matter (DOC) can be transported into deeper parts of the fracture zone. DOC then is further degraded by *heterotrophic* bacteria such as iron-reducing bacteria. The final product of biodegradation is the HCO_3^- according to:

$$DOC + Fe^{3+} \rightarrow HCO_3^- + Fe^{2+} \quad (4\text{-}3)$$

Not only the ferric iron is employed here as an electron acceptor, as reported by /Kotelnikova and Pedersen, 1999/, but other compounds such as Mn^{4+} and NO_3^- can also be employed as electron acceptors.

Observed concentrations of Mn^{2+} (Figure 4-4) show an increase after opening KR0013B. This could be due to Mn^{4+} or Mn^{3+} reduction yielding Mn^{2+} as part of biodegradation processes. Mn^{2+} is more soluble than Mn^{4+} and Mn^{3+}. Mn concentrations decrease after around 300 days, possibly be due to the second dilution stage which would have different behaviour from that of the first dilution stage.

* (see the Web page: World of Amber, http://www.emporia.edu/earthsci/amber/amber.htm, by Susie Ward Aber, Emporia State University, Kansas, USA).

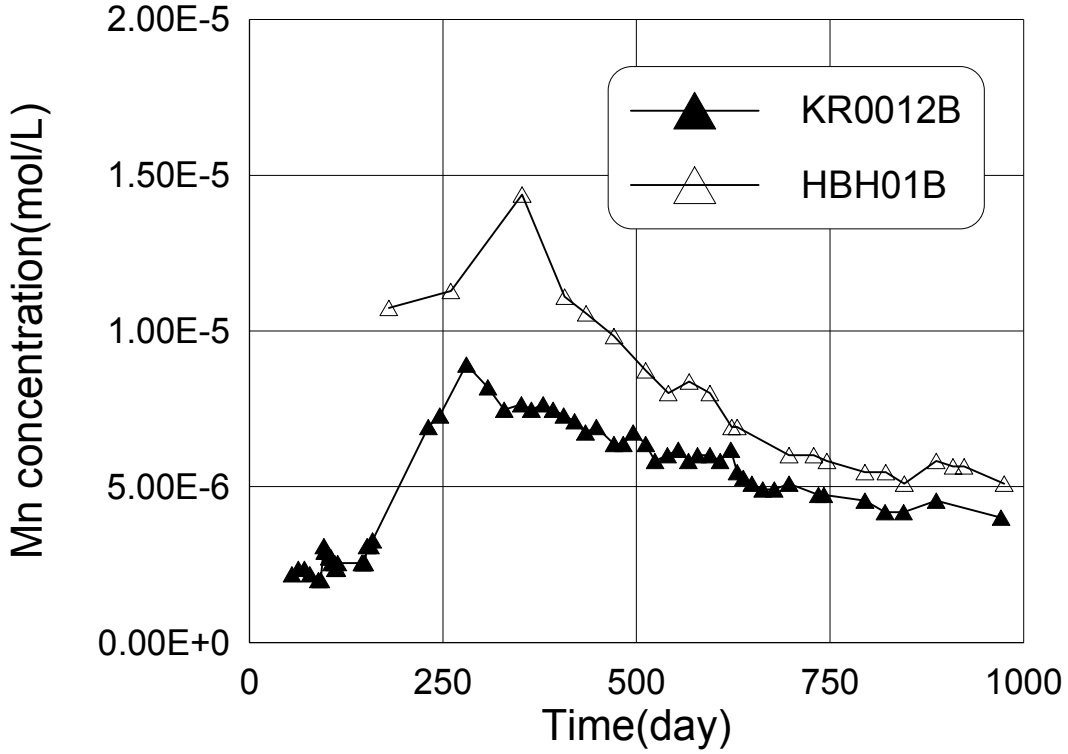

Figure 4-4. *Observed Mn^{2+} concentration evolution at HBH01B and KR0012B.*

The use of Mn as electron acceptor is limited by $Mn^{4+} \Leftrightarrow Mn^{2+}$ when the redox potential ranges from –0.05 to –0.15 V. According to Mn concentration evolution, it is believed that Mn is employed within the depth of 20–70 m. We conclude that the location of borehole KR0012B is more tightly connected to the location of HBH01 rather than with KR0015B, although KR0012B and KR0015B are closer to each other. Mn concentrations in KR0012B and KR0015B boreholes do not show the same behaviour in spite of the fact that they are located at the same depth. This could be due to the heterogeneity of the fracture zone.

In summary, possible microbial processes in the fracture zone include:

1) Fermentation of Particulate Organic Carbon (POC)

This is the first step of the decomposition of organic matters. Fermentation processes degrade insoluble macromolecular organic matters into various soluble organic acids, hydrocarbon chains and cycles which can be further degraded into aerobic, facultative aerobic, anaerobic and obligate anaerobic metabolism. These processes also release nitrogen and sulphur compounds because organic nitrogen and sulphur are common components of proteins and other macromolecular organic matters. Particulate organic matters (POC, insoluble macromolecular organic matters) at the Äspö site are originated from pine canopy in which a pronounced amount of organic sulphur is contained. The fermentation of these sulphur-containing organic matters releases sulphur compounds which could be one of the sulphate sources in the system under aerobic, facultative aerobic and some anaerobic conditions.

2) Aerobic degradation of dissolved organic matter

Dissolved organic matter released from fermentation processes is degraded first by dissolved oxygen yielding carbon dioxide or bicarbonate. This process is expected to happen in the shallow parts of the aquifer and/or near to the tunnel wall during excavation.

3) Anaerobic biodegradation by Fe (III) and/or Mn (IV) reduction

Fe and Mn reduction commonly takes place in anaerobic parts of the fracture zone, which causes an increase in bicarbonate concentration and ferrous mineral precipitation. These processes are expected to occur in the main part of the fracture zone.

After some time, dissolved Fe concentration in the tunnel inflows decreased to near zero for a period of a few weeks followed by a quasi stable low concentration. This could be taken as an indication of the arrival of an oxidation front to the tunnel position /Banwart et al, 1999/. Another possible explanation for the decrease in iron concentration is the aeration of the groundwater near the tunnel wall. The tunnel wall is in direct contact with the air. Diffusion of oxygen gas may oxidize Fe(II) and reduce the concentration of Fe. Oxygen diffusion through the tunnel wall can also induce aerobic biodegradation, yielding bicarbonate and causing an increase in bicarbonate concentration.

4.3 Previous microbial model of /Zhang, 2001/

Based on the reactive transport modelling work carried out by /Molinero, 2000/, Zhang constructed a hydrobiogeochemical reactive transport model which considers microbial iron reduction to evaluate whether microbially-driven DOC oxidation could explain the source of bicarbonate and sulphate /Zhang, 2001/. This model adopted all concepts of Molinero's water flow and abiotic geochemical reactive transport model and employed a different finite element mesh /Molinero, 2000/. Flow and transport parameters were calibrated again and got similar values to those of Molinero's model.

Fermentation of Particulate Organic Carbon (POC) takes place in the shallow anaerobic zone where POC can be enriched and the intrusion of oxygen coming from the surface can be consumed the aerobic metabolism near the surface. Fermentation provides the source of Dissolved Organic Carbon (DOC). In the fermentation processes, organic sulphur contained in POC is released in the form of reduced sulphur such as HS^-. DOC and HS^- are then transported and oxidized in deeper parts containing Fe (III)-mineral-enriched-zone.

These processes can be represented by:

$$POC+H_2O \Rightarrow DOC+HS^-+H^+ \quad (4\text{-}4)$$

$$DOC+Fe^{3+} \Rightarrow HCO_3+H_2O+ Fe^{2+} \quad (4\text{-}5)$$

$$HS^-+Fe^{3+} \Rightarrow SO_4^{2-}+Fe^{2+} \quad (4\text{-}6)$$

In fact, not only Fe^{3+} can be employed as an electron acceptor in the biodegradation of DOC. Other species such as Mn^{4+}, Mn^{3+}, NO_3^- as well as O_2 can also be employed as electron acceptors. /Kotelnikova and Pedersen, 1999/ and /Puigdomenech et al, 2001/ found that there are many diverse microorganisms in the fracture zone. Each microbial

species dominate in different positions (see Section 4.2). In the tunnel position, Fe^{3+} and Mn^{4+} are employed as electron acceptors.

In this model only Fe^{3+} was considered as the electron acceptor to account for the oxidation of DOC. By disregarding fermentation processes and other species as electron acceptors, the above iron reduction-DOC oxidation process was combined with other fermentation products, HS^- and H^+, (Equation 4-5 and Equation 4-6) into a single equation:

$$\alpha DOC+\beta HS^-+\gamma Fe^{+3}+\delta H^+ => \varepsilon HCO_3^- +\zeta SO_4^{2-} +\gamma Fe^{2+}+\delta H_2O \qquad (4\text{-}7)$$

The stoichiometric coefficients α, β, γ, δ, ε, ζ, γ and δ are uncertain because the molecular structure of DOC is unknown. Kinetic rates and proportionality coefficients must be calibrated. The rate of reaction (4.7) is assumed to be controlled by Monod kinetics according to:

$$R_{Fe-reducer} = \mu_{max} C_{Fe-reducer} \frac{C_{DOC}}{K_{DOC} + C_{DOC}} \frac{C_{Fe^{3+}}}{K_{Fe^{3+}} + C_{Fe^{3+}}}$$

with

$$R_{DOC} = \frac{R_{Fe-reducer}}{Y_{DOC}}$$

$$R_{HCO_3^-} = f_c R_{DOC},\ f_c = \frac{\varepsilon}{\alpha}$$

$$R_{Fe^{3+}} = f_a R_{DOC},\ f_a = \frac{\gamma}{\alpha}$$

where μ_{max} is the specific growth rate of iron-reducer (g biomass/day); C is concentration and subscripts represent the corresponding species (g biomass/L, g DOC/L and moles/L for chemical species); K is the half-saturation constant (g/L for DOC, moles/L/day for Fe^{3+}), R is the rate of the reaction (g/L/day for DOC and moles/L for chemical species). Y_{DOC} is the yield coefficient of DOC to iron reducer (g biomass/ g DOC), f_c is the transformation coefficient between DOC and HCO_3^- (moles HCO_3^-/g DOC), and f_a the proportional coefficient between DOC and Fe^{3+} (moles Fe^{3+}/g DOC).

Considering that HS^- is simultaneously and proportionally released from fermentation processes with DOC:

$$R_{HS^-} = f_s R_{DOC},\ f_s = \frac{\beta}{\alpha}$$

Then, one has:

$$R_{SO_4^{2-}} = R_{HS} = f_s R_{DOC}$$

The rate of H^+ is also related to that of DOC through:

$$R_{H^+} = f_H R_{DOC},\ f_H = \frac{\delta}{\alpha}$$

Microbial parameters are calibrated by fitting computed concentrations to measured values of bicarbonate and sulphate. Calibrated parameters are listed in Table 4-2.

Figures 4-5 and 4-6 show the computed concentration evolution of bicarbonate and sulphate as well as the comparison with measured data. Figure 4-7 illustrates the comparison of computed DOC and measured DOC at –70m.

Table 4-2 Calibrated microbial kinetic parameters and coefficients.

Parameters and coefficients	Values
Maximum growth rate (specific rate) of iron reducer (μ_{max})	0.11137 day^{-1}
Yield coefficient of DOC to iron-reducer (Y_{DOC})	6.5×10^{-3}g biomass/g DOC
Half-saturation coefficient of DOC (K_{DOC})	6.22×10^{-3} g/L
Half-saturation coefficient of Fe^{3+} ($K_{Fe^{3+}}$)	3.25×10^{-10} moles/L
Proportional coefficient between DOC and HCO_3^- (f_c)	– 0.052 mol HCO_3^-/g DOC
Proportional coefficient between DOC and Fe^{3+} (f_a)	0.021 mol Fe^{3+}/g DOC
Proportional coefficient between DOC and sulphate (f_s)	– 0.008 moles SO_4^{2-}/g DOC
Proportional coefficient between DOC and H^+ (F_H)	0.0032 moles SO_4^{2-}/g DOC

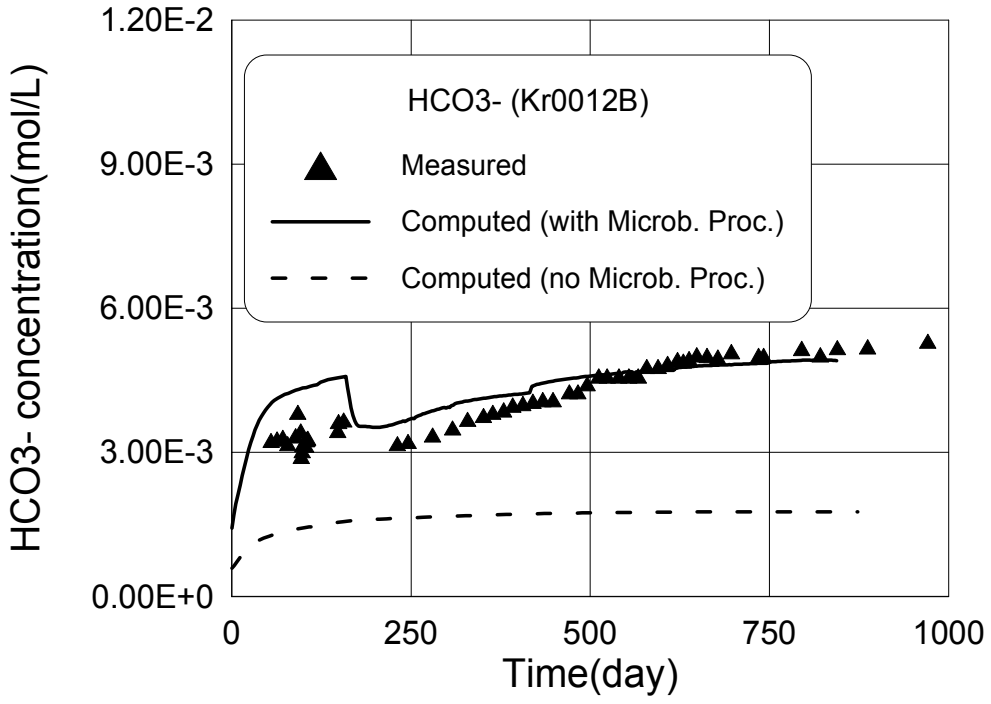

Figure 4-5. *Measured and computed bicarbonate concentrations with and without consideration of microbial oxidation of DOC (according to /Zhang, 2001/).*

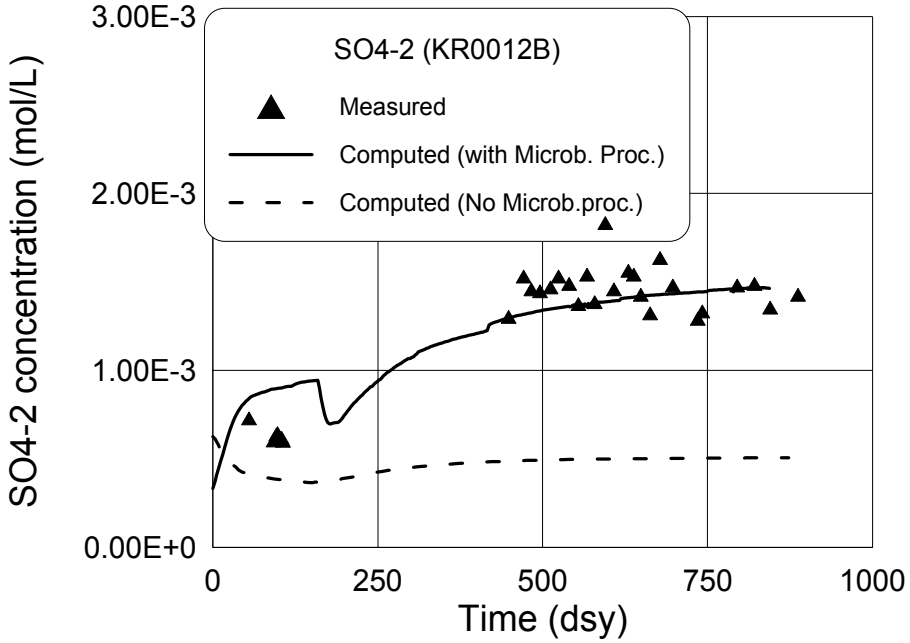

Figure 4-6. *Measured and computed sulphate concentrations with and without consideration of microbial oxidation of DOC (according to /Zhang, 2001/).*

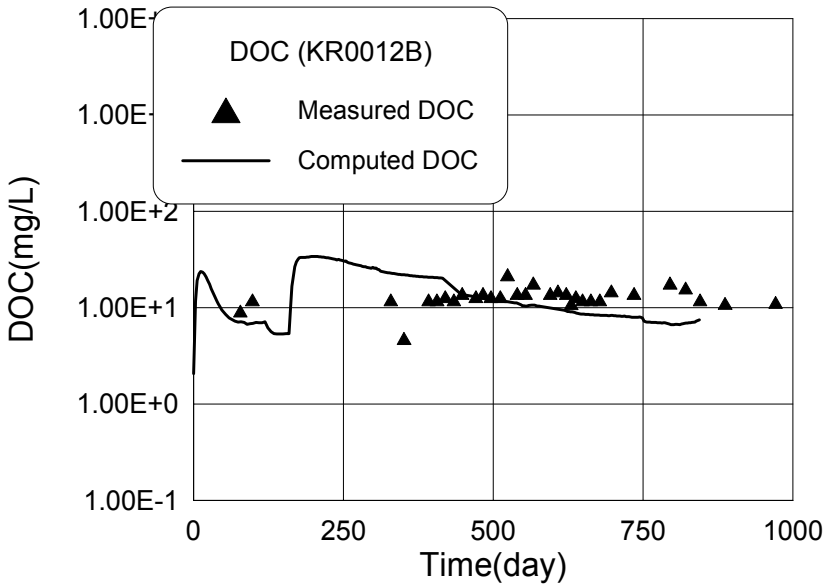

Figure 4-7. *Measured and computed concentration of dissolved organic carbon (DOC) (according to /Zhang, 2001/).*

/Zhang, 2001/ found that SO_4^{2-} and HCO_3^- concentrations were sensitive to permeability, especially the permeability of shallow granite, both before and after tunnel construction. With the calibrated hydraulic conductivity, the model match measured bicarbonate concentration at KR0012B. With a smaller permeability, HCO_3^- data cannot be properly reproduced (Figure 4-8).

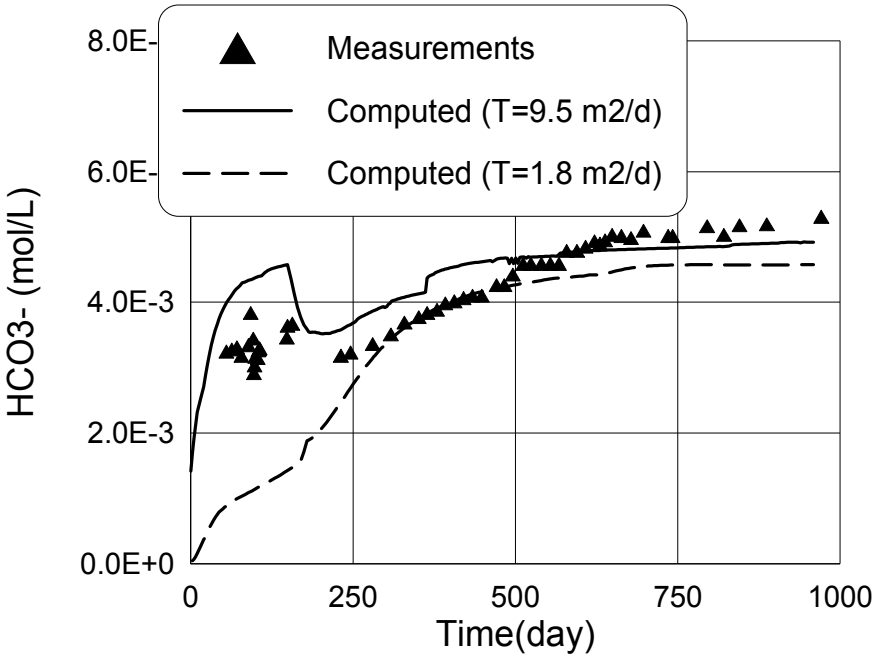

Figure 4-8. *Measured and computed bicarbonate concentration with different hydraulic conductivities for shallow granite at KR0012B (according to /Zhang, 2001/).*

Figure 4-9 shows that the computed bicarbonate concentrations at KR0012B with a model having a smaller permeability do not show the concentration jump which occurred at day 200. However, this behaviour coincides with the concentration evolution at borehole KR0015B although discrepancies occur between computed and measured concentrations (Figure 4-9).

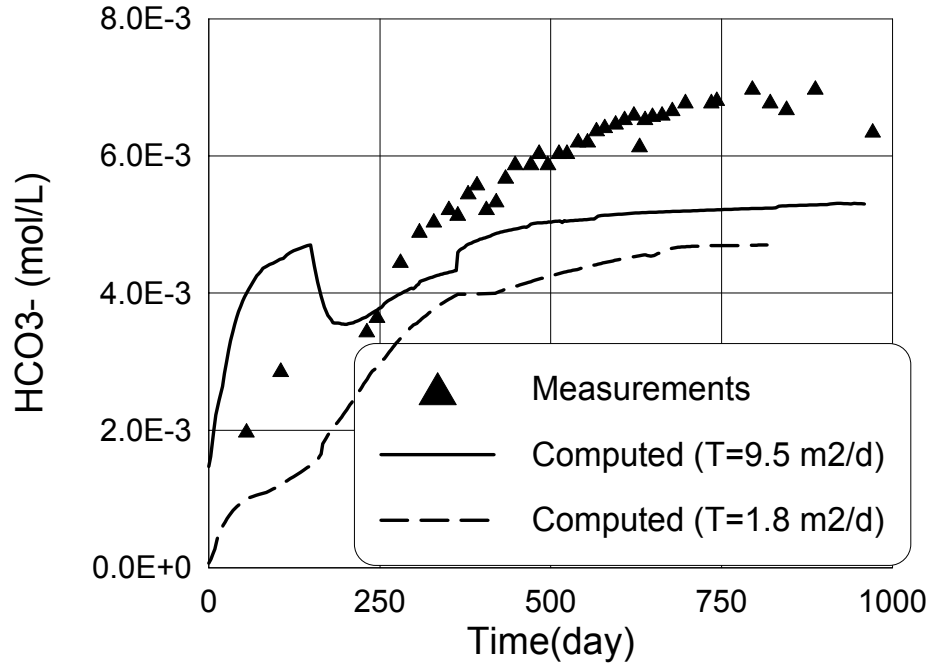

Figure 4-9. *Measured and computed bicarbonate concentrations with different hydraulic conductivities for shallow granite at KR0015B (according to /Zhang, 2001/).*

4.4 Updated microbial models coupled to hydrogeochemical reactive transport

4.4.1 Updated microbial models

As mentioned in Section 4.2, macromolecular organic matter containing sulphur compounds is firstly fermented in the shallow anaerobic zone releasing intermediate Dissolved Organic Carbon (DOC) and sulphur compounds. Then, DOC can be transported to deeper parts of the fracture zone and further degraded by heterotrophic bacteria which employ Fe(III), Mn^{4+}, Mn^{3+}, or NO_3^- as well as O_2 as electron acceptors. The final product of biodegradation is bicarbonate. Organic matter transformation by microbial processes is illustrated in Figure 4-10.

Previous hydrobiogeochemical models /Zhang, 2001/ only considered the oxidation of Dissolved Organic Carbon (DOC) by iron reducer and disregards the fermentation of POC was neglected. Such models can not provide the source of DOC degraded by heterotrophic bacteria (iron-reducer).

In addition, according to Figure 4-10, the amount of sulphur compounds released to the fracture zone depends on the amount of fermented POC by anaerobic bacteria (yeast). But in Zhang's model (Equation 4-7), in order to get the source of sulphate, the amount of sulphur compounds released to fracture zone were artificially related to the oxidation of DOC.

Fermentation of POC should be considered simultaneously with oxidation of DOC in the microbial model. The updated the microbial model presented below accounts for both microbial processes.

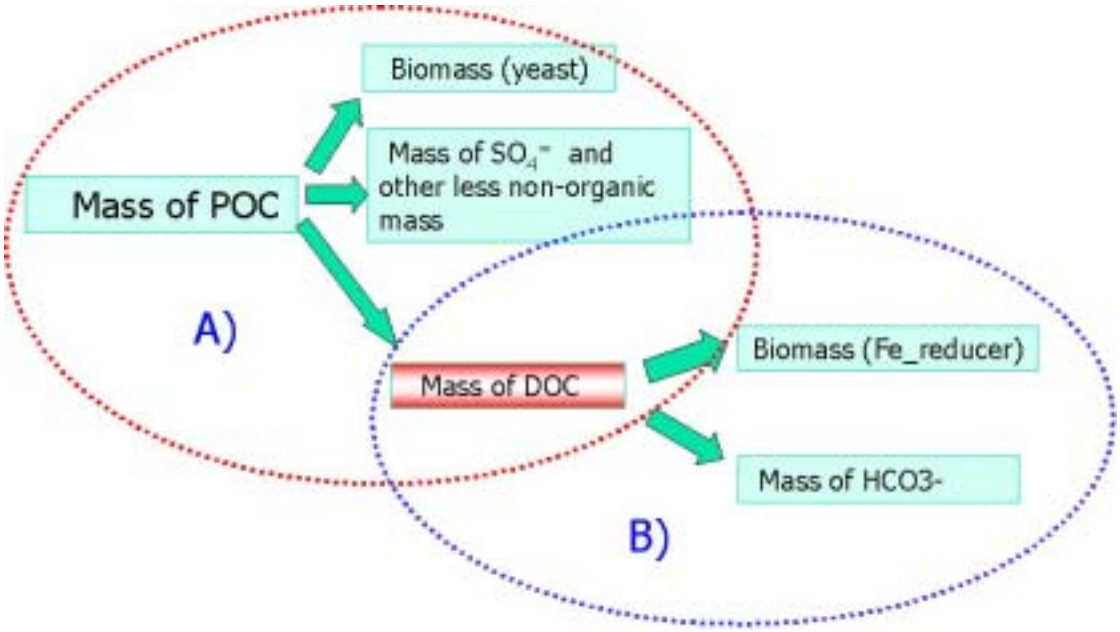

Figure 4-10. *Schematic representation of organic mass transformation. A) Fermentation of POC by yeast. B) Anaerobic biodegradation of DOC by Fe_reducer.*

4.4.1.1 Fermentation

Fermentation is carried out by many anaerobic bacteria. One of them is yeast. A microbial species 'yeast' is defined in the model to represent all fermentation-workers. POC is used as a substrate by yeast. During the fermentation, a lot of intermediate products are used as electron acceptors and these products are abundant. Therefore, the concentrations of electron acceptors do not limit the growth of the yeast. A single Monod expression can be employed to describe fermentation processes. Dissolved Organic Carbon (DOC) and HS^- are the products of POC fermentation. HS^- is oxidized by either O_2 (in local aerobic conditions) or Fe^{+3} minerals yielding SO_4^{-2}. Therefore SO_4^{-2} is assumed to be a direct product of fermentation in the updated microbial model.

The expression of POC fermentation by yeast is assumed to be:

$$\alpha_1 \text{ POC} \xrightarrow{\text{Yeast}} \beta_1 \text{ DOC} + \varepsilon_1 SO_4^{2-} + \gamma_1 \text{H}^+ \tag{4-8}$$

with

$$R_{Yeast} = \mu_{\max} C_{Yeast} \frac{C_{POC}}{K_{POC} + C_{POC}}$$

$$R_{POC} = \frac{R_{Yeast}}{Y_{POC}},$$

$$R_{DOC} = f_a R_{POC}, \; f_a = \frac{\beta_1}{\alpha_1}$$

$$R_{SO_4^{2-}} = f_b R_{POC}, \; f_b = \frac{\varepsilon_1}{\alpha_1}$$

$$R_{H^+} = f_H R_{POC}, \; f_H = \frac{\gamma_1}{\alpha_1}$$

where μ_{max} is the specific growth rate of yeast (gram of biomass/day); C_{Yeast} is concentration of yeast (g/L), C_{POC} is concentration of POC (g/L); K_{POC} is the half-saturation constant (g/L), R is the rate of the reaction. (g/L/day for POC and DOC and moles/L for chemical species); Y_{POC} is the yield coefficient of POC to yeast (g biomass/g POC), f_a is a transformation coefficient between POC and DOC, and f_b is a proportionality coefficient between POC and SO_4^{2-} (moles SO_4^{2-}/g POC).

4.4.1.2 Biodegradation of DOC

As a product of fermentation, DOC is further transported into the deeper part of the fracture zone and degraded by heterotrophic bacteria, such as, iron-reducing bacteria. In the fracture zone, not only Fe^{3+} can be employed as an electron acceptor in the biodegradation of DOC, but other species such as Mn^{4+}, Mn^{3+}, NO_3^- as well as O_2 can also be employed as electron acceptors. In this model Fe^{3+} is considered to be the only electron acceptor to account for the biodegradation of DOC. Taking DOC as a substrate and Fe^{+3} minerals as electron acceptors, iron-reducer grows yielding HCO_3^-. Iron (III) minerals are abundant in granitic rocks and the growth of the iron reducer should not be limited by Iron (III).

The expression of the biodegradation of DOC is assumed to be:

$$\alpha_2 DOC + \gamma_2 Fe^{+3} + \sigma_2 H^+ \Rightarrow \varepsilon_2 HCO_3^- + \gamma_2 Fe^{+2} + \sigma_2 H_2O \qquad (4\text{-}9)$$

with

$$R_{Fe-reducer} = \mu_{\max} C_{Fe-reducer} \frac{C_{DOC}}{K_{DOC} + C_{DOC}} \frac{C_{Fe^{3+}}}{K_{Fe^{3+}} + C_{Fe^{3+}}}$$

$$R_{DOC} = \frac{R_{Fe-reducer}}{Y_{DOC}}$$

$$R_{HCO_3^-} = f_c R_{DOC},\ f_c = \frac{\varepsilon_2}{\alpha_2}$$

$$R_{Fe^{3+}} = f_a R_{DOC},\ f_a = \frac{\gamma_2}{\alpha_2}$$

$$R_{H^+} = f_{H^+} R_{DOC},\ f_{H^+} = \frac{\delta_2}{\alpha_2}$$

4.4.2 Numerical model set-up

Based on the flow and reactive transport described in Chapters 2 and 3, an updated biogeochemical reactive transport model has been constructed considering fermentation and biodegradation of DOC to be the sources of bicarbonate and sulphate. Initially, the updated microbial model was coupled with a 2D reactive hydrogeochemical model. This reactive transport model adopts all the concepts of water flow and abiotic geochemical reactive transport model shown in Chapters 2 and 3, but with a new refined mesh. However, the large CPU time required to solve such a model together with the poor convergence behaviour led us to consider a simpler 1D reactive transport model. Based on this simple model, microbial parameters were calibrated easier. Then, a thorough sensitivity analysis was performed for most of the microbial parameters.

4.4.2.1 Coupled 2-D reactive and microbial transport model

Model domain and discretization. The fracture zone is conceptualized as a 2-D vertical confined aquifer. To avoid the uncertainty of boundary conditions, the domain of the numerical model is extended as explained in Chapter 2. The model domain is a rectangular vertical section 1360 m in length and 300 m in depth which is discretized with 3373 triangular elements and 1783 nodes (Figure 4-11). The model domain is divided into 5 material zones according to the zonation of permeability and fracture zone thickness (see Figure 4-12).

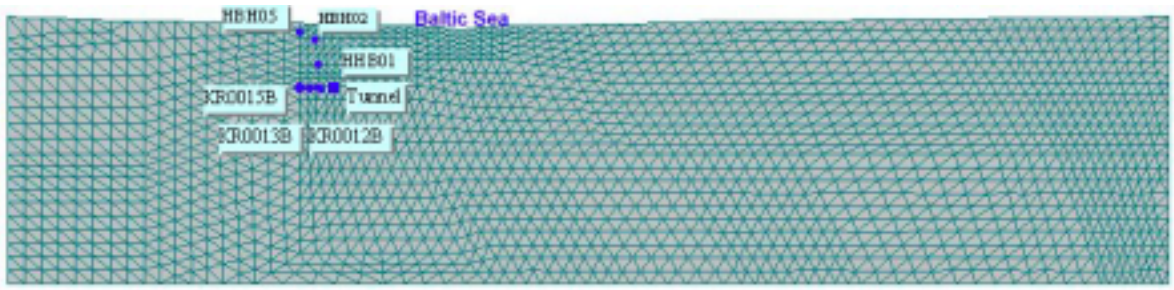

Figure 4-11. *Model domain and finite element mesh for 2D hydrobiogeochemical model.*

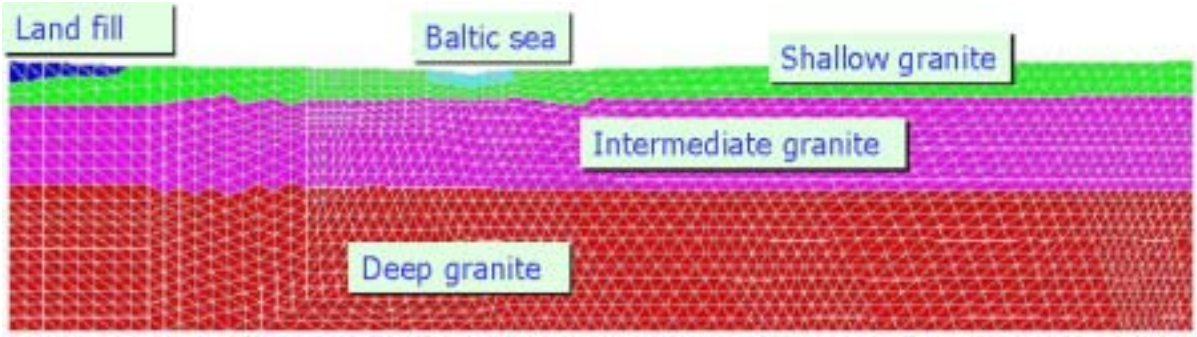

Figure 4-12. *Material zones.*

Geochemical and microbial processes. Chemical components are the same as those of the reactive transport model. The biogeochemical system is listed in Table 4-3. Thermodynamic equilibrium constants and stoichiometric coefficients for aqueous complexes and minerals are adopted from the thermodynamic database of EQ3/6 /Wolery, 1979/.

POC and DOC are treated as primary species in the biogeochemical system (see Table 4-3). Since POC is a macromolecular organic carbon, it is rarely mobile. In the model, POC is assumed to be an aqueous species rather than a solid phase. A large distribution coefficient is used to greatly reduce the mobility of POC. The distribution coefficient of POC is assigned a value of 100 dm^3/Kg.

Dissolved Organic Carbon (DOC) is subject to transport in the same manner as other aqueous species of the model.

Initial and boundary conditions. Initial conditions of water flow and solute transport are not well known. In order to adopt proper initial conditions the model was run for 90 years prior to the experiment by assuming a uniform head of 4.0 m and a uniform concentration of 10^{-4} (moles/L for non-organic, g/L for organic matter) as initial concentration for all species. The following boundary conditions were specified.

Table 4-3. Geochemical and microbial components and processes considered in the hydrobiogeochemical model.

Components:	Br^{-}, Ca^{+2}, Cl^{-}, Fe^{+2}, H_2O, H^{+}, HCO_3^{-}, K^{+}, Li^{+}, Mg^{+2}, Mn^{+2}, Na^{+}, $O_{2(aq)}$, $SiO_{2(aq)}$, SO_4^{-2}, Sr^{+2}, DOC, POC
Aqueous complexes:	$Ca(H_3SiO_4)_{2(aq)}$, $CaCl^{+}$, $CaCl_{2(aq)}$, $CaCO_{3(aq)}$, $CaH_2SiO_{4(aq)}$, $CaH_3SiO_4^{+}$, $CaHCO_3^{+}$, $CaOH^{+}$, $CaSO_{4(aq)}$, $CO_{2(aq)}$, CO_3^{-2}, $Fe(OH)_{2(aq)}$, $Fe(OH)_2^{+}$, $Fe(OH)_{3(aq)}$, $Fe(OH)_4^{-}$, Fe^{+3}, $FeCl^{+}$, $FeCl_{2(aq)}$, $FeCl_4^{-2}$, $FeCO_{3(aq)}$, $FeCO^{3+}$, $FeHCO_3^{+}$, $FeOH^{+2}$, $FeSO_{4(aq)}$, $H_{2(aq)}$, $H_2SiO_4^{-2}$, $H_4(H_2SiO_4)_4^{-4}$, $H_6(H_2SiO_4)_4^{-2}$, $HCl_{(aq)}$, HS^{-}, $HSiO_3^{-}$, HSO_4^{-}, $KBr_{(aq)}$, $KCl_{(aq)}$, $KHSO_{4(aq)}$, $KOH_{(aq)}$, KSO_4^{-}, $LiCl_{(aq)}$, $LiOH_{(aq)}$,$LiSO_4^{-}$, $Mg(H_3SiO_4)_{2(aq)}$, $MgCl^{+}$, $MgCO_{3(aq)}$, $MgH_2SiO_{4(aq)}$, $MgH_3SiO_4^{+}$, $MgHCO_3^{+}$, $MgSO_{4(aq)}$, $Mn(OH)_{2(aq)}$, $Mn_2(OH)_3^{+}$, Mn_2OH^{+3},$MnCl^{+}$, $MnCl^{3-}$, $MnCO_{3(aq)}$, $MnHCO^{3+}$, MnO_4^{-}, $MnOH^{+}$, $MnSO_{4(aq)}$, $NaBr_{(aq)}$, $NaCl_{(aq)}$, $NaCO_3^{-}$, $NaHCO_{3(aq)}$, $NaHSiO_{3(aq)}$, $NaOH_{(aq)}$, $NaSO^{4-}$, OH^{-}, $SrCl^{+}$, $SrCO_{3(aq)}$, $SrOH^{+}$, $SrSO_{4(aq)}$
Minerals:	Calcite, Hematite, Pyrite, Quartz
Exchangable Cations:	Ca^{+2}, Na^{+}
Microbes:	Iron reducer, Yeast

(1) Water flow

The upper boundary is treated with a Neumann (recharge) condition with an average recharge rate of 30 mm/year (see Chapter 2). Hydraulic head at the Baltic sea is prescribed to 0 m. The bottom boundary is treated with Dirichlet conditions with a fixed hydraulic head of 4.0 m. The lateral boundaries are impervious.

(2) Hydrogeochemistry

Concentrations of boundary waters are listed in Table 4-4. Concentrations of the deep saline water are later calibrated.

Computed concentrations under undisturbed conditions are used as initial concentrations for disturbed conditions. The initial concentrations of POC and DOC for disturbed conditions are shown in Figures 4-13 and 4-14.

Flow and transport parameters of each material zone were calibrated. Their values are listed in Table 4-5.

Model results reproduce water heads at borehole HBH01 (Figure 4-15), as well as measured concentrations for most species (Figure 4-16).

When microbial processes are incorporated into the model, severe convergence problems are found. Most runs consume a large of CPU time. CPU time for a run is about 3 hours on a PII 233 PC, while a run of the updated hydrobiogeochemical model needs 30 hours before the failure of the run.

Table 4-4. Concentrations (moles/L) of boundary waters.

Species	Recharge Fresh water	Bottom Boundary	Landfill water	Seafloor sediments Pore water
Mg^{+2}	1.64×10^{-4}	8.10×10^{-3}	4.92×10^{-9}	5.43×10^{-3}
H+	3.00×10^{-8}	3.16×10^{-8}	2.80×10^{-8}	3.16×10^{-8}
HCO_3^-	2.24×10^{-3}	1.05×10^{-3}	2.24×10^{-3}	1.47×10^{-3}
O2(aq)	1.48×10^{-66}	1.48×10^{-66}	1.48×10^{-66}	1.48×10^{-66}
Cl^-	1.69×10^{-4}	2.25×10^{-1}	1.69×10^{-4}	1.00×10^{-1}
K^+	6.65×10^{-5}	4.50×10^{-4}	6.65×10^{-5}	2.33×10^{-4}
Ca^{+2}	9.58×10^{-4}	4.96×10^{-2}	9.51×10^{-3}	2.43×10^{-3}
Fe^{+2}	1.00×10^{-5}	1.13×10^{-5}	1.00×10^{-5}	1.13×10^{-5}
$SO4^{-2}$	2.50×10^{-4}	4.95×10^{-3}	2.16×10^{-3}	2.60×10^{-2}
Br^-	1.00×10^{-4}	3.78×10^{-4}	1.00×10^{-20}	3.78×10^{-4}
SiO2(aq)	9.98×10^{-5}	9.32×10^{-5}	9.98×10^{-5}	9.32×10^{-5}
Mn^{+2}	6.55×10^{-6}	1.71×10^{-5}	6.55×10^{-6}	1.71×10^{-5}
Li^+	1.44×10^{-6}	8.00×10^{-5}	1.44×10^{-6}	4.61×10^{-5}
Na^+	6.69×10^{-4}	1.09×10^{-1}	6.69×10^{-4}	8.52×10^{-2}
Sr^{+2}	2.51×10^{-6}	2.45×10^{-4}	2.51×10^{-6}	2.45×10^{-4}
DOC(g/L)	3.00×10^{-2}	1.00×10^{-4}	3.00×10^{-2}	2.40×10^{-2}
POC(g/L)	3.00×10^{-2}	1.00×10^{-4}	3.00×10^{-2}	2.40×10^{-2}
Fe_reducer(mg/L)	1.058×10^{-6}	1.058×10^{-6}	1.058×10^{-6}	1.058×10^{-6}
Yeast (mg/L)	1.058×10^{-6}	1.058×10^{-6}	1.058×10^{-6}	1.058×10^{-6}

Table 4-5. List of calibrated flow and transport parameters.

Material zone	T (m^2/day)	S	Porosity	Longitudinal Dispersivity (m)	Transverse Dispersivity (m)
Landfill	100	2×10^{-3}	1%	30	15
Baltic sediments	10^{-4}	2×10^{-3}	10%	30	15
Shallow granite	100	7×10^{-3}	1%	30	15
Intermediate granite	0.13	4×10^{-3}	1%	30	15
Deep granite	0.09	2×10^{-3}	1%	30	15

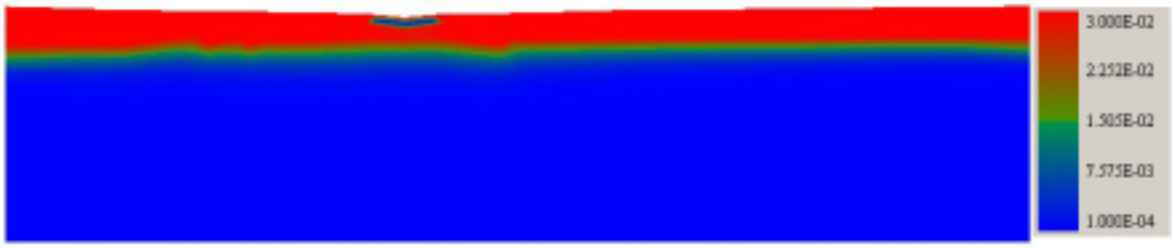

Figure 4-13. *Computed concentration of POC for initial undisturbed conditions.*

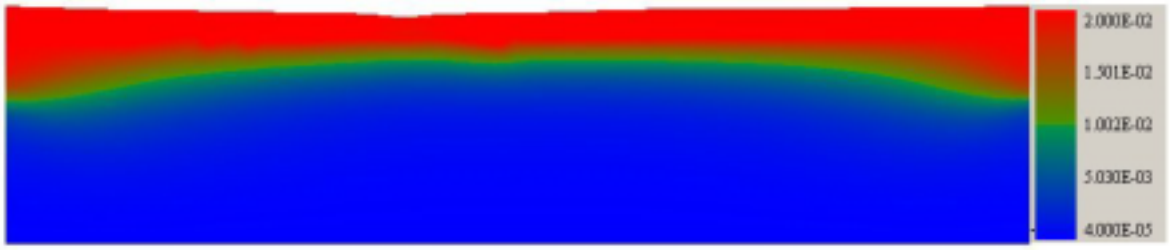

Figure 4-14. *Computer concentration of DOC for initial undisturbed conditions.*

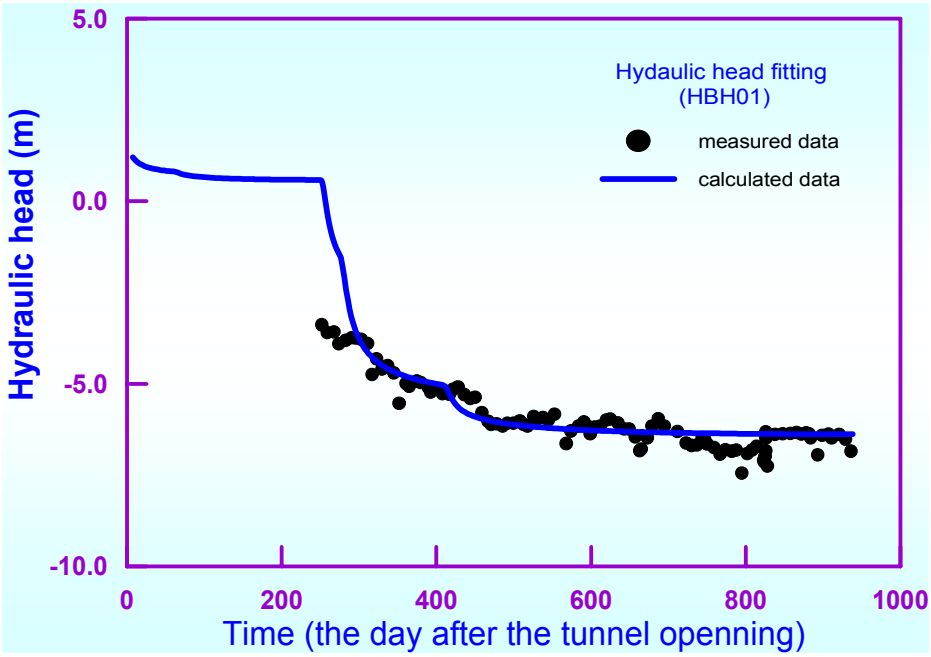

Figure 4-15. *Hydraulic head drawdown fitting.*

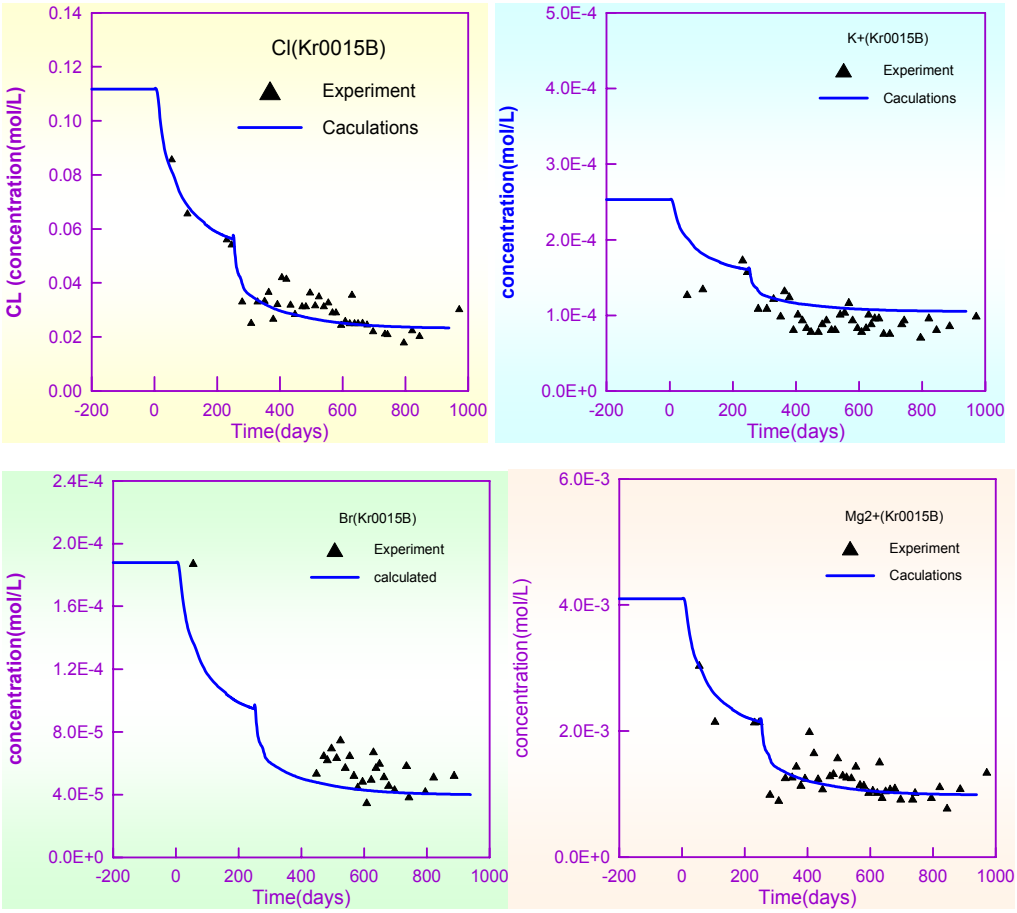

Figure 4-16. *Computed and measured concentrations breakthrough curves of Cl^-, K^+, Br^- and Mg^{+2} at –70 m.*

A great effort was devote to overcome such numerical problems. According to our own experience on groundwater flow and reactive transport modelling for the last 20 years, the following facts may contribute to understand this situation:

1) While available experience on chemically-reactive transport models spans on about 10 – 12 years, coupled models of microbial processes are more recent. UDC code BIOCORE was developed in year 2000.

2) Each type of problem has its own features. Microbial problems are much more non-linear than abiotic processes. In addition, they are intrinsically irreversible and usually have large rates.

3) The rate of microbial processes is extremely sensitive to key chemical and microbial parameters. Such large sensitivity translates into large changes in microbial and chemical concentrations when parameters are changed slightly.

4) The codes of the CORE series use a sequential iteration approach (SIA) for solving the coupled transport + chemistry + microbial processes. This approach is more efficient than the direct substitution approach (DSA) for problems with large grids and slow chemical and microbial processes. However, SIA is prone to lack of convergence for problems containing fast reactions. Improved versions of SIA are being developed to overcome this limitation.

In order to overcome the difficulties of the complex 2-D microbial model, it was decided to simplify the flow and transport model by considering a simple 1-D model which captures the essence of the flow system and has all the geochemical and microbial processes of the complex model. This model is called the simple model and is described next.

4.4.2.2 1-D reactive hydrogeochemical model (Simple model)

Native groundwater of the fracture zone at –70 m depth near the tunnel is a saline water of typical marine origin. Three weeks after the start of the experiment a front of fresh water arrived at the access tunnel, inducing a dilution and appearing a sharp decrease in Cl^-. This dilution is explained by mixing of native saline water with fresh water. Dilution of the saline native groundwater by fresh water is the dominant process controlling the hydrogeochemical evolution during the experiment /Banwart et al, 1995/. Figure 4-17 shows the conceptual model of the simple model.

A vertical column across the tunnel in the fracture zone is selected (Figure 4-17) with a length of 302 m, a width of 0.1 m and a thickness of 0.1 m. Fresh water and saline water flow into the column from top and bottom boundaries, respectively (Figure 4-17). A discharge point (tunnel and boreholes) is located at a depth of –70 m.

From top to bottom, the column is divided into 3 material zones: shallow granite with thickness of 37 m, intermediate granite with thickness of 83 m and deep granite with thickness of 182 m, which coincide with those of the 2D model. Flow and transport parameters for these 3 material zones are listed in Table 4-5.

Geochemical and microbial processes of the simple model are the same as those of the 2-D model (see Table 4-3).

The top and bottom boundaries of the column are treated as prescribed water flux conditions. Concentrations of fresh water (top) and saline (bottom) are listed in Table 4-4. Initial concentrations of chemical species are the same as those of the 2-D model.

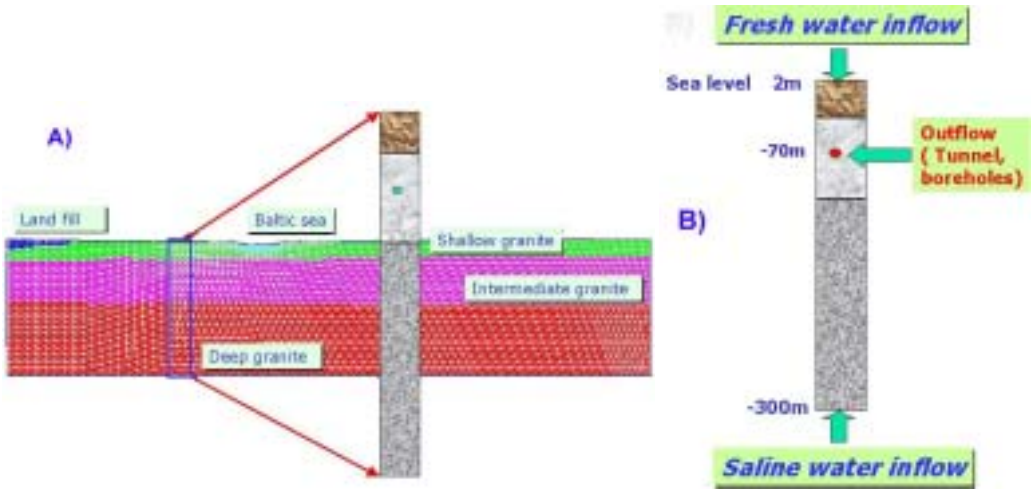

Figure 4-17. *Conceptual model of simple model.*

4.4.3 Model calibration

Model calibration is aimed at reproducing the dilution processes of non-organic species by adjusting the discharge rate at a depth of –70 m, and estimating microbial parameters such as specific growth rate of microbes, half saturation, yield production, proportionality coefficients, and POC and DOC initial and boundary concentrations

Flow and transport parameters were not calibrated. Those of the 2-D model parameters were directly used for the simple model.

4.4.3.1 Dilution process

Fresh water coming from the shallow part of the fracture zone dilutes the native saline water at the tunnel position. The dilution process causes a decrease in concentration of conservative solutes such as Cl^- and Br^-. The simple model can reproduce the dilution of these species (Figure 4-18).

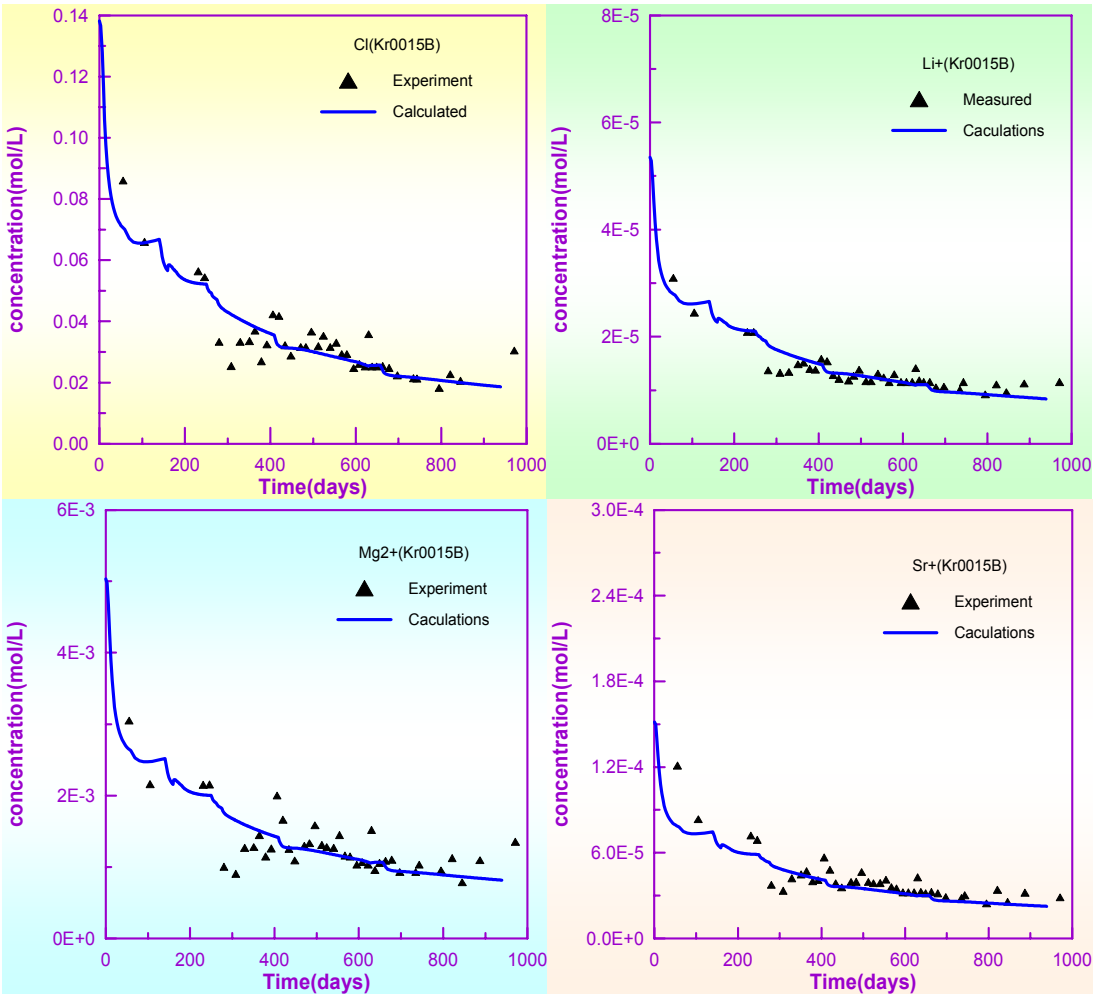

Figure 4-18. *Measured breakthrough curves (symbols) of Cl^-, Li^+, Mg^{2+} and Sr^+ at –70 m and computed values with the sinple model.*

4.4.3.2 Abiotic geochemical processes

The simple model also accounts for other abiotic geochemical processes, including aqueous complexation, acid-base, redox processes, mineral dissolution-precipitation and cation exchange.

Concentration of $SiO_{2(aq)}$ is controlled by both dilution processes and dissolution-precipitation of quartz. It is known that the dissolution-precipitation of quartz is too slow to reach thermodynamic equilibrium in a 3 years-experiment. $SiO_{2(aq)}$ is known in all boundary waters to be in a quasi equilibrium state. So, there is no dilution occurring for disturbed condition. One can see in Figure 4-19 that the concentration of $SiO_{2(aq)}$ remains almost constant.

According to /Viani and Bruton, 1997/ the behaviour of Na^+ and Ca^{2+} is consistent with cation exchange, with preferential exchange of dissolved Ca^{2+} and displacement of exchanged Na^+ during the dilution process. Model results indicate that incorporating of this process is consistent with the concentration evolution of Ca^{2+} and Na^+ (Figure 4-20). This result also coincides with the conclusions of Chapter 3.

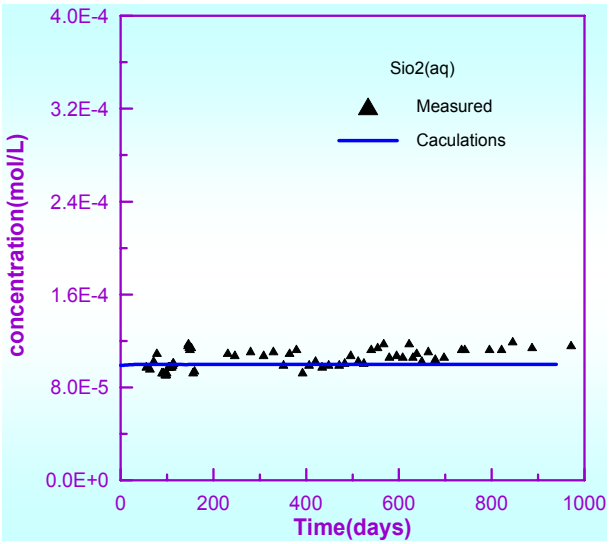

Figure 4-19. *Fitting of aqueous SiO_2 concentration at a depth of 70 m (1-D model).*

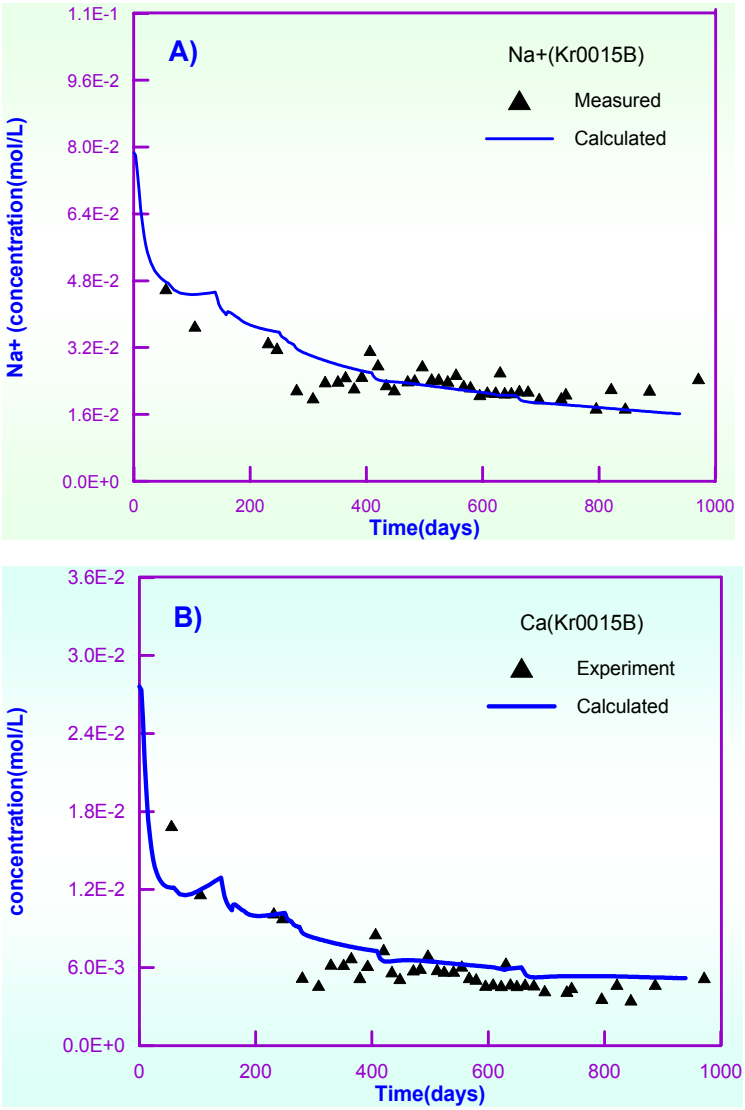

Figure 4-20. *Computed and measured concentrations curves of Ca^{+2} and Na^{+} at a depth of 70 m (simple 1-D model).*

4.4.3.3 Microbial processes

Microbial parameters (Equations 4.8 and 4.9) were calibrated by comparing computed concentrations of bicarbonate and sulphate with their measured data at a depth of 70 m.

Microbial kinetic processes are very sensitive to specific growth rate, half-saturation constant and yield coefficients. Given the lack of measured data about microbial parameters, most of them were estimated by trial and error.

In the updated microbial model, the two microbial processes are inter-related because dissolved organic carbon not only is produced by fermentation of POC, but also serves as a substrate of iron-reducer (see Figure 4-10). So, calibration of this model is time consuming and highly difficult.

Calibrated microbial parameters were obtained after many trail runs (see Tables 4-6 and 4-7).

Table 4-6. Calibrated microbial parameters and coefficients for yeast.

Parameters and coefficients	Values
Specific growth rate of yeast (μ_{max})	0.16746 day^{-1}
Yield coefficient of POC to Yeast (Y_{POC})	3.076×10^{-3} g biomass/g POC
Half-saturation coefficient of POC (K_{POC})	7.60×10^{-3} g/L
Proportionality coefficient between POC and DOC (f_a)	– 0.9 DOC/ POC
Proportionality coefficient between POC and SO_4^{-2} (f_H)	–0.019 moles of SO_4^{-2} /g POC
Proportionality coefficient between POC and H^+ (f_H)	–0.05 moles of $\mathbf{H^+}$ /g POC

Table 4-7. Calibrated microbial parameters and coefficients for iron reducer.

Parameters and coefficients	Values
Specific growth rate of iron reducer (μ_{max})	0.15084 day^{-1}
Yield coefficient of DOC to iron-reducer (Y_{DOC})	8.48×10^{-3} g biomass/g DOC
Half-saturation coefficient of DOC (K_{DOC})	6.60×10^{-3} g/L
Half-saturation coefficient of Fe^{3+} (K_{Fe+3})	3.25×10^{-10} moles/L
Proportionality coefficient between DOC and HCO_3^- (f_c)	–0.0606 mol. of HCO_3^-/g DOC
Proportionality coefficient between DOC and Fe^{3+} (f_a)	0.021 moles of Fe^{3+}/g DOC
Proportionality coefficient between DOC and H^+ (f_H)	0.01 moles of $\mathbf{H^+}$ /g DOC

Figures 4-21 and 4-22 show the evolution of computed concentrations of bicarbonate and sulphate with and without microbial processes. They are compared to measured data.

Figure 4-23 illustrates the computed and measured DOC at a depth of 70 m. Figure 4-24 shows the evolution of pH at a depth of 70 m. One can see that pH remains stable.

The numerical model considers 4 minerals (see Table 4-4). They are calcite, hematite, pyrite and quartz. As mentioned before, $SiO_{2(aq)}$ is in quasi equilibrium with respect to quartz, the dissolution-precipitation rate of this mineral is very small. Calcite tends to precipitate (positive values) due to the increase in bicarbonate concentration. Hematite and pyrite tend to dissolve at a depth of –70 m (Figure 4-25).

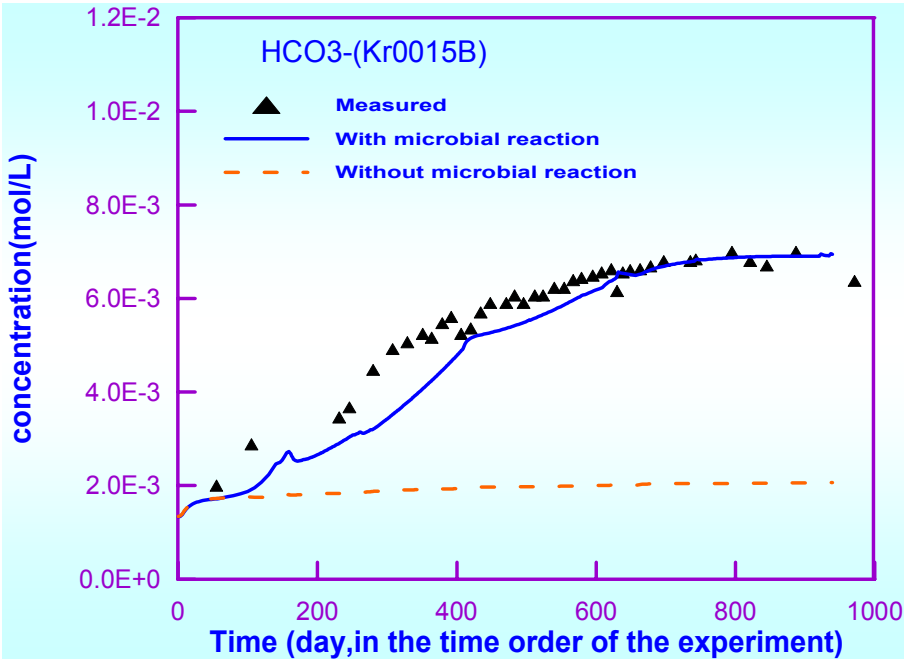

Figure 4-21. *Measured and computed bicarbonate concentrations with and without consideration of microbial processes.*

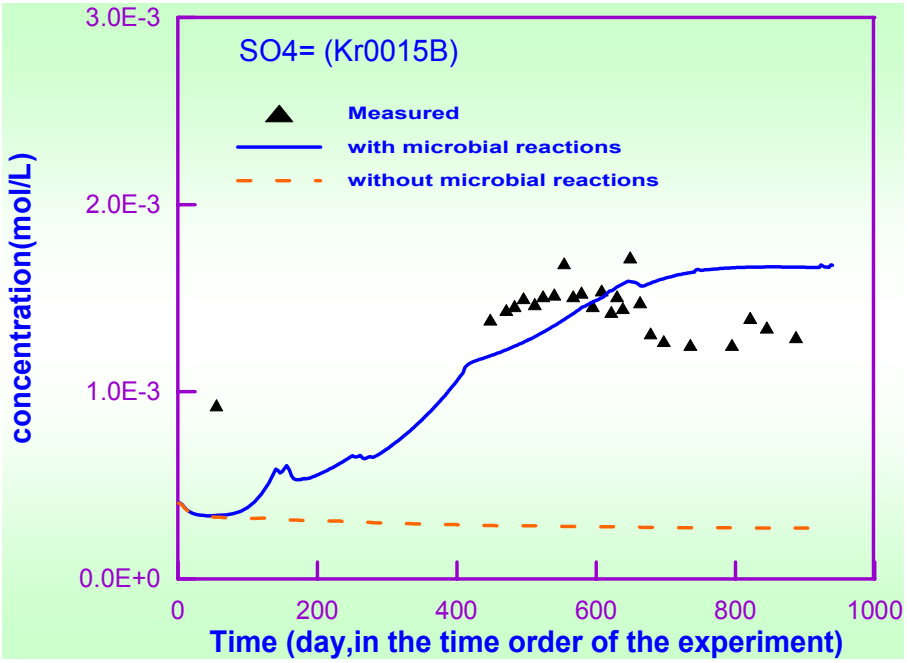

Figure 4-22. *Measured and computed sulphate concentrations with and without consideration of microbial processes.*

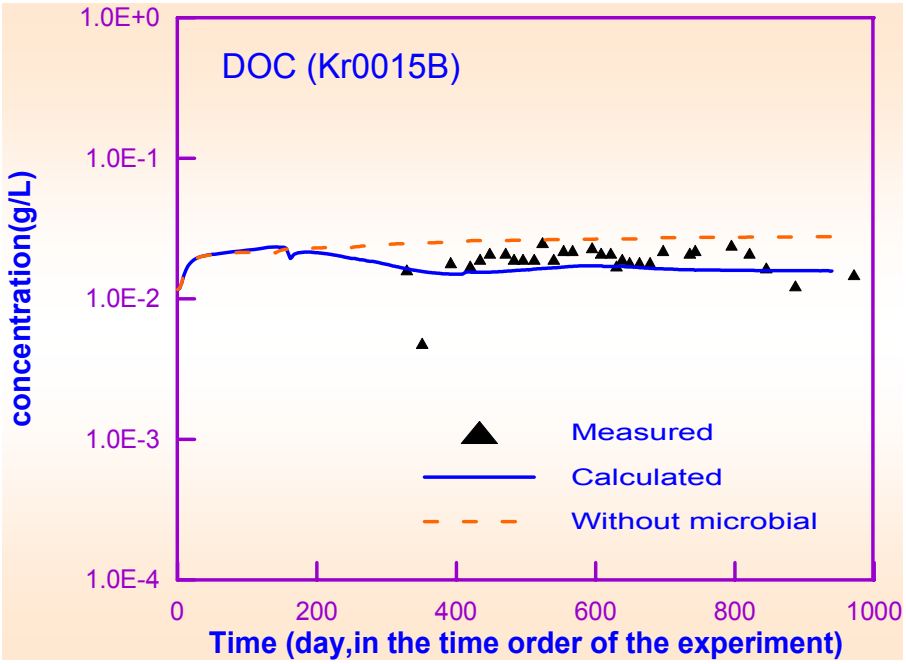

Figure 4-23. *Measured and computed concentrations of dissolved organic carbon (DOC) at –70 m.*

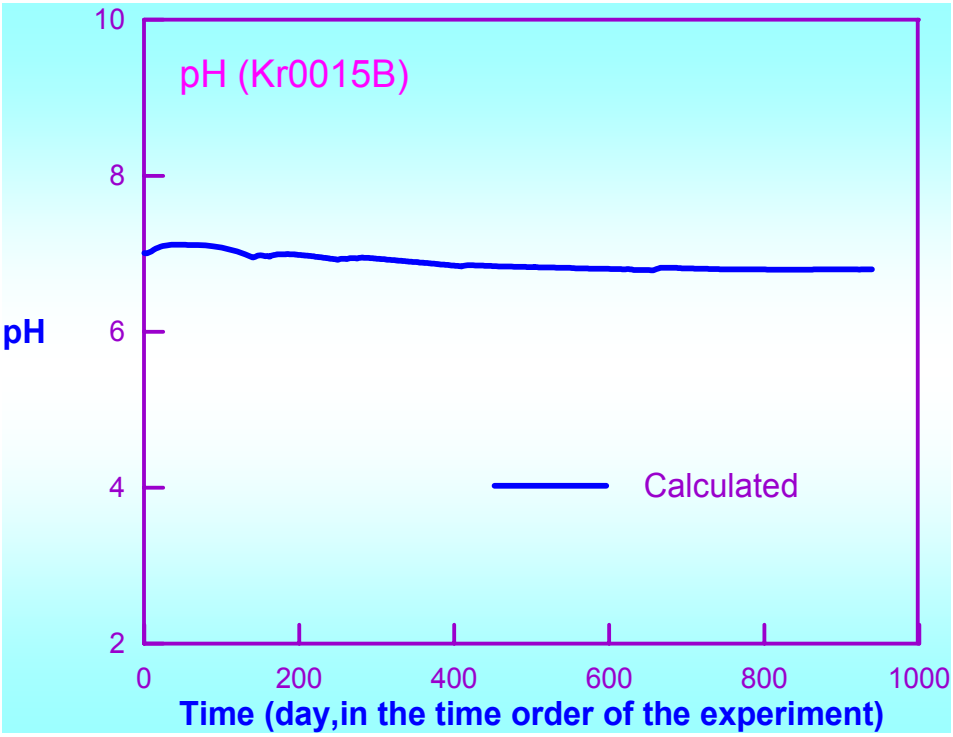

Figure 4-24. *Computed pH at –70 m.*

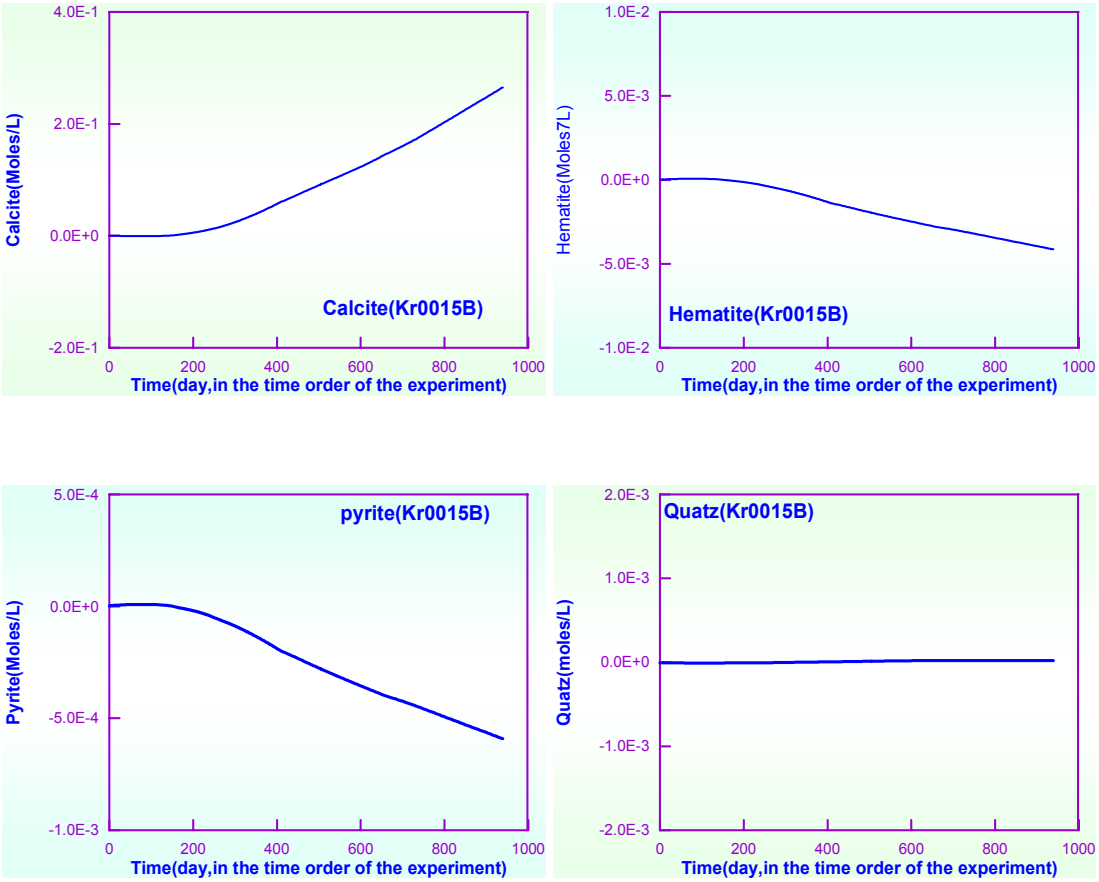

Figure 4-25. *Mineral dissolution-precipitation trends at the depth of –70m (positive values indicate precipitation, negative values are for dissolution).*

4.4.4 Sensitivity analysis

During the calibration stage it was found that model results were extremely sensitive to all parameters, especially to specific growth rates, half-saturation constants and proportional coefficients. This section presents the results of the sensitivity analysis about these parameters as well as initial and boundary concentrations of organic species. This sensitivity analysis was performed with the simple model.

4.4.4.1 Sensitivity to specific growth rates

According to the microbial models (Equations 4.8 and 4.9), if specific growth rates increase and enough substrates and electron acceptors for microbial growth are provided, the growth rate of microbes will increase. Then the rate of production of other product species will also increase because they are related by the reaction rate of substrate which is equal to the microbial growth rate divided by the yield coefficient.

Figure 4-26 shows the sensitivity of DOC and HCO_3^- to different specific growth rate of iron-reducer. The specific growth rate increases from 0.151 day^{-1} of the base run to 0.1716 day^{-1} for run1. As the growth rate increases, bicarbonate increases (Figure 4-26a), while the substrate is depleted of other product species (Figure 4-26b).

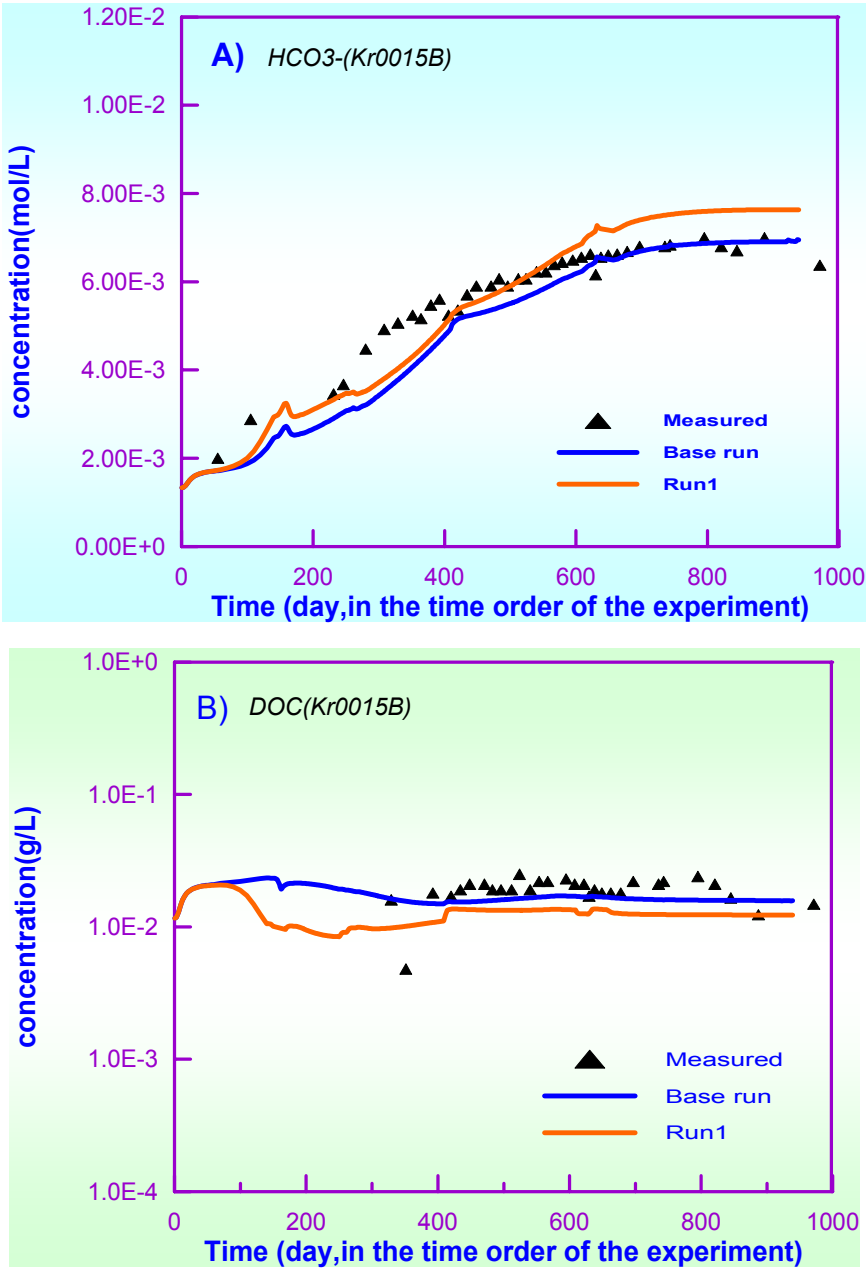

Figure 4-26. *Sensitivity of the concentrations of HCO_3^- (A) and DOC (B) to specific growth rate of iron-reducer. Base run: growth rate=0.1508 day^{-1}. Run1: growth rate=0.1716 day^{-1}.*

Figure 4-27 shows the sensitivity of the concentrations of sulphate (Figure 4-27a) and bicarbonate (Figure 4-27b) to changes in the specific growth rate of yeast. The specific growth rate of yeast decreases from 0.1675 day^{-1} (base run) to 0.1623 day^{-1} (run2). By decreasing the growth rate, sulphate decreases (see Figure 4-27a). Bicarbonate shows the same trend. The explanation for the smaller bicarbonate is that DOC decreases with the growth of yeast. The smaller the quantity of substrate (DOC), the smaller the growth of iron-reducer.

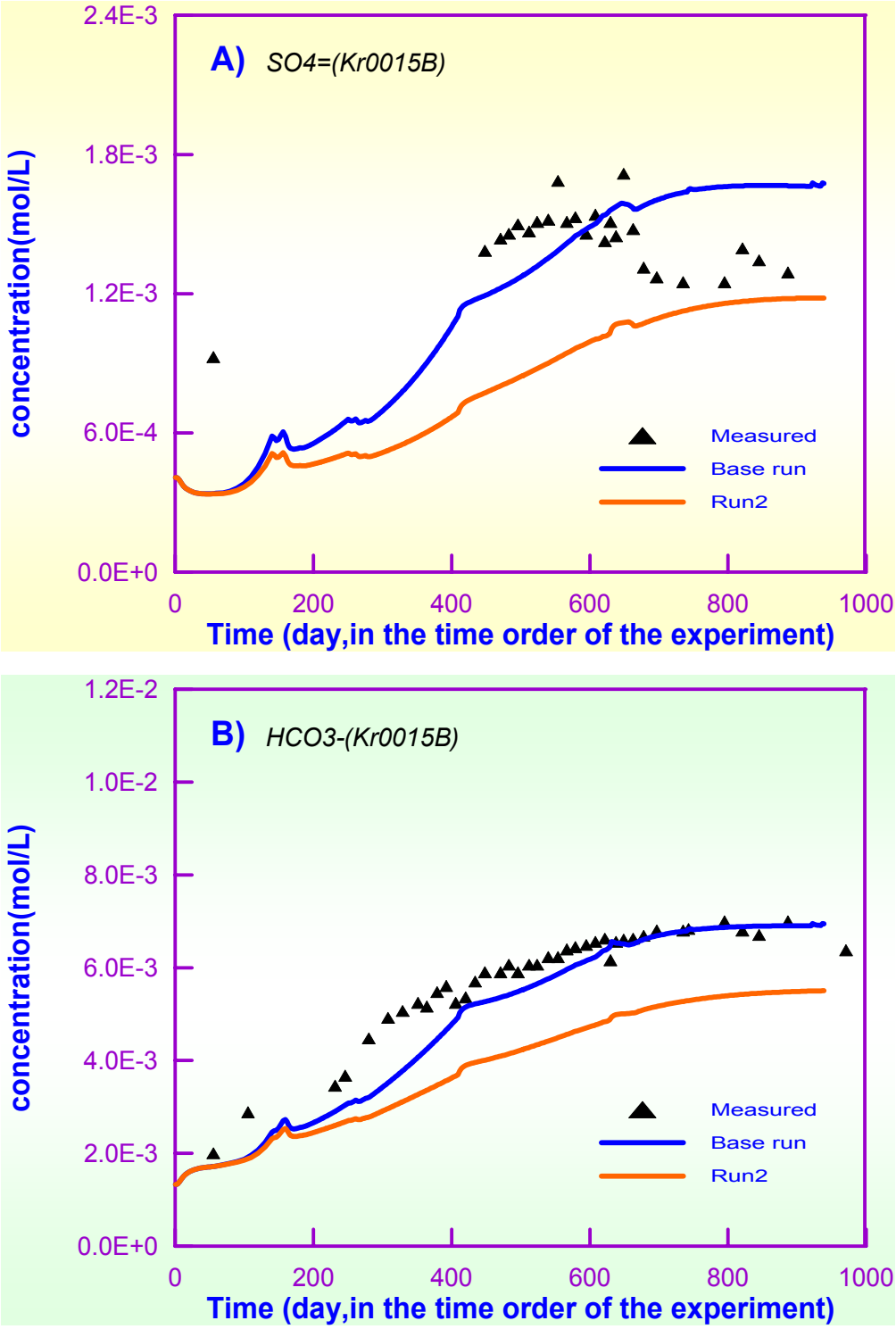

Figure 4-27. *Sensitivity of the concentrations of SO_4^{2-} (A) and HCO_3^- (B) to specific growth rate of yeast. Base run: Specific growth rate= 0.1675 day^{-1}. Run2: Specific growth rate=0.1623 day^{-1}.*

4.4.4.2 Sensitivity to half-saturation constants

Half-saturation constants control the dependence of microbial growth on substrate concentration. Here we analyze the sensitivity with respect to the half-saturation constant of the two microbial processes. Let F be the term of the Monod kinetic expression,, $\frac{C_s}{K + C_s}$. If C_s is not equal to 0, then

$$F = \frac{C_s}{K + C_s} = \frac{1}{\frac{K}{C_s} + 1}$$

where C_s is concentration of substrate and K is the half-saturation constant.

When the half-saturation constant is much smaller than the concentration of the substrate, F will be close to 1, i.e. the substrate does not limit microbial growth. The growth process behaves like a first-order kinetic process and the dependence of the growth rate on substrate concentration decreases. When the half-saturation constant has a value similar to the substrate concentration, the limitation term depends strongly on substrate concentration and the growth process has a mixed order behaviour.

The results of the sensitivity analysis show that the growth process is sensitive to variations of this parameter. Figure 4-28 shows the sensitivity of bicarbonate and DOC to the half-saturation constant of Iron-reducer.

The smaller value enhances the growth and transformation rate. One can see in Figure 4-28 that bicarbonate (Figure 4-28a) with half-saturation 3.6×10^{-3} g/L in run3 is larger than that with 6.6×10^{-3} in the base run. On the contrary, DOC is depleted in run 3 compared to the base run (Figure 4-28b).

Conclusions are similar for the half-saturation of POC. Figure 4-29a illustrates sensitivity of sulphate to different values of half-saturation constant of POC. Figure 4-29b shows the sensitivity of bicarbonate to different values of half-saturation constant of POC. Although HCO_3^- is not produced by the fermentation of POC, a smaller half-saturation constant of POC enhances the growth of yeast and provides more source of DOC. Meanwhile, as a substrate of iron-reducer, DOC stimulates the growth of iron-reducer and leads to more bicarbonate.

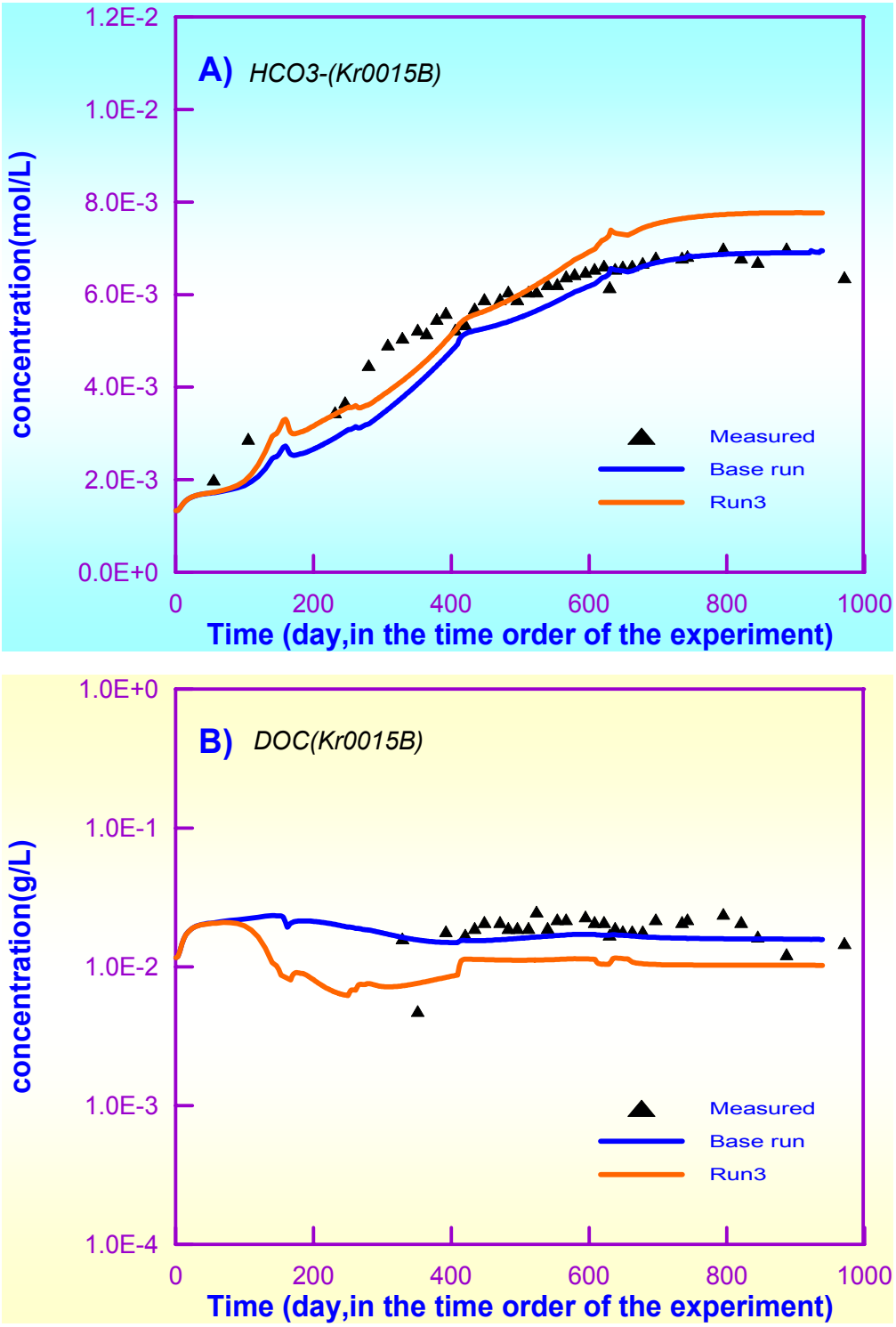

Figure 4-28. *Sensitivity of the concentrations of HCO_3^- (A) and DOC (B) to different half-saturation constant of DOC. Base run: Half saturation of DOC= 6.6×10^{-3} g/L. Run 3: Half saturation of DOC= 3.6×10^{-3} g/L.*

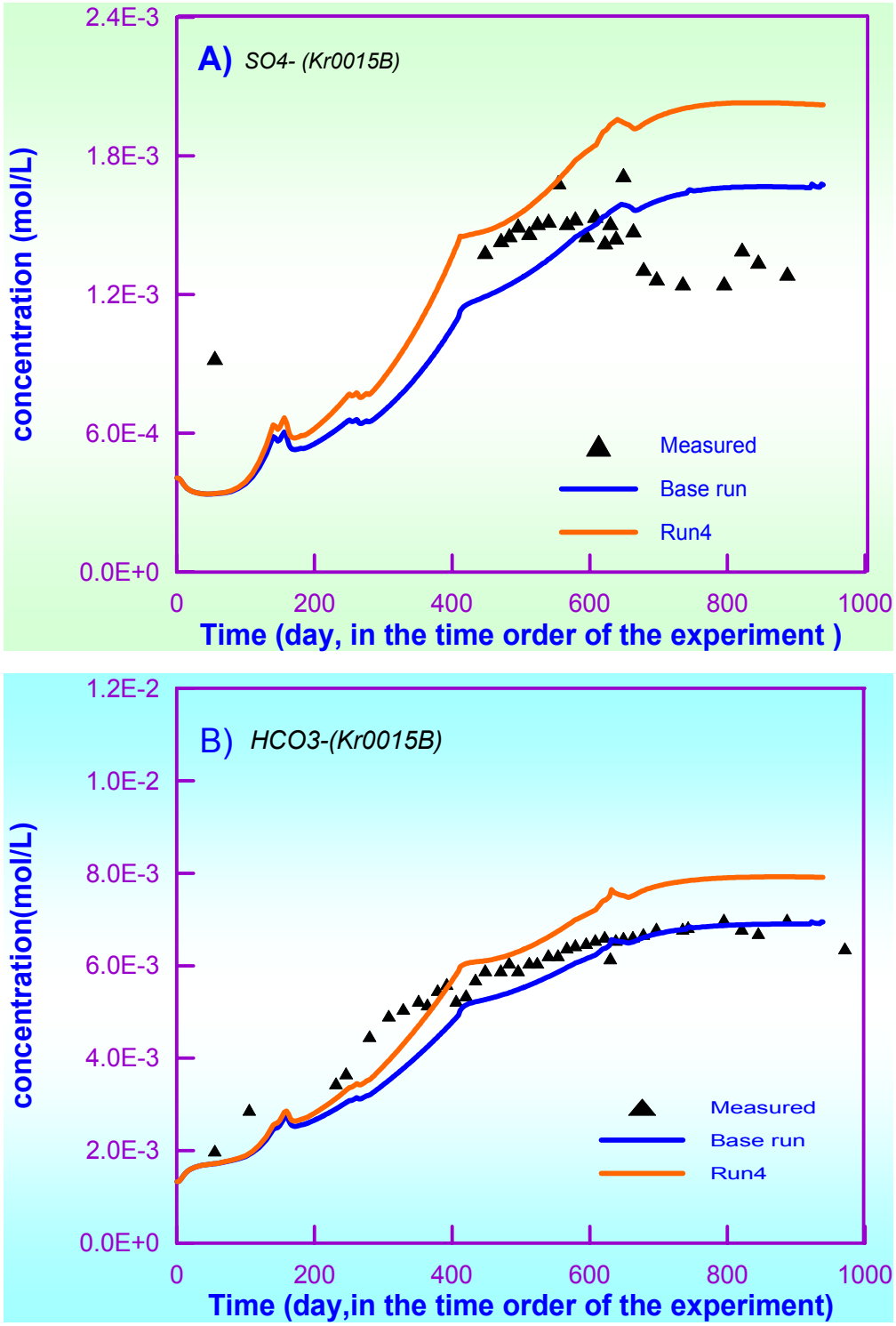

Figure 4-29. *Sensitivity of concentrations of SO_4^{2-} (A) and HCO_3^- (B) to half-saturation constant of POC. Base run: Half saturation of POC = 7.6×10^{-3} g/L. Run 4: Half saturation of POC = 7.0×10^{-3} g/L.*

4.4.4.3 Sensitivity to yield coefficients

The yield coefficient is defined as the ratio between the part used to build cell materials, equal to the biomass growth, and the total consumption of the substrate /Zhang, 2001/. According to the mass balance, the total amount of consumed substrate should be equal to the sum of the increased biomass and mass of products. So, if the yield coefficient is increased, more substrate is transformed to microbial mass. Then, less amount of substrate that is not consumed by microbes constitutes the production of microbial metabolism.

Figure 4-30 shows the sensitivity of bicarbonate to the yield coefficient of DOC to iron-reducer. One can see that bicarbonate is not sensitive to an increase in the yield coefficient.

Figure 4-31 shows the sensitivity of sulphate (Figure 4-31a) and bicarbonate (Figure 4-31b) to changes in the yield coefficient of POC to yeast.

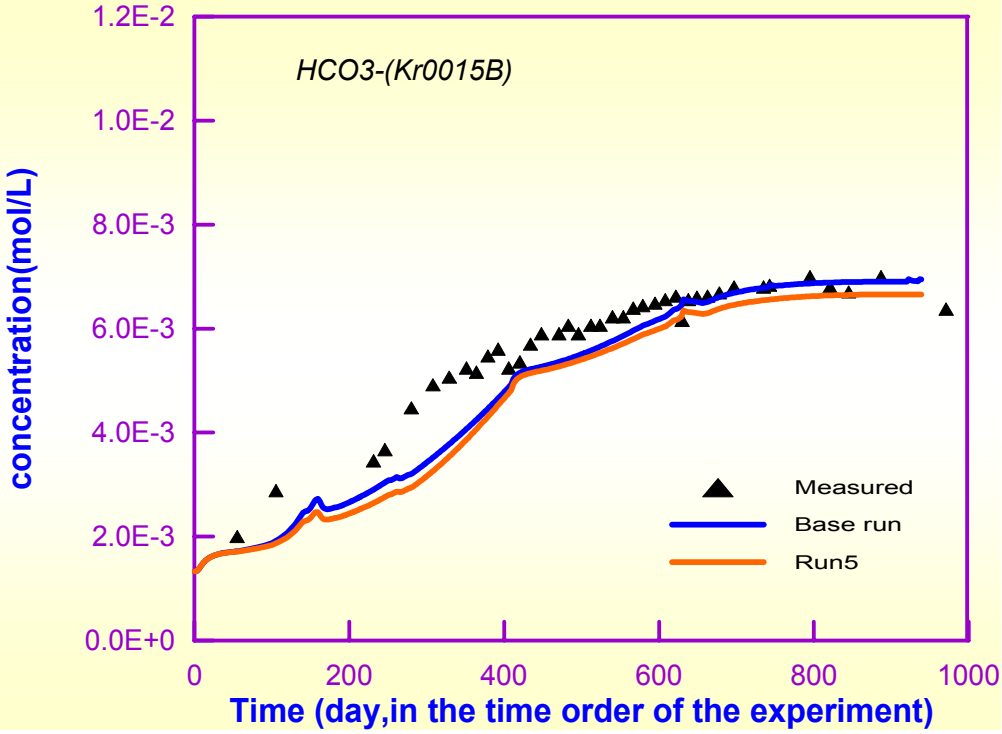

Figure 4-30. *Sensitivity of the concentrations of HCO_3^- to yield coefficient. Base run: yield coefficient of DOC to iron-reducer=$8.48x10^{-3}$ g biomass/g DOC. Run 5: yield coefficient of DOC to iron-reducer=$22.48x10^{-3}$ g biomass/g DOC.*

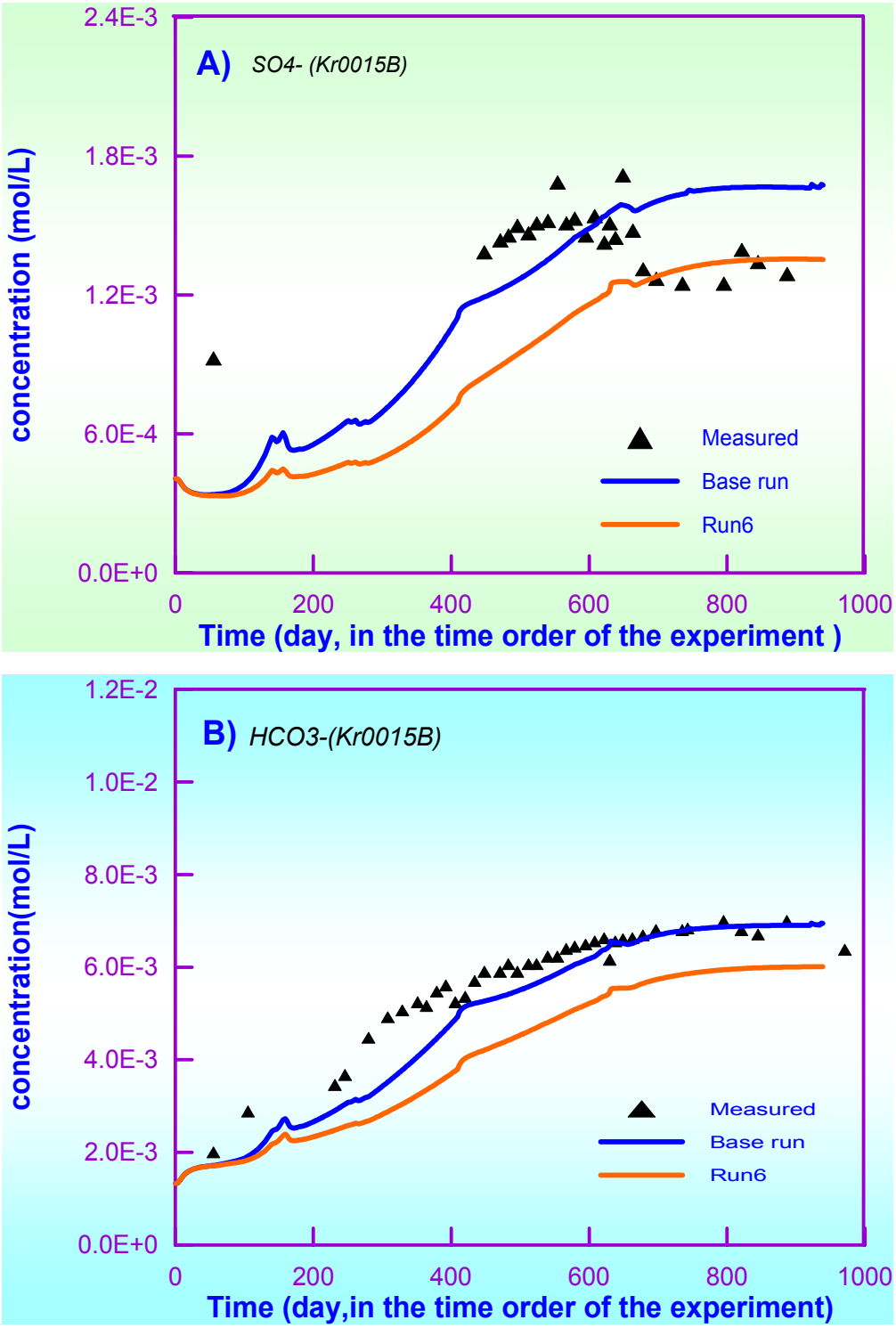

Figure 4-31. *Sensitivity of concentrations of SO_4^{2-} (A) and HCO_3^- (B) to the yield coefficient of POC to yeast. Base run: Yield coefficient of POC to Yeast=3.076x10^{-3} g biomass/g POC. Run 6: Yield coefficient of POC to Yeast=8.076x10^{-3} g biomass/g POC.*

4.4.4.4 Sensitivity to proportionality coefficients

Proportionality coefficient is defined as the ratio between the reaction rate of products and that of substrate. So, by increasing the proportionality coefficient, one gets more amount of products or by decreasing the proportionality coefficients one gets less amount of products.

Figure 4-32 shows the sensitivity of DOC (Figure 4-32a) and bicarbonate (Figure 4-32b) calculated to the proportionality coefficient of DOC to POC. One can see that the smaller proportionality coefficient of DOC to POC the smaller the amount of DOC, and therefore, the smaller the amount of DOC that can be degraded to bicarbonate (Figure 4-32b).

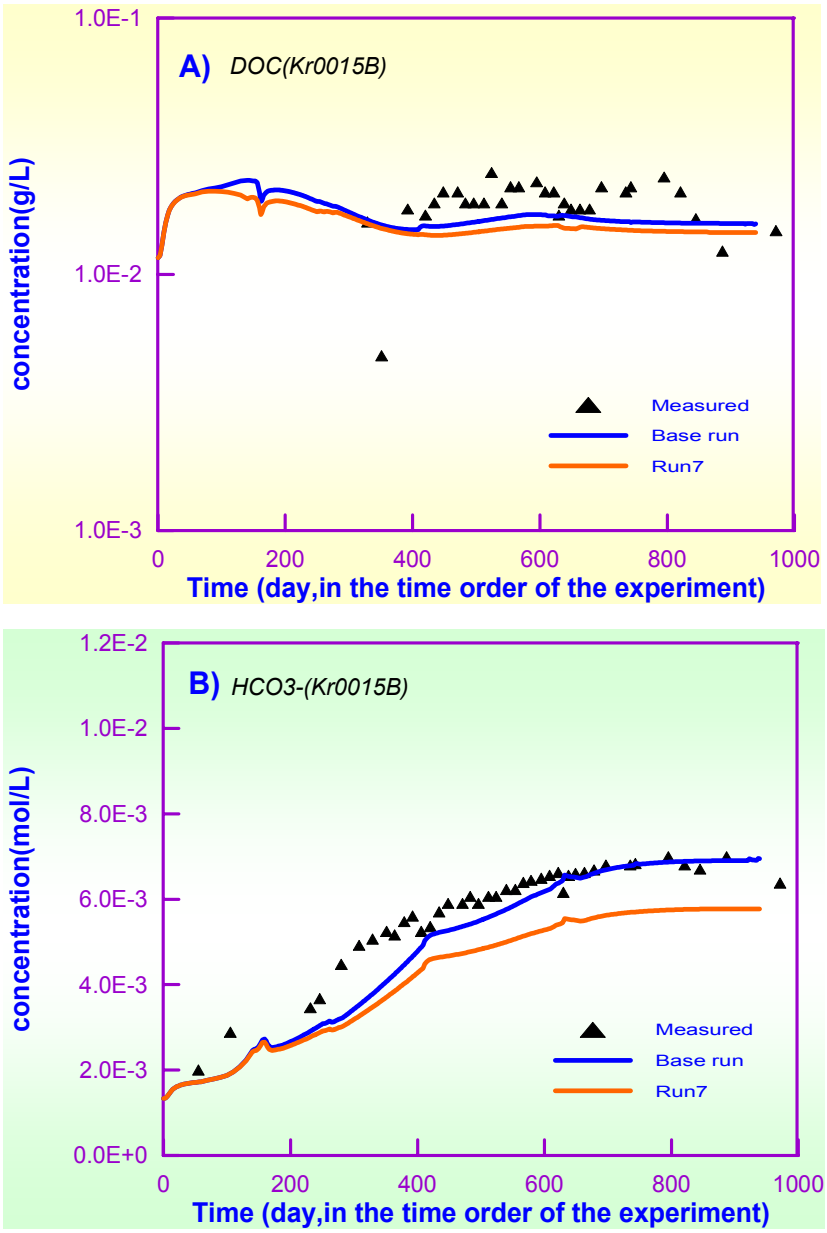

Figure 4-32. *Sensitivity of concentrations of DOC^{-} (A) and HCO_3^{-} (B) to proportionality coefficient of POC to DOC. Base run: proportionality coefficient of POC to DOC=0.9 g/g. Run 7: proportionality coefficient of POC to DOC=0.5 g/g.*

Figure 4-33 shows the sensitivity of sulphate to the proportionality coefficient of SO_4^{2-} to POC. Again, the same conclusion obtained, the smaller the proportionality coefficient of SO_4^{2-} to POC the smaller the amount of SO_4^{2-}.

Figure 4-34 shows the sensitivity analysis of proportionality coefficient of bicarbonate to DOC. One can see the smaller the proportionality coefficient the smaller the amount of bicarbonate.

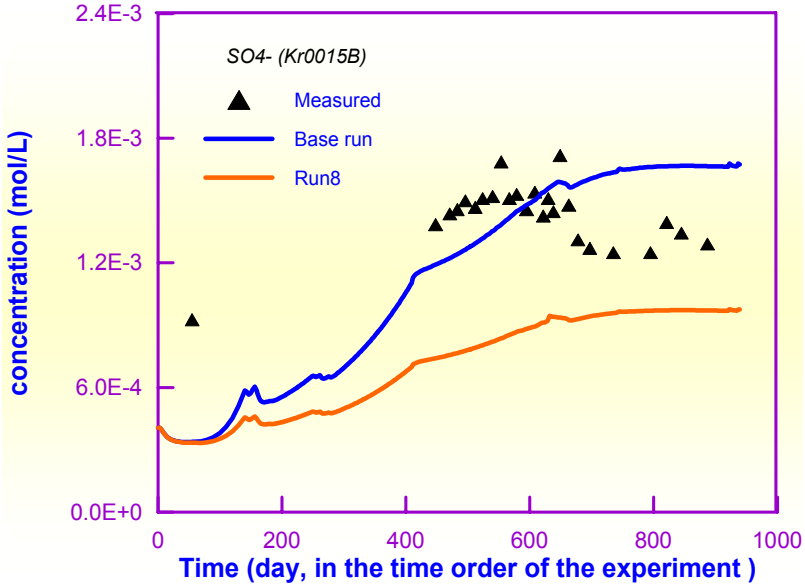

Figure 4-33. *Sensitivity of concentrations of SO_4^{2-} to different proportionality coefficient SO_4^{2-} to POC. Base run: proportionality coefficient of SO_4^{2-} to POC=0.023 mol/g. Run 8: proportionality coefficient of SO_4^{2-} to POC=0.0115 mol/g.*

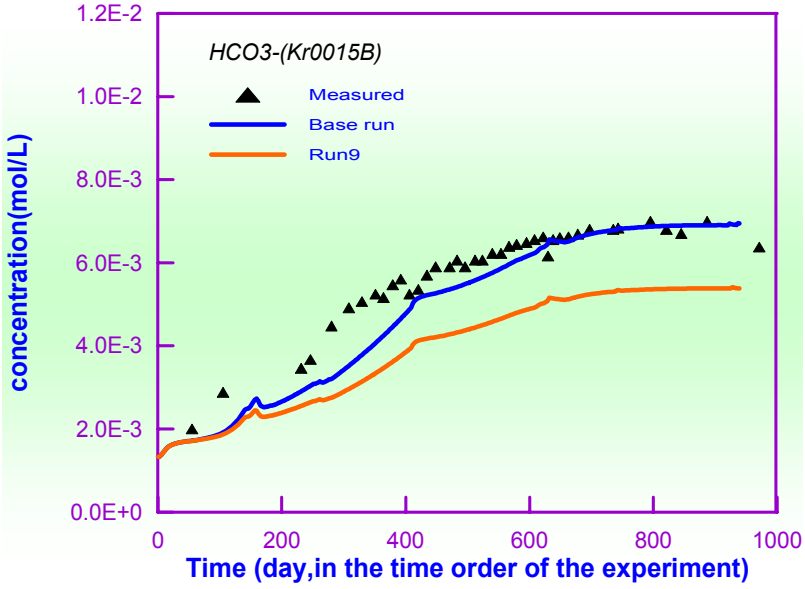

Figure 4-34. *Sensitivity of concentrations of $HCO3^-$ to proportionality coefficient of $HCO3^-$ to DOC. Basic run: proportionality coefficient of $HCO3^-$ to OC=0.0606 mol/g. Run 9: proportionality coefficient of $HCO3^-$ to DOC=0.0303 mol/g.*

4.4.4.5 Sensitivity to initial concentrations of DOC and POC

Figure 4-35 shows the sensitivity of concentration of bicarbonate to initial concentration of DOC at the top layer. From this figure, it can be concluded bicarbonate is not sensitive to the initial concentration of DOC at the top layer.

The sensitivity analysis to initial concentration of POC at the top layer shows a different trend. Figure 4-36 shows the results of sensitivity to initial concentration of POC at the top layer. By decreasing initial concentration of POC at the top layer, the amount of sulphate (Figure 4-36b) and DOC (Figure 4-36a) decreases which leads to a smaller amount of bicarbonate (Figure 4-36C).

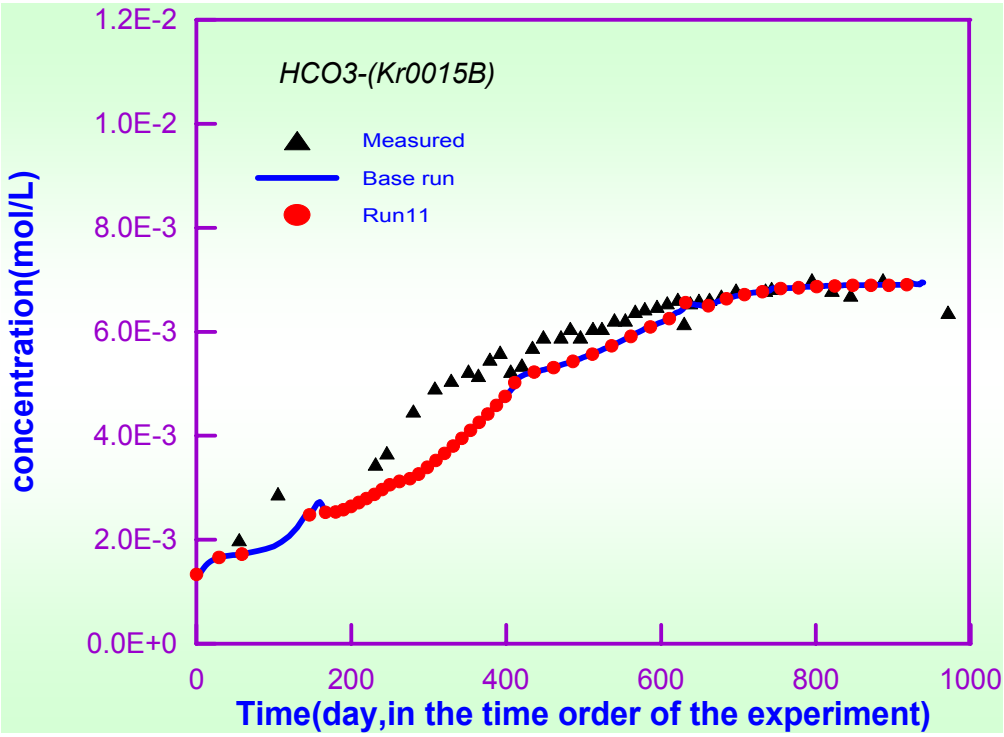

Figure 4-35. *Sensitivity of concentrations of HCO_3^- to initial concentration of DOC at the top layer. Base run: Initial concentration at top layer DOC 22 mg/L. Run 11: Initial concentration at top layer DOC 18 mg/L.*

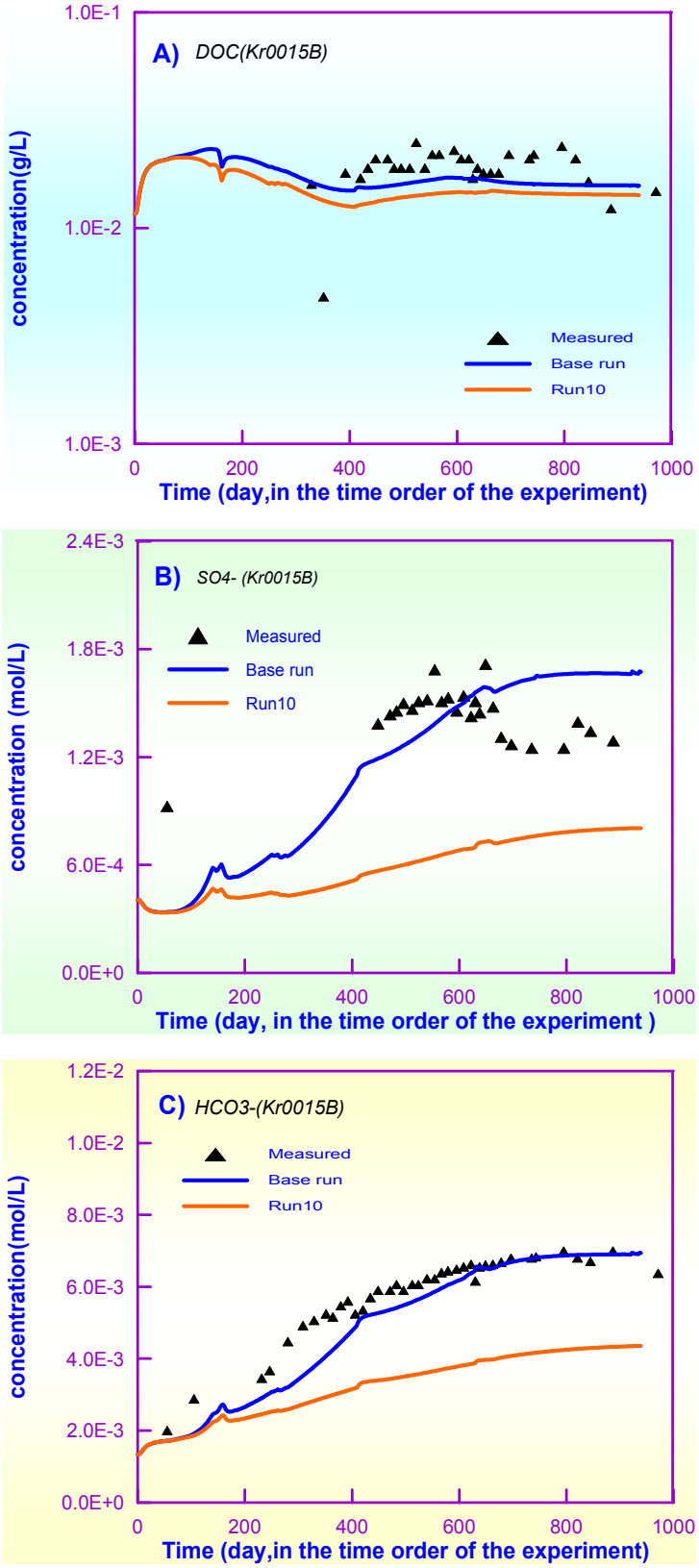

Figure 4-36. *Sensitivity of concentrations of DOC^- (A), SO_4^{2-} (B) and HCO_3^- (C) to initial concentrations of POC at the top layer. Base run: Initial concentration of POC = 30 mg/L. Run 10: Initial concentration of POC = 15 mg/L.*

4.4.4.6 Sensitivity to boundary concentrations of DOC and POC

The source of organic matter to the fracture zone comes mainly from the top boundary with the fresh water. In the simple model, the concentrations of organic species at the bottom boundary are assumed very small, 1.0×10^{-4} g/L. There are no measured data for the concentrations of organic species at the top boundary. During the calibration of the model, it found that the results of the model are sensitive to the concentration of DOC at the top boundary, but insensitive to the concentration of POC.

Figure 4-37 shows sensitivity of bicarbonate to top-boundary concentration of DOC. One can see that the boundary concentration of DOC in the upper boundary affects strongly the amount of bicarbonate.

Figure 4-38 shows the sensitivity of DOC, sulphate and bicarbonate to the upper boundary concentration of POC. One can see that the concentrations of DOC, sulphate and bicarbonate are not sensitive to the boundary concentration of POC. The reason is that the POC is specified a very high distribution coefficient.

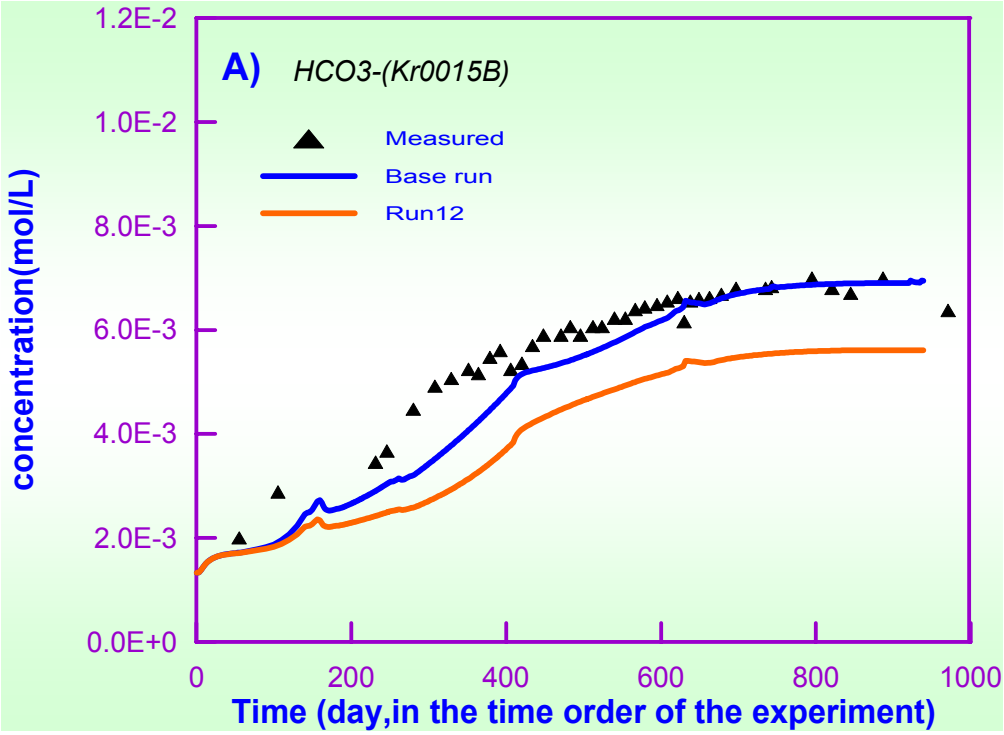

Figure 4-37. *Sensitivity of concentrations of HCO_3^- to the upper boundary concentration of DOC. Base run: concentration of DOC = 30 mg/L. Run 12: concentration of DOC =15 mg/L.*

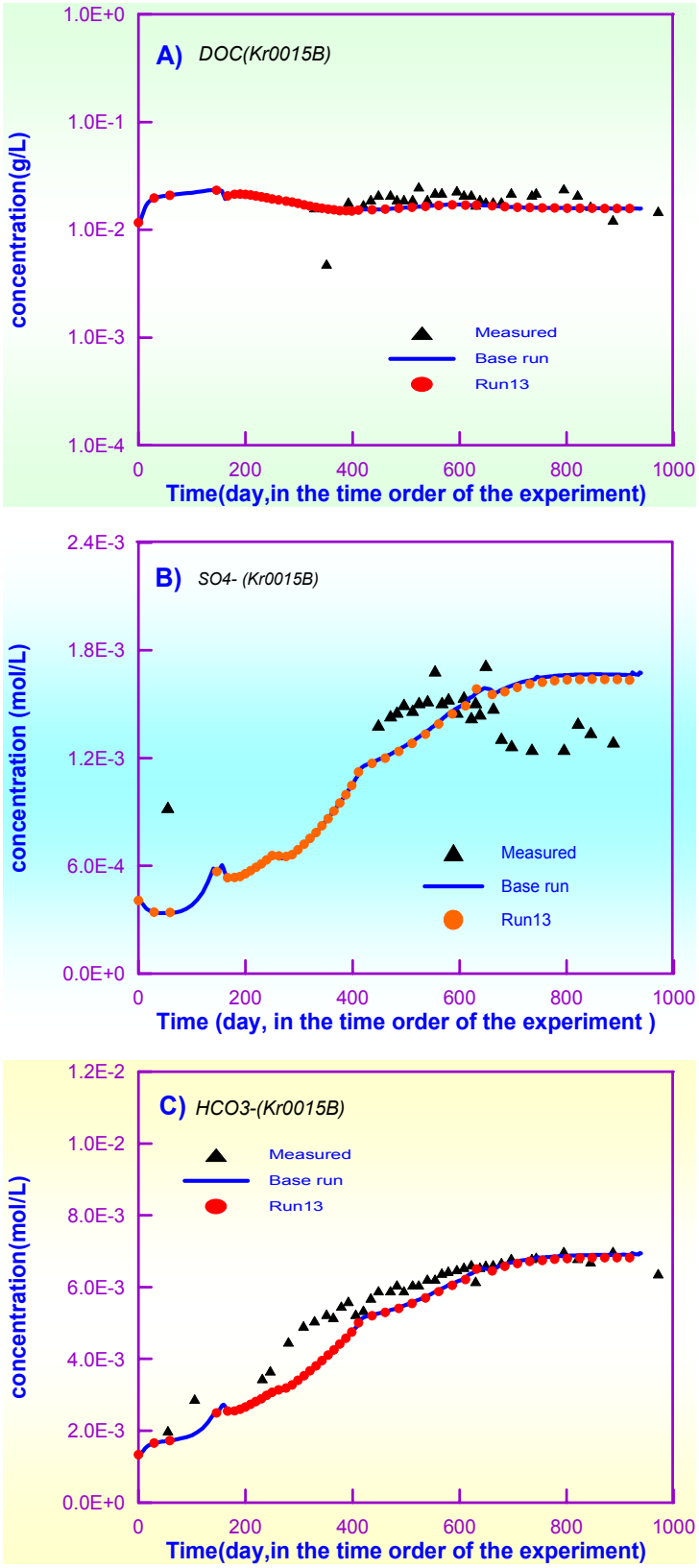

Figure 4-38. *Sensitivity of concentrations of DOC^- (A), SO_4^{2-} (B) and HCO_3^- (C) to the upper boundary concentration of POC. Base run: concentration of top boundary POC = 30 mg/L. Run 12: concentration of top boundary POC = 15 mg/L.*

4.5 Chapter conclusions

Microbially-driven organic matter fermentation and oxidation by iron-reducer are considered as the dominant microbial processes controlling the redox status and the concentration evolution of bicarbonate and sulphate.

The updated microbial model considers fermentation of particulate organic matter by yeast and the oxidation of dissolved organic matter (by iron-reducer bacteria) which is the main product of fermentation processes. Dissolved organic matter is produced by yeast and also serves as a substrate for iron-reducer. These two microbial processes are interdependent.

The other product of fermentation of sulphur-containing organic matter is sulphate. It can give a possible explanation for the increase of the observed concentration of sulphate in the fracture zone. Results of the updated microbial model confirm this conclusion.

Bicarbonate is an end-prod of microbial processes. Model results reproduce the increase in bicarbonate concentration. This also confirms that the source of bicarbonate could be the oxidation of organic matter.

Model results indicate that pH and Eh are relatively stable. The dissolution-precipitation trends of hematite, pyrite and calcite also coincide with those indicated by the conceptual model.

A suite of sensitivity runs was performed. Their results indicate that the model is sensitive to most microbial parameters, such as specific growth rate, half saturation constant, proportionality coefficient and yield coefficient. But the results seem less sensitive to the yield coefficient of DOC to iron-reducer. Changes in the microbial parameters of fermentation affect the growth of iron-reducer.

Sensitivity analyses have been performed also for boundary and initial concentrations of organic matter. The results indicate that concentrations of bicarbonate and sulphate are sensitive to the initial concentration of POC and the boundary concentration of DOC, but not sensitive to the initial concentration of DOC and the boundary concentration of POC. POC cannot migrate because of its large molecular weight while DOC can move dissolved into water.

Although the simple model can reproduce the observed increase of concentrations of bicarbonate and sulphate at a depth of –70 m, further work is needed to improve the 2D hydrobiogeochemical model to characterize the microbial processes in the fracture zone.

5 Conclusions

5.1 Flow and solute transport model

Finite element numerical models of groundwater flow and solute transport of the Redox Zone Experiment have been presented which have proved to be useful for evaluating the effects of the construction of the access tunnel on the hydrogeological and hydrochemical conditions of this fracture zone. The first model was constructed on the basis of the conceptual model used by /Banwart et al, 1994, 1999/ to interpret hydrochemical data. This numerical model fails to reproduce simultaneously the observed drawdowns and the decrease in salinity at the tunnel location. The limitations of this model are overcome by revising Banwart's hydrogeological conceptual model. An improved conceptual and numerical flow and transport model has been presented which relies directly on available hydrogeological and transport parameters, is based on the identification of appropriate flow and transport boundary conditions and uses, when needed, solute data extrapolated from nearby fracture zones. This revised model is consistent with head and concentration data collected prior to tunnel construction and its results match both observed drawdowns and the chemical dilution induced by the construction of the tunnel.

A major outcome of this numerical model is that quantitative analyses of hydrochemical data should rely on sound conceptual flow and transport models in order to ensure consistency of hydrochemical and hydrogeological data /NEA, 1999/. Numerical modeling of water flow and solute transport provides the appropriate framework for checking the consistency of hydrodynamic and hydrochemical data. This framework can be subsequently used for quantitative analyses of complex chemically-reactive species and biological processes by means of reactive transport models.

As a broader conclusion regarding mixing freshwater induced by the tunnel construction, the results of the model confirm that this is a relevant process for a potential repository at least for the conditions prevailing in the Scandinavian region. Chemical data from deeper portions of Äspö tunnel indicate that freshwater mixing takes place whenever the tunnel intersects a major fracture zone. Most of the measured inflows to the tunnel take place along fracture zones. This is also confirmed by numerical models /Molinero et al, 2002/. Therefore, fresh water mixing at a potential repository will be relevant if the repository intersects one of such fracture zones.

5.2 Coupled flow and reactive transport model

The flow and transport model has been used to perform coupled groundwater flow and reactive solute transport simulations of the Redox Zone Experiment. The reactive transport numerical model accounts for more than 60 homogeneous reactions, including aqueous complexation, acid-base, gas dissolution and redox processes, as well as 5 heterogeneous reactions including mineral dissolution/precipitation and cation exchange. The model reproduces the observed concentrations of most dissolved species both before and after tunnel construction.

Numerical analyses indicate that fresh recharge waters have reducing conditions which are consistent with measured values of dissolved iron at a depth of 5 m. In addition, it is found that hematite is the iron mineral phase controlling dissolved iron in groundwaters.

Numerical calibration of the cation exchange capacity leads to a larger value than that evaluated on the basis of reported clay contents. Numerical results are consistent with an average clay content on the order of 5%.

Although calcite dissolution is taking place in the surroundings of the tunnel, this process is not able to explain the increase of bicarbonate concentrations measured near the tunnel. Microbially-mediated degradation of organic matter through iron (III) reduction is a likely chemical process which can explain such observations. The analysis of measured data of bicarbonate, iron, ^{13}C and ^{14}C in water samples collected at different boreholes allows one to conclude that the rock landfill could be a "hot spot" for organic matter degradation.

The model predicts also the dissolution of pyrite around the tunnel but this process cannot explain the measured sulphate evolution. Numerical results support the hypothesis of sulphate-reducing bacteria being present in the fracture zone prior to tunnel intersection. After the start of the experiment, fresh groundwater flowing towards the tunnel increases the input of suitable electron donors (organic matter) in the tunnel surroundings. This could have enhanced the activity of iron reducing bacteria, which at the same time could inhibit the growth of sulphate-reducer microorganisms by out-competition.

The coupled groundwater flow and reactive solute transport numerical model has been used to test additional hydrochemical hypotheses. Numerical results rule out the possibility of a source of sulphate coming from alkaline sulphate-rich waters leaching from a nearby rock landfill. They also rule out the hypothesis of dissolution of iron monosulphides within Baltic seafloor sediments as being responsible for the evolution of sulphate. By discarding these hypotheses one is left with competitive anion adsorption as a likely geochemical process influencing sulphate behaviour during the Redox Zone Experiment.

Coupled flow and reactive transport numerical model results are markedly different than those computed with a model of pure mixing and chemical reactions. Computed results not only are different but they show opposite trends in mineral behaviour. It can be concluded that end-members mixing and reaction models are inappropriate for modeling hydrodynamic systems.

5.3 Coupled flow, reactive transport and microbial model

The preliminary microbial model of /Zhang, 2001/ has been updated by accounting for microbially-driven organic matter fermentation and organic matter oxidation which are considered to be the dominant microbial processes controlling the evolution of redox conditions and the concentrations of bicarbonate and sulphate.

This updated microbial model considers simultaneously the fermentation of particulate organic matter by yeast and the oxidation of dissolved organic matter, a product of fermentation. Dissolved organic matter is produced by yeast and serves also as a substrate for iron-reducing bacteria. These two microbial processes are therefore interconnected.

Another important product of fermentation of sulphur-rich organic matter is sulphate. It provides a plausible explanation for the observed increase in the concentration of sulphate in the fracture zone. Results of the updated microbial model confirm this conclusion.

Bicarbonate is a product of microbial processes. Model results reproduce the increase in bicarbonate concentration. This also confirms that the source of bicarbonate may be the oxidation of organic matter.

Model results indicate that pH and Eh are relatively stable. The dissolution-precipitation trends of hematite, pyrite and calcite also coincide with those indicated by the conceptual model.

A thorough sensitivity analysis has been performed for the most relevant microbial parameters as well as for initial and boundary POC and DOC concentrations. The results of such analysis indicate that computed concentrations of bicarbonate, sulphate and DOC are sensitive to most of the microbial parameters, including specific growth rates, half-saturation constants, proportionality coefficients and yield coefficients. Model results, however, are less sensitive to the yield coefficient of DOC to iron-reducer bacteria. The sensitivity analysis indicates that changes in fermentation microbial parameters affect the growth of the iron-reducer, thus confirming the interconnection of both microbial processes. Computed concentrations of bicarbonate and sulphate are found to be sensitive to changes in the initial concentration of POC and the boundary concentration of DOC, but they lack sensitivity to the initial concentration of DOC and the boundary concentration of POC. The explanation for such result is related to the fact that POC has a low mobility due to its large molecular weight. DOC, however, can migrate downwards.

Although a coupled hydro-bio-geochemical 1-D model can reproduce the observed "unexpected" increase of concentrations of bicarbonate and sulphate at a depth of 70 m, further modelling work is required in order to obtain a similar conclusion under the more realistic two dimensional conditions of the fracture zone.

Acknowledgements

The work presented here has been funded by SKB through a Research Grant signed with the University of La Coruña. The code used for coupled geochemical and microbial modeling, BIOCORE, was developed within the framework of R&D projects funded by ENRESA and Spanish Ministry of Science and Technology (CICYT Project HID98-0282). Authors want to acknowledge the support on geochemical mixing calculations which was provided by Luis Montenegro (UDC). Thanks are especially given to Ignasi Puigdomenech and Peter Wikberg for their support and suggestions as well as to Marcus Laaksoharju and Steve Banwart for the estimulating discussions and comments about the Redox Zone Experiment.

References

Atkins M, Glasser F P, 1992. Application of portlandite cement-based materials to radiactive waste inmobilization. Waste Management, 12, 105–131.

Banwart S, Gustafsson E, Laaksoharju M, Nilsson A-N, Tullborg E-L, Wallin B, 1994. Large-scale intrusion of shallow water into a vertical fracture zone in crystalline bedrock: Initial hydrochemical perturbation during tunnel construction at the Äspö Hard Rock Laboratory, southeastern Sweden. Water Resources Research, 30:6, 1747–1763.

Banwart S, Laaksoharju M, Pitkänen P, Snellman M, Wallin B, 1995. Development of a site scale model for reactive element dynamics. In: The Redox Experiment in Block Scale. Final Reporting of Results from the Three year Project. Chapter 6. Steven Banwart (Ed). SKB Progress Report 25-95-06.

Banwart S, Tullborg E-L, Pedersen K, Gustafsson E, Laaksoharju M, Nilsson A-C, Wallin B, Wikberg P, 1996. Organic carbon oxidation induced by large-scale shallow water intrusion into a vertical fracture zone at the Äspö Hard Rock Laboratory (Sweden). Journal of Contaminat Hydrology, 21, 115–125.

Banwart S, 1997. Aqueous speciation at the interface between geological solids and groundwater. In: Modelling in Aquatic Chemistry (Grenthe I and Puigdomenech I, Eds.). The Nuclear Energy Agency (NEA) of the OECD. Paris.

Banwart S, 1999. Reduction of iron(III) minerals by natural organic matter in groundwater. Geochimica et Cosmochimica Acta. 63:19/20, 2919–2928.

Banwart S, Gustafsson E, Laaksoharju M, 1999. Hydrological and reactive processes during rapid recharge to fracture zones. The Äspö large scale redox experiment. Applied Geochemistry, 14, 873–892.

Bear J, 1972. Dynamics of Fluids in Porous Media. New York, Dover Publications, Inc. pp 764.

Berner U R, 1992. A thermodynamic description of the evolution of pore water chemistry and uranium speciation during the degradation of cement. PSI Report 62 and NAGRA Technical Report NTB-91-12.

Beverskog B, Puigdomenech I, 1996. Revised Pourbaix diagrams for iron at 25–300ºC. Corrosion Science, 38 (12). 2121–2135.

Bruton C J, Viani B E, 1997. Ion sorption onto hydrous ferric oxides: effect on major element fluid chemistry at Äspö (Sweden). In: Evolution of the Groundwater Chemistry at the Äspö Hard Rock Laboratory. Proceedings of the second Äspö International Geochemistry Workshop. (Laaksoharju M and Wallin B, Eds.). SKB International Cooperation Report 97-04.

Chilakapati A B, 1997. Solution to the CONTA Problem (Chilakapati). *Pacific Northwest National Laboratories. Interim Report.*

Custodio E, 1983. Relaciones agua dulce-agua salada en las regiones costeras. In: Hidrología Subterránea, Vol. II, Chapter 13. (Custodio E and Llamas M R, Eds.) Ed. Omega, S.A. Barcelona. 1315–1385. (In Spanish)

Freeze R A, Cherry J A, 1979. Groundwater. Prentice-Hall, Inc. New Jersey.

Garrels R M, Christ C L, 1965. Solutions, Minerals and Equilibria. Freeman. San Francisco, CA.

Gustafsson E, Andersson-Ludvigson J E, Gentzschein B, 1994. Pressure build-up interference tests in the Redox Fracture Zone. The Äspö Redox Experiment in Block Scale. In: Hydraulic modelling and tracer tests in the Redox Experiment in the Äspö Hard Rock Laboratory Tunnel. E. Gustafsson (ed). SKB Progress Report 25-94-37.

Hautojärvi A, Koskinen L, Löfman J, 1994. Hydraulic modelling of the Large Scale Redox Experiment at Äspö HRL. In: Hydraulic modeling and tracer tests on the Redox Experiment in the Äspö Hard Rock Laboratory tunnel. (Gustafsson et al. Eds.). SKB Progress Report 25-94-37.

Kotelnikoba S, Pedersen K, 1999. The microbe REX Project: Microbial O2 comsuption in the Äspö tunnel. SKB Technical Report. Stockholm.

Laaksoharju M (ed), Gustafsson G, Pedersen K, Rhén I, Skarman C, Tullaborg E L, Wallin B, Wikberg P, 1995. Sulphate reduction in the Äspö HRL tunnel. SKB Technical Report, 95-25.

Laaksoharju M, Wallin B, 1997. Evolution of the groundwater chemistry at the Äspö Hard Rock Laboratory. Proceedings of the second Äspö International Geochemistry Workshop, June 6–7, 1995. SKB, International Cooperation Report 97-04.

Laaksoharju M, Tullborg E-L, Wikberg P, Wallin B, Smellie J, 1999. Hydrogeochemical conditions and evolution at the Äspö HRL, Sweeden. Applied Geochemistry, 14, 835–860.

Landström O, Aggeryd I, Marthiasson L, Sundblad, 1994. Chemical composition of sediments from the Äspö area and interactions between the biosphere and geosphere. SKB Status Report AR 94-03. Stockholm.

Lichtner P C, Seth M, 1996. "Multiphase-Multicomponent Nonisothermal Reactive Transport in Partially Saturated Porous Media." *Proceedings of the International Conference on Deep Geological Disposal of Radioactive Waste, Canadian Nuclear Society*, 3-133 to 3-142. Toronto, Ontario, Canada: Canadian Nuclear Society. TIC: 237969

Lovley D R, 1991. Dissimilatory Fe(III) and Mn(IV) reduction. Microbiological Reviews, 55, 259–287.

Molinero J, 2000. Testing and validation of numerical models of groundwater flow, solute transport and chemical reactions in fractured granites: A quantitative study of the hydrogeological and hydrochemical impact produced by the construction of the Äspö Underground Laboratory (Sweden). Ph. D. Dissertation. University of A Coruña. Spain.

Molinero J, Samper J, Montenegro L, Puigdomenech I, 2000. Groundwater flow and reactive transport models in fractured granites: case study in the Äspö island system (Sweden). In: Groundwater 2000 (Bjerg, P.; Engesgaard, P. and Krom. T. Eds). Proceedings of the International Conference on Groundwater Research, Copenhagen. A.A. Balkema. 111–112.

Molinero J, Samper J, Juanes R, 2002. Numerical modeling of the transient hydrogeological response produced by tunnel construction in fractured bedrocks. Engineering Geology, 64, 369–386.

Molinero J, Samper J, 2003. Groundwater Flow And Solute Transport In Fracture Zones: An Improved Model For A Large-Scale Field Experiment At Äspö (Sweden). Journal of Hydraulic Research, Vol. 42, Extra Issue on Groundwater Hydraulics. In Press.

Molinero J, Samper J, Zhang G, 2004. Groundwater flow and solute transport in fracture zones: II. Reactive transport model of the Redox Zone Experiment at Äspö (Sweden). In Preparation.

NEA, Nuclear Energy Agency, 1999. Use of Hydrogeochemical Information in Testing Groundwater Flow Models, Workshop Proceedings, Borgholm, 1–3 Sep. 1997, 356 p.

Parkhurst D L, Appelo C A J, 1999. User's guide to PHREEQC (version 2)-A computer program for speciation, batch-reaction, one dimensional transport, and inverse geochemical calculations Water-Resources Investigations Report 99-4259 U.S. GEOLOGICAL SURVEY.

Pedersen K, Arlinger J, Jahromi N, Ekendahl S, Hallbeck L, 1995. "Microbiological investigations". In: The Redox Experiment in Block Scale. Final Reporting of Results from the Three year Project. Chapter 7. Steven Banwart (Ed). SKB Progress Report 25-95-06.

Pitkänen P, Löfman J, Koskinen L, Leino-Forsman H, Snellman M, 1999. Application of mass-balance and flow simulation calculations to interpretation of mixing at Äspö, Sweden. Applied Geochemistry, 14, 893–905.

Pourbaix M, 1945. Ph.D. Thesis. Technische Hogeschool Delft. The Netherlands

Pourbaix M, Zubov N, 1963. Atlas d'Equilibres Electrochimiques (Pourbaix, M. Ed.). Gauthier-Villars and Cie. Paris.

Puigdomenech I, 1999. MEDUSA: Make Equilibrium Diagrams Using Sophisticated Algorithms. Vers. 2 Nov. 1999. Inorganic Chemistry, Royal Institute of Technology (KTH). Stockholm. (http://www.inorg.kth.se)

Puigdomenech I, Ambrosi J-P, Eisenlohr L, Lartigue J-E, Banwart S A, Bateman K, Milodowski A E, West J M, Griffault L, Gustafsson E, Hama K, Yoshida H, Kotelnikova S, Pedersen K, Michaud V, Trotignon L, Rivas Perez J, 2001. O_2 depletion in gratitic media, The REX project. TR-01-05. Svensk Kärnbränslehantering AB.

Reardon E J, 1992. Problems and approaches to the prediction of the chemical composition in cement/water systems. Waste Management, 12, 221–239.

Rhén I, Bäckbom G, Gustafson G, Stanfors R, Wikberg P, 1997. Results from pre-investigations and detailed site characterization. Summary Report. SKB Technical Report 97-03.

Salvage K M, Yeh GT, 1998. Development and Application of a Numerical Model of Kinetic and Equilibrium Microbiological and Geochemical Reactions (BIOKEMOD), *Journal of Hydrology*, Vol. 209 (27–52).

Samper J, Delgado J, Juncosa R, Montenegro L, 1998. CORE-LE-2D: A Code for water flow and reactive transport. User's manual. *Universidad de A Coruña*. Spain. Unpublished.

Samper J, Juncosa R, Delgado J, Montenegro L, 2000. CORE^{2D}: A code for non-isothermal water flow and reactive solute transport. Users manual version 2. *ENRESA* Technical Publication 06/2000: 131 pp.

Samper J, Molinero J, Zhang G, Yang C B, 2003. Modeling groundwater flow and solute transport in fracture zones: III. Coupled reactive transport and microbial processes in the Redox Zone Experiment at Äspö (Sweden). In Preparation.

SKB, 1995. This is how we manage Sweden's radioactive waste. Activities 1995. Swedish Nuclear Fuel and Waste Management Company, SKB. Stockholm.

SKB, 1996. Äspö Hard Rock Laboratory. 10 years of research. Swedish Nuclear Fuel and Waste Management Company, SKB. Stockholm.

Smellie J A T, Laaksoharju M, Wikberg P, 1995. Äspö, SE Sweden: a natural groundwater flow model derived from hydrogeochemical observations. Journal of Hydrology, 172, 145–169.

Steefel C I, Lichtner P C, 1994. Diffusion and reaction in rock matrix bordering a hyperalkaline fluid-filled fracture. Geochimica et Cosmochimica Acta, vol. 58, nº 17, 3595–3612.

Sundblad B, Mathiasson L, Holby O, Landström O, Lampe S, 1991. Chemistry of soil and sediments, hydrology and natural exposure rate measurements at the Äspö Hard Rock Laboratory. SKB Progress Report 25-91-08.

Sundblad B, Mathiasson L, 1994. Recipient studies at the Äspö Hard Rock Laboratory. Water turnover, sediment and conceptual models. SKB Status Report 94-52.

Svensson U, 1997. A regional analysis of groundwater flow and salinity distribution in the Äspö area. SKB Technical Report 97-09.

Tullborg E-L, 1995. Mineralogical/Geochemical investigations in the Fracture Zone. In: The Redox Experiment in Block Scale. Final Reporting of Results from the Three year Project. Chapter 4. Steven Banwart (Ed). SKB Progress Report 25-95-06.

Tullborg E-L, Gustafsson E, 1999. ^{14}C in biocarbonate and dissolved organics – a useful tracer?. Applied geochemistry, 14, 927–938.

Valocchi A J, Tebes C, 1997. Benchmark problem: A workshop on Subsurface Reactive transport Modeling, 29 October – 1 November 1997, Pacific Northwest Laboratory, Richland, WA.

Viani B, Bruton C, 1997. In assessing the role of cation exchange in controlling groundwater chemistry during fluid mixing in a fracture granite at Äspö, Sweden. In: Laaksoharju and Wallin (Eds). 2nd Äspö Internat. Chem. Workshop. SKB-ICR-97/04.

Wallin B, 1995. Sulphur cycling in the Fracture Zone. In: The Redox Experiment in Block Scale. Final Reporting of Results from the Three year Project. Chapter 6. Steven Banwart (Ed). SKB Progress Report 25-95-06.

Wallin B, Tullborg E-L, Pettersson C, 1995. "Carbon cycling in the Fracture Zone". In: The Redox Experiment in Block Scale. Final reporting of results from the three year project. Chapter 5. Steven Banwart (Ed). SKB Progress Report 25-95-06.

Wikberg P, Wallin B, Tullborg E V, Laaksoharju M, 1997. Usefulness of isotope techniques for assessment of the hydrochemical conditions at the Äspö Hard Rock Laboratory. In: Use of hydrogeochemical Information in Testing Groundwater Flow Models, Borgholm (Sweden), 1–3 September 1997. Workshop Proceedings. AEN-NEA. 355–356.

Wolery T J, 1979. Calculation of equilibrium between aqueous solution and minerals: the EQ3/6 software package. Lawrence Livermore National Laboratory. CA, USA. UCRL-52658.

Zhang G, Samper J, 2001. Biohydrogeochemistry "A new face" of groundwater chemistry. Proceeding of the conference: Las caras del agua subterranea. Universidad Politécnica de Cataluña. Barcelona.

Zhang G, 2001. Nonisothermal hydrobiogeochemical models in porous media. Ph. D. Dissertation. University of A Coruña. Spain.

Appendix I

Brief description of BIO-CORE

A1.1 Main features of the code

BIO-CORE /Zhang and Samper, 2001/ is an extended version of code CORE^{2D} /Samper et al, 2000/. BIO-CORE copes with both thermodynamically controlled non-isothermal abiotic geochemical processes and subsurface microbial processes in two-dimensional variably saturated porous media. The code defines the hydrogeochemical system as an integration of motion and transformation of substance and energy in subsurface environment. Substance, including water and rock matrix, is represented by parameterized porous medium, quantified chemical species, including water, in both aqueous and solid, adsorbed and crystallized (mineral) phase, active microbiological species, in both attached phase or free cells in water. Temperature, referring to heat transfer processes, hydraulic head, referring to water flow and concentrations, referring to solute transport, are state variables of the system which measure the distribution and evolution of energy and mass in the system. They are governed by partial differential equations (PDEs) describing water flow, solute and heat transport, and nonlinear algebraic equations (AEs), describing chemical reactions. The code uses the Galerkin finite element method to solve the PDEs and the Newton-Raphson method to solve the AEs. The PDEs and AEs are coupled in a sequential iterative manner.

BIO-CORE is capable to deal with any number of chemical and microbial species in both aqueous and solid phases (adsorbed, minerals and attached microbial species). Aqueous reactions, adsorption/desorption, exchange and dissolution/precipitation reactions are optionally considered as either equilibrium or kinetic processes. The code deals with growth-consumption processes with consideration of metabolic competition, decay and attachment/detachment. It also considers the availability of the substrates for attached microorganisms by coupling a diffusion layer model to account for the biofilm resistance. The code has been verified and applied to the interpretation of the field experiments /Zhang, 2001/.

A1.2 A verification example of BIO-CORE against the results of FEREACT

This problem was originally set up from extending a batch biogeochemical system by /Valocchi and Tebes, 1997/ using FEREACT and has been known as benchmark problem usually used to verify reactive transport codes. So far there are some codes that have been able to solve this problem (BIOKEMOD, /Salvage and Yeh, 1998/; MULTIFLO, /Lichtner and Seth, 1996/; RAFT, /Chilakapati, 1997/ and a non released version of PHREEQC, /Parkhurst and Appelo, 1999/). We take this example to verify the performance of BIO-CORE dealing with coupled equilibrium aqueous speciation, kinetic biodegradation and adsorption/desorption reactions.

A1.2.1 Problem description

This problem considers transport of multiple reacting species through a 1-D column. The objective of the analysis is to model the coupled effects of a set of equilibrium speciation reactions and kinetic biodegradation and adsorption/desorption reactions.

The physical parameters used in the simulation are given in Table A1-1.

A Dirichlet (specified hydraulic head with specified concentrations) boundary condition is used at the inlet of the column, while the end of the column is a solute exit boundary. The duration of the simulation is 75 hours. For the first 20 hours of the simulation, a pulse containing cobalt (Co^{2+}) and nitrilotriacetate (NTA^{3-}) is injected at the entrance of the column. After 20 hours, the fluid injected at the entrance has the same composition as the original background solution in the column (Table A1-2).

A1.2.2 Speciation reactions

The chemical system consists of seven aqueous components and three immobile components. Table 2 lists the component species and provides the initial conditions and the total concentrations of each component in the injected fluid. The pH and the total concentrations of the aqueous and immobile component species are allowed to vary under the influence of kinetic reactions. The aqueous components undergo equilibrium speciation reactions to form 14 complex species. The appropriate stoichiometric coefficients and equilibrium constants for each complex are given in Table A1-3.

Table A1-1. Physical parameters.

Length of column	10 m
Porosity	0.4
Bulk density	1.5×10^3 g/L
Pore water velocity	1 m/hr
Longitudinal dispersivity	0.05 m

Table A1-2. Total concentration of component species.

Component	Type	Pulse Concentration	Background concentration
H^+	Aqueous	pH = 6	pH = 6
H_2CO_3	Aqueous	4.9×10^{-7} moles/L	4.9×10^{-7} moles/L
NH_4^+	Aqueous	0.0	0.0
O_2	Aqueous	3.125×10^{-5} moles/L	3.125×10^{-5} moles/L
NTA^{3-}	Aqueous	5.23×10^{-6} moles/L	0.0
Co^{2+}	Aqueous	5.23×10^{-6} moles/L	0.0
Buffer	Aqueous	0.0 & 10^{-3} moles/L	0.0 & 10^{-3} moles/L
Biomass	Immobile	——	1.36×10^{-4} g/L
CoNTA(ads)	Immobile	——	0.0
Co(ads)	Immobile	——	0.0

Table A1-3. Stoichiometric coefficients and equilibrium constants for complex species.

Complex	Stoichiometric coefficients							log Keq
	H^+	H2CO3*	$NH4^+$	O2	NTA^{3-}	Co^{2+}	Buffer	
H_3NTA	3	0	0	0	1	0	0	14.9
H_2NTA^-	2	0	0	0	1	0	0	13.3
$HNTA^{2-}$	1	0	0	0	1	0	0	10.3
$CoNTA^-$	0	0	0	0	1	1	0	11.7
$CoNTA2^{4-}$	0	0	0	0	2	1	0	14.5
$CoOHNTA^{2-}$	–1	0	0	0	1	1	0	0.5
$CoOH^+$	–1	0	0	0	0	1	0	–9.7
$Co(OH)_2^-$	–2	0	0	0	0	1	0	–22.9
$Co(OH)_3^-$	–3	0	0	0	0	1	0	–31.5
HCO_3^-	–1	1	0	0	0	0	0	–6.35
CO_3^{2-}	–2	1	0	0	0	0	0	–16.68
NH_3	–1	0	1	0	0	0	0	–9.3
OH^-	–1	0	0	0	0	0	0	–14.0
HBuffer	1	0	0	0	0	0	1	6

A1.2.3 Biodegradation of $HNTA^{2-}$

The biodegradation of the complex HNTA 2– is represented by the following reaction.

$$HNTA^{2-} + 1.620\ O_2 + 1.272\ H_2O + 2.424\ H^+ \Longrightarrow 0.576\ C_5H_7O_2N + 3.120\ H_2CO_3 + 0.424\ NH_4^+ \quad (1)$$

The rate of substrate degradation (R_{HNTA}) is modeled with multiplicative-Monod kinetics:

$$R_{HNTA^{2-}} = -q_m X_m \frac{[HNTA^{2-}]}{K_s + [HNTA^{2-}]} \frac{[O_2]}{K_A + [O_2]} \quad (2)$$

where Xm is the biomass concentration, $[HNTA_2^-]$ is the concentration of $HNTA_2^-$ and $[O_2]$ is the concentration of oxygen. The parameters used in equation (2) are defined in Table A1-4. The rates of change in the concentration of O_2, H^+, H_2CO_3, and NH_4^+ are proportional to the rate of substrate degradation. Using the stoichiometry of reaction (1), the appropriate rate expressions are:

$$R_{O2} = 1.620\ RHNTA^{2-} \quad (3)$$

$$R\ H^+ = 2.424\ RHNTA^{2-} \quad (4)$$

$$R\ H_2CO_3^- = 3.120\ RHNTA^{2-} \quad (5)$$

$$R\ NH_4^+ = 0.424\ RHNTA^{2-} \quad (6)$$

The net rate of microbial growth is given by the synthesis rate minus a first-order decay rate.

Table A1-4. Biodegradation rate parameters

Parameter	Description	Value
KS	half-maximum-rate concentration for donor	7.64×10^{-7} moles/L
KA	half-maximum-rate concentration for acceptor	6.25×10^{-6} moles/L
Qm	maximum specific rate of substrate utilization	1.407×10^{-3} moles NTA/gcells/hr.
Y	microbial yield coefficient	65.14 g cells/mole NTA
b	first-order microbial decay coefficient	0.00208 hr^{-1}

$$R\ cells = -YR\ HNTA^{2-} - bXm \tag{7}$$

where Y is the yield coefficient and b is the decay coefficient.

A1.2.4 Adsorption/Desorption of Co^{2+} and $CoNTA^{-}$

The sorption reactions are represented by a linear kinetic model, which is given by the following rate expression.

$$R_{X_{aq}} = \frac{d[X]}{dt} = -K_m([X] - \frac{\overline{X}}{K_d}) \tag{8}$$

where [X] denotes the aqueous concentration of species X in moles/L, X denotes the adsorbed concentration of species X in moles/gram, km is the mass transfer coefficient in hr^{-1}, and Kd is the distribution coefficient for linear equilibrium adsorption. Equation (4) is used to calculate the rate of change in the aqueous concentration of species X due to sorption. The corresponding rate expression for the change in the adsorbed concentration of species X is given by:

$$R_{X_{ad}} = \frac{d\overline{X}}{dt} = -\frac{\theta}{\rho}\frac{d[X]}{dt} = \frac{\theta}{\rho}K_m([X] - \frac{\overline{X}}{K_d}) \tag{9}$$

In this problem, uncomplexed cobalt (Co^{2+}) and $CoNTA^{-}$ are retarded due to the process of ad-sorption. The mass transfer coefficient is set equal to 1 hr^{-1} for both sorption reactions. The distribution coefficients for Co^{2+} and $CoNTA^{-}$ are assumed to be equal to 5.07×10^{-3} L/g and 5.33×10^{-4} L/g, respectively. It should be noted that these distribution coefficients were selected to give retardation coefficients of 20 and 3 for Co^{2+} and $CoNTA^{-}$, respectively. The Kd values were calculated using the following formula:

$$K_d = \frac{\theta}{\rho}(R_f - 1) \tag{10}$$

The Kd values do not necessarily represent realistic sorption behaviour.

A1.2.5 Results

The following simulations were performed with $\Delta x = 0.1$m. Parts A and B used maximum $\Delta t = 0.1$ hr and part C used maximum $\Delta t = 0.05$ hr.

Part A. Perform the simulation with 10^{-3} moles/L of buffer in both the pulse solution and the background solution. The presence of the buffer will keep the pH approximately constant at a value of 6.

Part B. Perform the simulation with the total aqueous concentration of buffer equal to 0.0 moles/L in both the pulse solution and the background solution. In this case, the biodegradation reaction (1) will cause the pH to rise (to a maximum value of about 6.94 at a time of 30 hours at the end of the column). This increase in pH results in a redistribution of species in solution. Specifically, as pH rises, $CoNTA^-$ forms at the expense of Co^{2+} and $HNTA^{2-}$. The rise in pH affects the results of the simulation in two ways:

Since $HNTA^{2-}$ is the biodegradable form of NTA, the increase in pH causes a decrease in the overall amount of biodegradation in the column. This can be confirmed by comparing the concentration vs. time curves for biomass in parts A and B at any given point along the column.

Since $CoNTA^-$ ($Rf \approx 3$) does not adsorb as strongly as uncomplexed cobalt (Co^{2+}, $Rf \approx 20$), the increase in the concentration of $CoNTA^-$ relative to that of Co^{2+} allows cobalt to migrate through the column more quickly. A comparison of the concentration vs. time curves for the adsorbed species in parts A and B reveals that at the end of the simulation, less cobalt remains adsorbed in the column for part B.

Part C. Repeat Part B with the sorption mass transfer coefficient increased to 1000 hr^{-1}. Setting the mass transfer coefficient to 1000 hr^{-1} approximates equilibrium for the sorption reactions. This results in sharper concentration fronts.

The plots below (Figure A1-1 through A1-6) show Comparisons between the concentration vs. time curves calculated by BIO-CORE and that of Tebes and Valocchi for selected species at the end of the 10 m column for parts A, B, and C.

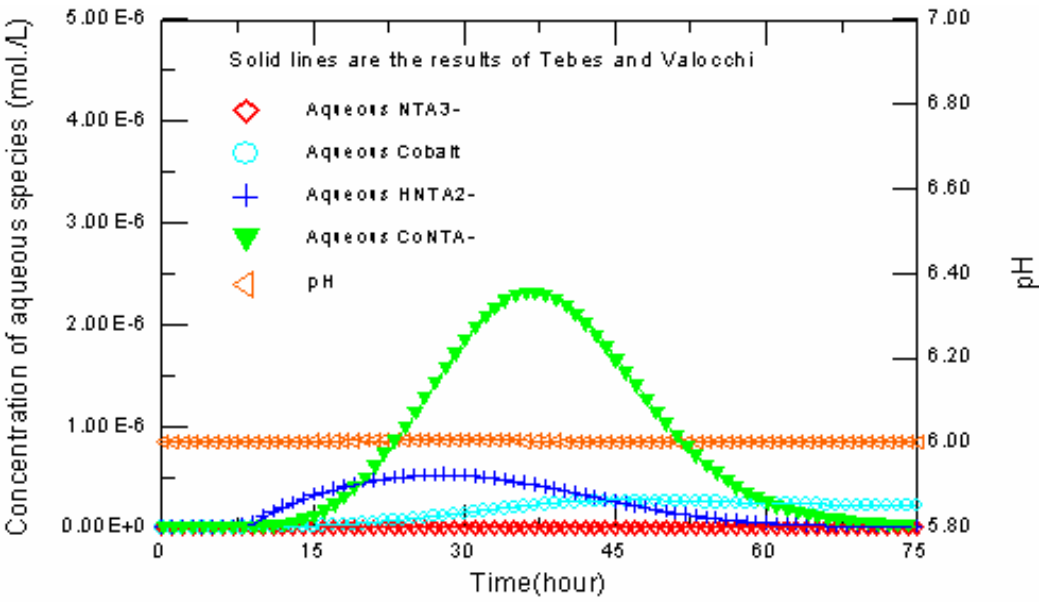

Figure A1-1. *Concentration time evolution curves of aqueous species (Part A). Solid lines correspond to Tebes and Valocchi; Symbols correspond to BIO-CORE.*

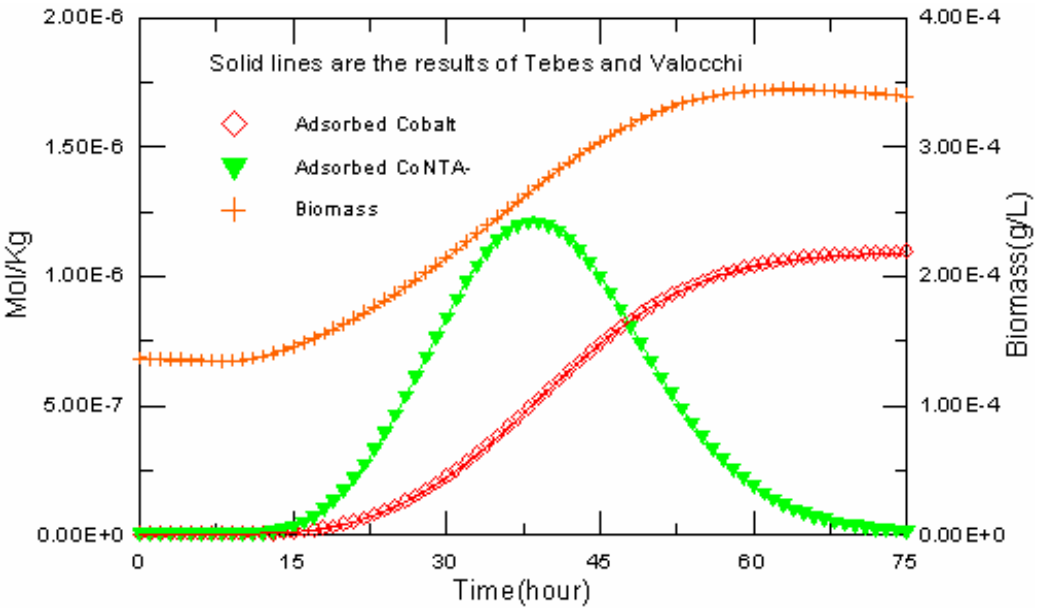

Figure A1-2. *Concentration time evolution curves of adsorbed species (Part A). Solid lines correspond to Tebes and Valocchi; Symbols correspond to BIO-CORE.*

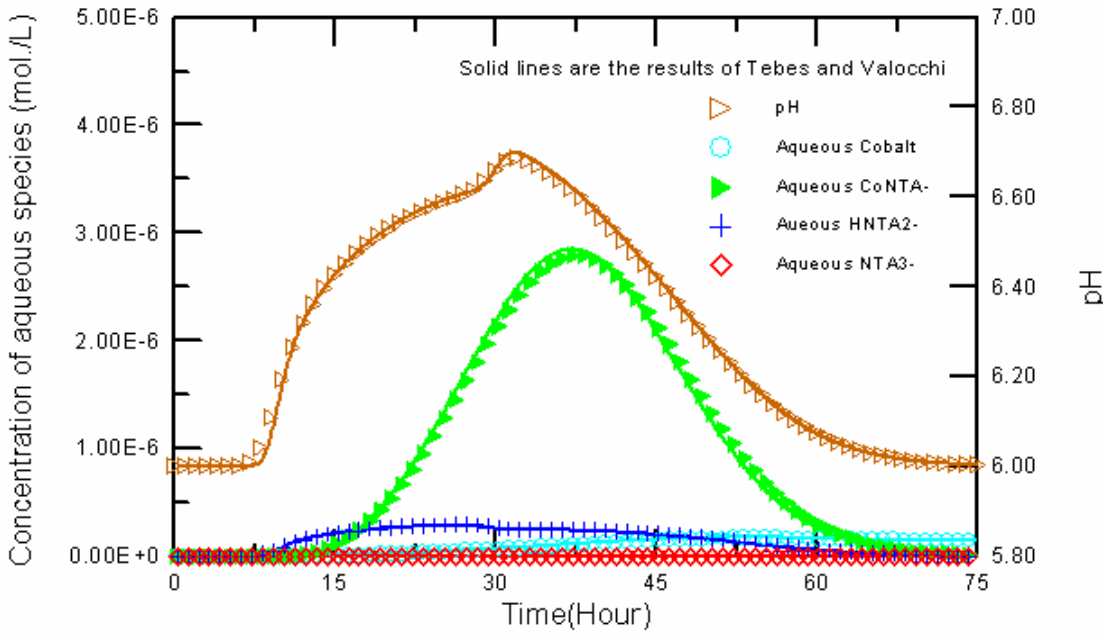

Figure A1-3. *Concentration time evolution curves of aqueous species (Part B). Solid lines correspond to Tebes and Valocchi; Symbols correspond to BIO-CORE.*

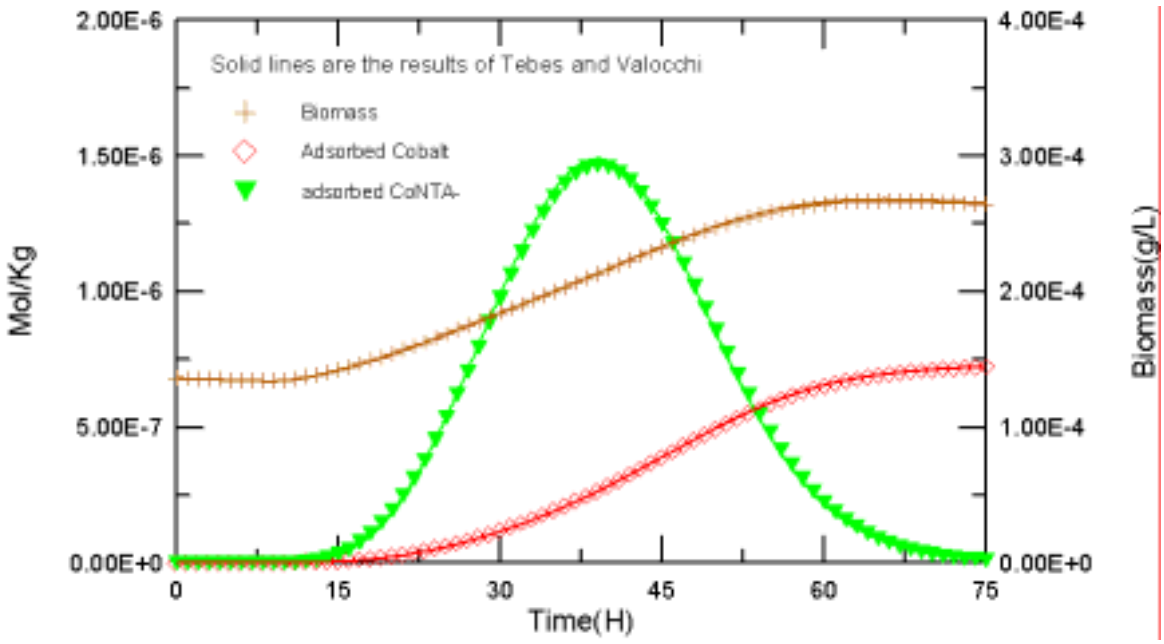

Figure A1-4. *Concentration time evolution curves of adsorbed species (Part B). Solid lines correspond to Tebes and Valocchi; Symbols correspond to BIO-CORE.*

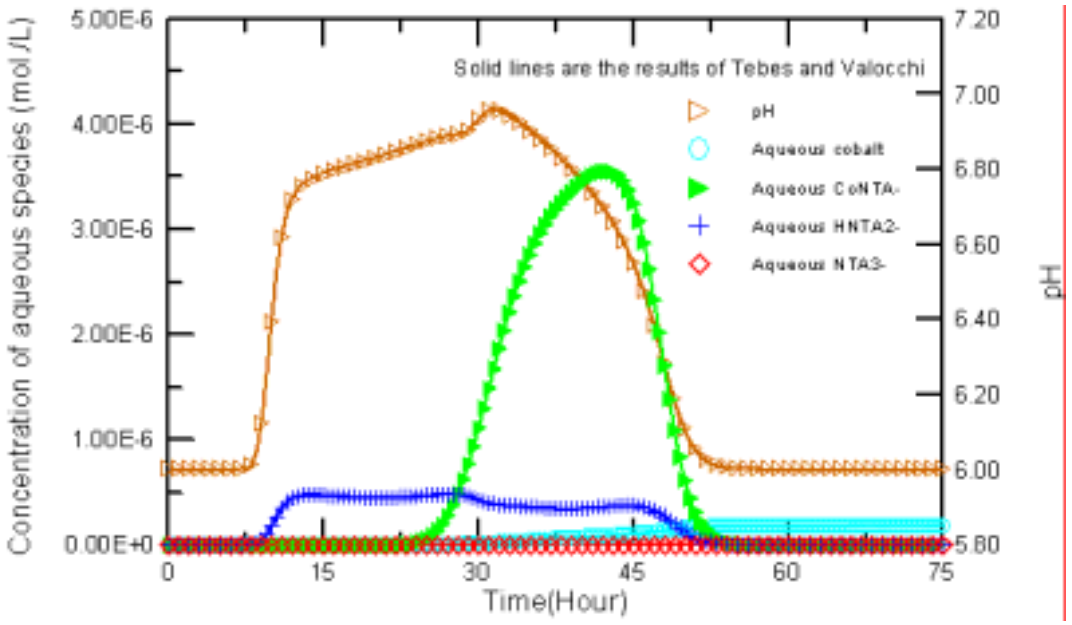

Figure A1-5. *Concentration time evolution curves of aqueous species (Part C). Solid lines correspond to Tebes and Valocchi; Symbols correspond to BIO-CORE.*

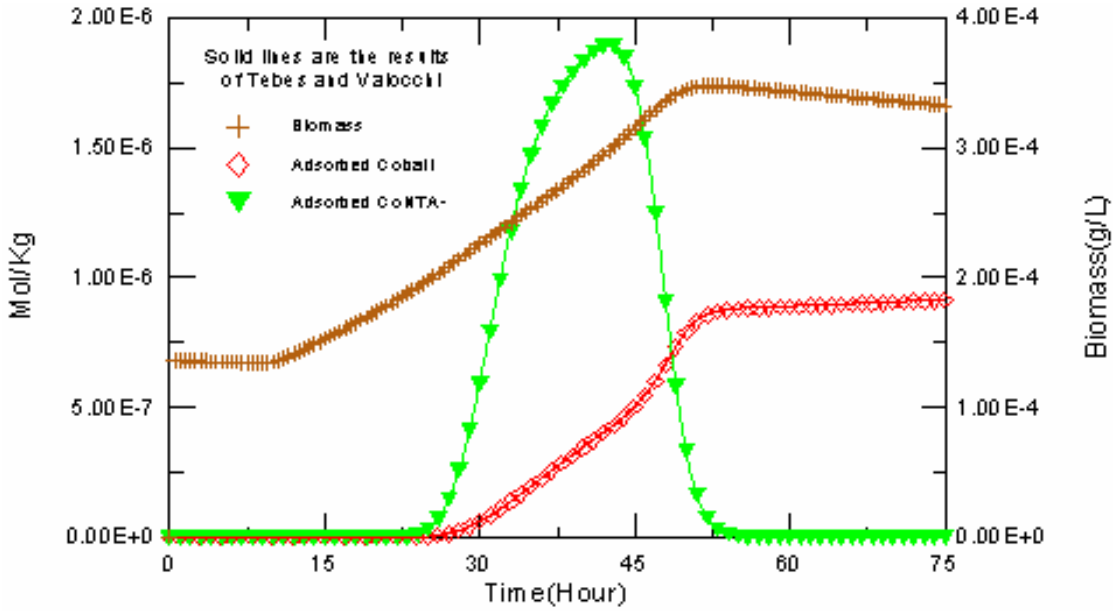

Figure A1-6. *Concentration time evolution curves of adsorbed species (Part C). Solid lines correspond to Tebes and Valocchi; Symbols correspond to BIO-CORE.*

ISSN 1404-0344

CM Digitaltryck AB, Bromma, 2003